Aus dem Institut für Immunologie
im Biomedizinischen Zentrum
der Ludwig-Maximilians-Universität München
Vorstand: Prof. Dr. Thomas Brocker

Development of tools for detection of phosphatidylserine exposure *in vitro* and *in vivo*

Dissertation
zum Erwerb des Doktorgrades der Naturwissenschaften
an der Medizinischen Fakultät der
Ludwig-Maximilians-Universität zu München

vorgelegt von
Tilman Kurz
aus Waiblingen

2020

Mit Genehmigung der Medizinischen Fakultät
der Universität München

Betreuer:	Prof. Dr. Thomas Brocker
Zweitgutachterin:	Prof. Dr. Kirsten Lauber
Dekan:	Prof. Dr. med. dent. Reinhard Hickel
Tag der mündlichen Prüfung:	09.03.2021

Author’s declaration

Ich erkläre hiermit an Eides statt, dass ich die vorliegende Dissertation mit dem Thema „Development of tools for detection of phosphatidylserine exposure *in vitro* and *in vivo*” selbständig verfasst, mich außer der angegebenen keiner weiteren Hilfsmittel bedient und alle Erkenntnisse, die aus dem Schrifttum ganz oder annähernd übernommen sind, als solche kenntlich gemacht und nach ihrer Herkunft unter Bezeichnung der Fundstelle einzeln nachgewiesen habe.
Ich erkläre des Weiteren, dass die hier vorgelegte Dissertation nicht in gleicher oder in ähnlicher Form bei einer anderen Stelle zur Erlangung eines akademischen Grades eingereicht wurde.

Tilman Kurz

München, 20. April 2021

This thesis contains data that will be presented in the following publication:
Kurz, T., Kranich, J., Jiahui F., Knobloch, G., Ladurner, A., Schulz, C., Brocker, T.
Novel multimers for the detection of apoptotic cells *in vivo* and *in vitro*
Manuscript in preparation

Kranich, J., Chlis, N-K., Rausch, L., Latha, A., Schifferer, M., Kurz, T., Foltyn-Arfa Kia, A., Simons, M., Theis, F.J., Brocker, T. (2020) *In vivo* identification of apoptotic and extracellular vesicle-bound live cells using image-based deep learning. *Journal of Extracellular Vesicles*

Abbreviations

aa	Amino acids
AF647	Alexa Fluor 647
APS	Ammonium persulfate
ATP	Adenosine triphosphate
BSA	Bovine serum albumin
CD	Cluster of differentiation
cDNA	Complementary DNA
CHAPS	3-[(3-cholamidopropyl)dimethylammonio]-2-hydroxy-1-propanesulfonate
CV	Column volume
DAPI	4‘,6-Diamidin-2-phenylindol
DC	Dendritic cell
DMEM	Dulbecco’s modified eagle medium
DNA	Deoxyribonucleic acid
dNTP	Deoxynucleoside triphosphate
Dsb A / C	Disulfide bond A / C (protein name)
DTNB	5,5’-Dithiobis 2-nitrobenzoic acid
DTT	Dithiothreitol
E. coli	*Escherichia coli*
EDTA	Ethylenediaminetetraacetic acid
EGF	Epidermal growth factor
EGFP	Enhanced green fluorescent protein
ELISA	Enzyme-linked immunosorbent assay
ER	Endoplasmic reticulum
EV	Extracellular vesicle
FACS	Fluorescence activated cell sorting (used synonymous for flow cytometry)
FITC	Fluorescein isothiocyanate
GFP	Green fluorescent protein
GST	Glutathione S-tranferase
Gy	Gray (SI unit for ionizing radiation)
HBS	HEPES buffered saline
HEK	Human embryonal kidney (mammalian cell line)
HEPES	4-(2-hydroxyethyl)-1-piperazineethanesulfonic acid

Abbreviations

HRP	Horseradish peroxidase
IPTG	Isopropyl ß-D-1-thiogalactopyranoside
LB	Lysogeny broth (bacterial medium)
ld	live/dead (viability dye / staining)
MFG-E8	Milk fat globule-EGF factor 8
MFI	Mean fluorescence intensity
MHC	Major histocompatibility complex
MW	Molecular weight
NTA	Nitrilotriacetic acid
OD_{600}	Optical density at 600 nm
OSB	Optimized stabilizing buffer
PAGE	Polyacrylamide gel electrophoresis
PBS	Phosphate buffered saline
PCR	Polymerase chain reaction
PE	Phosphatidylethanolamine *or* Phycoerythrin
PI	Propidium iodide (viability dye / staining)
POI	Protein of interest
PS	Phosphatidylserine
RNA	Ribonucleic acid
SA	Streptavidin
SDS	Sodium dodecyl sulfate
SEC	Size exclusion chromatography
Senp2	Sentrin-specific protease 2
sfGFP	Superfolder green fluorescent protein
SLE	Systemic lupus erythematosus
SN	Supernatant
SS	Signal sequence
SUMO	Small ubiquitin-like modifier
TCR	T cell receptor
TEV protease	Tobacco etch virus protease
TUNEL	TdT-mediated dUTP nick end labeling assay
TrxA	Thioredoxin A
WT	Wild type

Table of Contents

1 Summary

Cell death is a process which is essential to sustain the life of all multicellular organisms. Detection of cell death is an important tool in diagnostics, e.g. to monitor the success of anti-cancer therapies or unravel diverse processes in basic research like immune cell development, developmental biology and tissue homeostasis. One central hallmark of dying cells is the exposure of the phospholipid phosphatidylserine (PS) on the outer leaflet of the cell membrane. This circumstance can be taken advantage of utilizing the PS-binding protein MFG-E8 with two homologous F5/8 type C domains as a marker for extracellular PS exposure. In this study, MFG-E8 was characterized with the aim to develop tools for imaging of cell death. Whereas the PS binding activity was already published for the C2 domain of MFG-E8, this feature has not been shown for its C1 domain so far. With single domain studies performed using overexpressed protein from HEK293T cells strong PS binding activity for the C1 domain of the human MFG-E8 homologue could be proven and approaches were started to further enhance its binding properties and produce the full-length molecule in a bacterial expression system.

In addition, single C domains of the murine homologue (mMFG-E8) were produced in bacteria and site-specifically modified with a biotin-containing peptide in a Sortase reaction after purification. These single domains formed the basis for multimerization with the homotetramer Streptavidin to form a cost-efficient and versatile platform for detection of PS exposure. C1 and C2 multimers showed increased avidity compared to the respective monomers. These multimers proved to be an effective and Ca^{2+}-independent alternative to Annexin V, an already established PS-binding molecule. Also, they could be used in the depletion of dead cells and debris from cell suspensions and reliably detected dead cells and cell-associated PS^{+} vesicles *in vivo*.

2 Zusammenfassung

Zelltod ist ein wichtiger Prozess um das Leben aller multizellulären Organismen zu erhalten. Die Detektion von Zelltod stellt ein wichtiges Werkzeug in der Diagnostik dar, zum Beispiel um den Erfolg von Krebstherapien zu überwachen. Zudem können verschiedene Prozesse in der Immunzellentwicklung, Entwicklungsbiologie und Zellhomöostase im Gewebe in der Grundlagenforschung aufgedeckt werden. Ein zentrales Merkmal sterbender Zellen ist die Exposition des Phospholipids Phosphatidylserin (PS) auf der Außenseite der Zelle. Dieser Umstand kann mit der Verwendung des PS-bindenden Proteins MFG-E8 mit zwei homologen C-Domänen vom Typ F5/8 als extrazellulärer Marker für PS Exposition genutzt werden.

In dieser Arbeit wurde MFG-E8 charakterisiert mit dem Ziel Hilfsmittel für den Nachweis von Zelltod zu entwickeln. Obwohl PS-Bindung bereits für die C2-Domäne von MFG-E8 publiziert wurde, konnte dies noch nicht für die C1-Domäne gezeigt werden. Unter Verwendung von überexprimiertem Protein aus HEK293T-Zellen konnte in Experimenten mit den Einzeldomänen eine starke PS-Bindung für die humane C1-Domäne nachgewiesen werden. Es wurden Versuche unternommen, die Bindeeigenschaften zu verbessern und das Volllänge-Molekül in einem bakteriellen Expressionssystem herzustellen.

Einzelne C-Domänen des murinen Homologes wurden ebenfalls in Bakterien produziert und nach der Reinigung in einer Sortase-Reaktion zielgerichtet mit einem Biotin-Peptid modifiziert. Diese Einzeldomänen bildeten die Grundlage für eine Multimerisierung mit dem Homotetramer Streptavidin um eine kosteneffiziente und vielfältige Plattform für die Detektion von PS-Exposition zu schaffen. C1- und C2-Multimere wiesen eine erhöhte Avidität im Vergleich mit den jeweiligen Monomeren auf. Diese Multimere konnten als effektive und Ca^{2+}-unabhängige Alternative zu Annexin V eingesetzt werden, einem bereits etablierten PS-bindenden Molekül. Außerdem entfernten sie erfolgreich tote Zellen und Zellbruchstücke aus Zellsuspensionen und detektierten zuverlässig tote Zellen und zell-assoziierte, PS^{+}-Vesikel *in vivo*.

3 Introduction

3.1 Cell death

The life of multicellular organisms is accompanied, shaped by and critically dependent on cell death. Every day, more than 10^9 cells die in the body (Elliott and Ravichandran, 2010). Targeted deletion of cells by apoptosis plays a role in processes like normal tissue homeostasis, the removal of old cells to provide space for new ones and developmental processes, for example in the embryonic formation of limbs. Furthermore, in immune cell development deletion of cells recognizing self-antigens, inflammation and immune responses like elimination of virus-infected cells by cytotoxic T cells, targeted cell removal is an essential process in multicellular organisms.
The pathways leading to cell death and their nomenclature are manifold (Galluzzi et al., 2018), but the outcome concerning cell morphology features and impact on the organism will be narrowed down to apoptosis and necrosis in this work.

3.1.1 Apoptosis is a regulated form of cell death

The term ‘Apoptosis’ was coined in 1972 by Kerr and colleagues and morphological features of apoptotic cells characterized (Kerr et al., 1972). Cells undergoing apoptosis show typical budding of the plasma membrane, so called ‘blebbing’ until they fragment into apoptotic bodies in the final stage. This is part of a tightly controlled and regulated molecular process, therefore apoptosis is also referred to as ‘programmed cell death’.

Initiation of the apoptotic pathway can occur via extrinsic (death factor pathway) or intrinsic stimuli for the respective cell (Fig. 1.1). During the extrinsic pathway, interaction of death factors with death receptors presented on the cell surface transmits the signal via adapter proteins like FADD (Fas-associated death domain) to the apoptotic machinery. It is employed by e.g. cytotoxic T cells and natural killer cells to remove virus-infected or cancer cells (Ashkenazi and Dixit, 1998).
The intrinsic pathway on the other hand is triggered by cellular stress like infliction of excessive DNA damage by chemicals and radiation. Also, the withdrawal of cytokines like Interleukin-2 (IL-2) leads to the death of T effector cells (Duke and Cohen, 1986). Initiation of the intrinsic pathway ultimately results in the release of Cytochrome c from mitochondria which induces oligomerization of apoptotic protease activating factor 1 (Apaf-1) (Shakeri et al., 2017).

3.1 Cell death

For both, the intrinsic and extrinsic pathway the signal from an initial stimulus is relayed and converges at proteolytic enzymes called Caspases (Cysteinyl-aspartic acid-proteases). Initiator Caspases like Caspase 8 and 9 start a cascade enhancing the signal and proteolytically activate e.g. Caspase 3 as effector Caspase (Riedl and Shi, 2004).

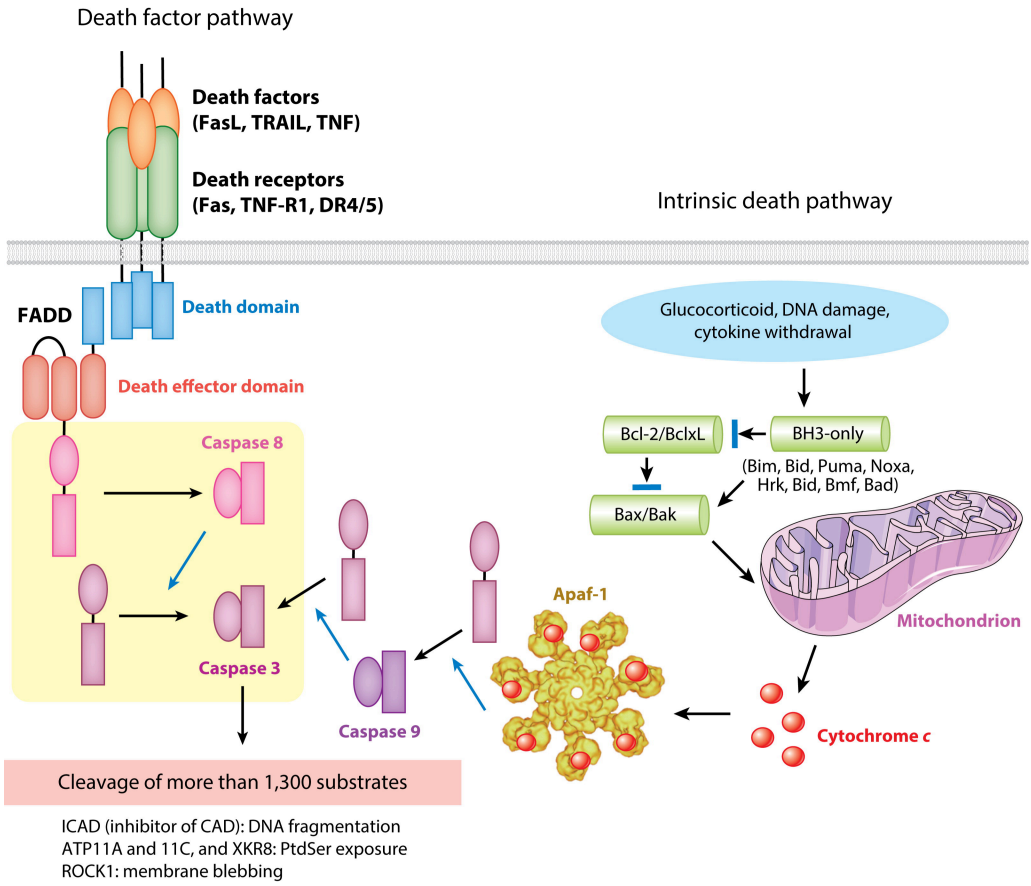

Fig.1.1: The process of extrinsic and intrinsic apoptosis induction is channeled at the level of Caspases. In the death factor or extrinsic pathway, a death factor interacts with death receptors exposed on the target cell surface. By an intracellular death domain and a FADD adapter protein the signal is relayed through the cytoplasm and activates e.g. the initiator Caspase-8. The intrinsic death pathway is triggered in reaction to cellular stress. Anti-apoptotic proteins like Bcl-2 or Bcl-xL are inhibited and the pro-apoptotic Bax/Bak pathway leads to release of Cytochrome c from mitochondria. Apaf-1 serves as an adapter protein, binding Cytochrome c and activating the initiator Caspase-9. Both Caspase-8 and -9 in turn cleave and activate e.g. effector Caspase-3 which culminates in the cleavage of a multitude of substrates such as ICAD, ATP11A/C, XKR8 and ROCK1 paving the way for apoptotic processes. Image from (Nagata, 2018)

Proteolytic processing of the respective effector Caspase substrates ultimately leads to the cells' demise by DNA fragmentation, formation of apoptotic bodies retaining the cytoplasmic compartment and presentation of ligands for phagocytic cell receptors on the cell surface.

In contrast, necrosis is distinguishable to the highly regulated apoptotic process by release of cytoplasmic components via a disrupted cell membrane, also leading to inflammatory processes. This energy-independent form of cell death is often induced by an excess of cytotoxic stimuli (Elmore, 2007).

3.1 Cell death

3.1.2 Exposure of phosphatidylserine serves as an ‘eat me’ signal

Once the cell death program has been initiated, steps are already taken for removal of the dying cell. This is especially important in light of the immune system’s discrimination between ‘self’ and ‘non-self’. Uncontrolled and extensive release of intracellular autoantigens, previously not encountered by the immune system, would lead to autoimmunity. To prevent this from happening, dying cells mark themselves by an elaborate mechanism for removal by phagocytes.

In healthy cells, an asymmetry of phospholipids is maintained between the outer and inner cell membrane leaflet. Phosphatidylserine (PS) and phosphatidylethanolamine (PE) make up 12 and 25 % of the total phospholipid pool, respectively (Leventis and Grinstein, 2010). Both are restricted to the cytoplasmic leaflet by the action of ATP-dependent aminophospholipid translocases, also called flippases. In human cells, ATP11C was found to be a representative of this protein family, being inactivated by Caspase cleavage upon induction of apoptosis (Segawa et al., 2014). Alongside with flippase inactivation, Caspases activate another protein class, called Scramblase like Xkr8 (Suzuki et al., 2013) (Fig. 1.2). Scramblases destroy phospholipid asymmetry by ATP-independent transbilayer transport of PS and PE. Exposure of PS on the outer membrane leaflet and therefore on the cell surface serves as an ‘eat me’ signal for phagocytes. Recognition by membrane-anchored or soluble PS receptors leads to binding and engulfment of apoptotic cells by phagocytes and their removal from the system (Segawa and Nagata, 2015).

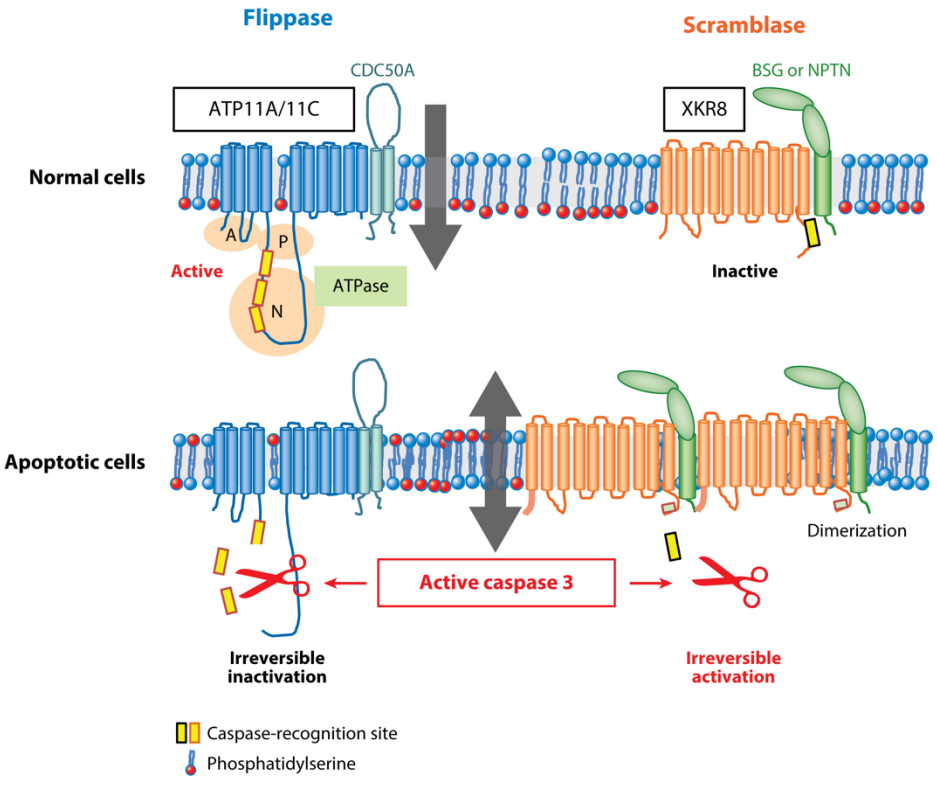

Fig. 1.2: Flippases and Scramblases are enzymes involved in transbilayer transport of phospholipids. In live cells, phospholipids like PS are restricted to the inner membrane leaflet in an ATP-dependent process by Flippases (upper panel). Upon induction of apoptosis and activation of e.g. the effector Caspase 3, Flippase is inactivated by proteolytic action of Caspase, Scramblase is activated, dimerizes and establishes an equilibrium of PS between the outer and inner membrane leaflet (lower panel). Image from (Nagata, 2018)

3.2 MFG-E8 is a bivalent protein with binding activity towards integrins and PS

Milk fat globule-EGF factor 8 (MFG-E8) or Lactadherin was first identified as a soluble glycoprotein associated with the milk fat globule membrane in mammary tissue with highly elevated mRNA levels in lactating mice (Stubbs et al., 1990). Subsequently, the respective homologues were characterized in other vertebrates like humans (Larocca et al., 1991), bovine (Aoki et al., 1995) and rat (Ogura et al., 1996). One hallmark of all MFG-E8 homologues is the occurrence of at least one epidermal growth factor (EGF)-like domain with similarity to the Notch-1 protein of *Drosophila.* Furthermore, domains featuring high sequence identity with the C domains of blood coagulation factor V and VIII were initially described in mouse MFG-E8 (mMFG-E8) (Stubbs et al., 1990).

MFG-E8 has been shown to act as a bridging protein utilizing both its EGF-like and C domains to link apoptotic cells to phagocytes (Hanayama et al., 2002), which will be described in detail below. The work presented in this thesis is based on the mouse and human homologue (hMFG-E8). Despite sharing basic functions as mentioned above they slightly differ in domain composition (Fig. 1.3).

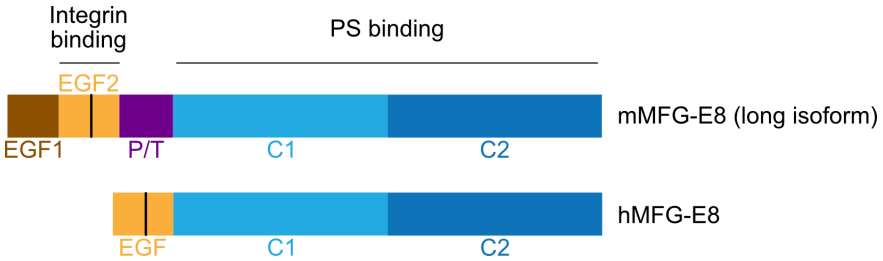

Fig. 1.3: mMFG-E8 and hMFG-E8 share a basic domain structure. hMFG-E8 features one N-terminal EGF-like domain and two C domains. The second EGF-like domain (EGF2) of mMFG-E8 is functionally related to the one of hMFG-E8, carrying the RGD motif (black line) for integrin binding. In addition, it carries another EGF-like domain at the N-terminus (EGF1). Both are separated by a proline/threonine-rich domain from the C domains which mediate association with PS.

3.2 MFG-E8 is a bivalent protein with binding activity towards integrins and PS

The smallest common denominator in all MFG-E8 homologues are the PS-binding C domains (see 3.2.2) and one EGF-like domain with an RGD cell attachment motif (see 3.2.1). One striking feature of mMFG-E8 is the proline/threonine (P/T)-rich sequence (Fig. 1.3) in the long isoform, representing a splice variant which is strongly upregulated in lactating mammary gland (Oshima et al., 1999). The P/T rich sequence has been found to increase binding of mMFG-E8 for PS-coated microtiter plates (Hanayama et al., 2002), which made the long isoform the mMFG-E8 variant of choice for this study. In direct comparison, mMFG-E8 also showed a higher affinity to PS than hMFG-E8 (Yamaguchi et al., 2008). For hMFG-E8, several isoforms exist as well but the work for this thesis focused on the most common isoform 1.

To exert its role as a bridging molecule enabling phagocytosis of apoptotic cells, MFG-E8 is produced and secreted not only by epithelial cells and macrophages in mammary glands (Hanayama and Nagata, 2005) but also thioglycolate-activated macrophages (Hanayama et al., 2002), immature dendritic cells (DCs) (Miyasaka et al., 2004) and follicular DCs (Kranich et al., 2008). The great importance of MFG-E8 for prevention of autoimmune diseases is exemplified by impaired removal of apoptotic cells and age-dependent appearance of autoantibodies in MFG-E8-deficient mice (Hanayama et al., 2004).
Furthermore, aberrant splicing (Yamaguchi et al., 2010), abnormal expression (Yamaguchi et al., 2008) and genetic polymorphism (Hu et al., 2009) of the MFG-E8 gene have been implicated in the development of the autoimmune disease systemic lupus erythematosus (SLE) in humans.

Besides its discovery of being associated with the milk fat globule membrane and its assigned role of linking phagocytes to apoptotic cells, MFG-E8 was also found associated with membrane vesicles secreted by cultured cells via its C domains (Oshima et al., 2002). It also represented a major component of DC-derived exosomes (Thery et al., 1999). Exosomes are vesicles of endosomal origin, between 50 - 100 nm small and result from the fusion of multivesicular endosomes with the plasma membrane. Alongside with microvesicles (200 nm – 1 µm) budding from the plasma membrane and a multitude of other vesicle types they are generally categorized as extracellular vesicles (EVs) (D'Souza-Schorey and Schorey, 2018). EVs are thought to confer long-range intercellular communication with their ability to transport cargo like proteins, lipids and nucleic acids between cells (van Niel et al., 2018). Due to their lack of ATP production, EVs expose phospholipids like PS and PE on their outer surface either via passive or active, scramblase-mediated transport (Record et al., 2018).

3.2 MFG-E8 is a bivalent protein with binding activity towards integrins and PS

3.2.1 The EGF-like domain features an RGD motif for cell attachment

The MFG-E8 homologues differ in their N-terminal domain structure with one EGF-like domain for hMFG-E8 (Couto et al., 1996) and two for mouse (Stubbs et al., 1990), rat (Ogura et al., 1996) or bovine MFG-E8 (bMFG-E8) (Aoki et al., 1995). Whereas the role for the first EGF-like domain remains elusive, the purpose of the second was determined to serve as a scaffold for presentation of an Arg-Gly-Asp (RGD) sequence (Taylor et al., 1997, Couto et al., 1996). This tripeptide represents a cell-adhesion motif recognizing integrins (Takagi, 2004, Takada et al., 2007).

For MFG-E8, binding to $\alpha_v\beta_5$ (Andersen et al., 1997) and a_vb_3 integrins (Taylor et al., 1997) has been demonstrated. An MFG-E8 variant with the RGD-integrin binding sequence mutated to RGE suppresses engulfment of apoptotic cells in cell culture by mouse fibroblasts engineered to express a_vb_3 integrins (Hanayama et al., 2006, Hanayama et al., 2002) and resulted in production of autoantibodies after intravenous injection into mice (Asano et al., 2004).

3.2.2 The F5/8 type C domains mediate high-affinity binding to PS

After sequence analysis of MFG-E8 cDNA from mouse mammary glands it was discovered that the C-terminal part of the protein shares 42% sequence identity with the C1 and C2 domain of coagulation factor V and VIII (Stubbs et al., 1990). The authors therefore proposed binding activity towards anionic phospholipids. In one study, bMFG-E8 bound to phosphatidylserine, phosphatidylethanolamine, phosphatidylinositol, phosphatidic acid, phosphatidylglycerol and cardiolipin in a solid phase ELISA (Andersen et al., 1997). However, in later reports PS was found to be the major phospholipid ligand (Castellanos et al., 2016) and even stereoselective interaction with phosphatidyl-L-serine was proven (Shi et al., 2004).

The structure of the bMFG-E8 C2 domain shows high similarity to the C2 domain of factor V and VIII with a discoidin-like fold, termed a F5/8 C domain with two sheets of five and three strands opposing each other (Lin et al., 2007). The borders of the C2 and C1 domain are defined by cysteine residues forming disulfide bridges (Shao et al., 2008, Hvarregaard et al., 1996). Binding of the C2 domain to PS and integration into the membrane environment is achieved by electrostatic interactions with positively charged aa residues playing a critical role as well as solvent-exposed hydrophobic residues at loops protruding from the structure (Ye et al., 2013, Shao et al., 2008, Lin et al., 2007). Among PS-binding proteins, MFG-E8 was found

to be an efficient, high-affinity competitor to Annexin V and factor V / VIII for binding sites in membranes (Shi and Gilbert, 2003), detecting as little as 0.03% PS in a sensitive assay (Otzen et al., 2012).
In the literature, PS binding activity of MFG-E8 has been mostly conferred to the C2 domain using stopped-flow kinetics (Otzen et al., 2012) or solid-phase ELISA (Andersen et al., 2000). A fusion of C2 with fluorescent proteins was also successfully applied as a biosensor to investigate intracellular PS distribution by fluorescence microscopy (Yeung et al., 2008) or additionally with electron microcopy (Fairn et al., 2011). On the other hand, C1 produced in COS-7 cells did not show binding in ELISA (Oshima et al., 2002). However, for detection of the MFG-E8 protein variants in ELISA polyclonal antibodies were used with no uniform antigenic target and therefore doubtful readout. The isolated MFG-E8 C1 domain has rarely been in focus for binding assays so far making it an interesting object of study to shed light on the MFG-E8 mode of PS binding.

3.3 Opportunities and challenges for detection of cell death

For detection of apoptosis and cell death *in vitro*, several methods have been developed. The TUNEL assay (TdT-mediated dUTP nick end labeling) takes advantage of the DNA fragmentation and extensive generation of double-strand DNA breaks during apoptosis (Gavrieli et al., 1992, Gorczyca et al., 1992). The huge increase of free 3'-hydroxy groups in fragmented DNA can be detected on single-cell level by direct or indirect labeling with fluorescent or biotin-conjugated dUTP analogs by the enzyme Terminal deoxynucleotidyl transferase (TdT). However, specificity of the TUNEL method is not given for apoptotic cells since during necrosis DNA breakdown may also occur (Bar, 1996).
Caspase-3, one of the central proteases in the apoptosis pathway can also be used for detection of apoptotic cells. A cleavage fragment of Caspase-3, rising after its activation can be specifically detected by antibody staining (Namura et al., 1998). Caspase-3 activation is an early marker of apoptosis in relation to the TUNEL assay (Glamoclija et al., 2005). Both can be applied in flow cytometry (Darzynkiewicz et al., 2008, Crowley and Waterhouse, 2016) but share the need for cell permeabilization prior to analysis in experiments *in vitro*, making their use inconvenient, time-consuming and restricted to specific assays.

Detection of PS exposed on the cell surface is an easy-to-perform alternative which was established with fluorescent Annexin V (Vermes et al., 1995). The method described by Vermes and colleagues also included propidium iodide (PI), a DNA dye. Since this dye only stains cells with compromised membrane integrity the procedure allowed for discrimination

between apoptotic cells with an intact cell membrane or necrotic cells with already permeabilized membrane. Annexin V is easy to produce (Brumatti et al., 2008, Logue et al., 2009) and its wide commercial availability made it a popular tool for cell death detection approaches. However, binding of the Annexin protein family is strictly dependent on the presence of Ca^{2+} ions (Raynal and Pollard, 1994), which restricts its usage to a respective Ca^{2+}-containing binding buffer. Concentrations of at least 3 mM are needed for efficient binding of Annexin V (Stuart et al., 1998) and with a Ca^{2+} concentration in blood serum ranging between 0.94 – 1.33 mM (Moore, 1970) Annexin V is not the optimal choice for *in vivo* approaches.

To overcome this limitation, an MFG-E8-based imaging system with its Ca^{2+}-independent binding mode could be used. In direct comparison, MFG-E8 proved to be a much more sensitive PS-binding probe than Annexin V (Dasgupta et al., 2006, Shi and Gilbert, 2003, Albanyan et al., 2009). Association of fluorescent MFG-E8 with synthetic membranes was detected at a PS content ≥ 0.5% and PS-dependent proportional increase in binding shown, whereas the range for Annexin V was 2.5 - 8%, depending on the membrane's PE content (Shi et al., 2006).

3.4 Application of PS-binding proteins for research and as diagnostic tools

Staining of cells *in vitro* after preparation of cell suspensions might give an obscured view on the actual number of dying cells in the tissue. During organ preparation, previously intact cells will become damaged or stressed and might spontaneously induce the apoptosis program. With staining of dying cells *in vivo* these problems are circumvented making a precise analysis of e.g. individual cell development and fate decisions possible. Besides applications in research, PS-binding proteins have gained attention in diagnostic approaches for non-invasive imaging of apoptosis during tumor therapy. Methods like Computed Tomography (CT) or Magnetic Resonance Imaging (MRI) are time-consuming since they mostly rely on detection of tumor shrinkage. Monitoring of cancer therapy progress and effectiveness of chemotherapeutics will take possibly weeks with the patient losing valuable time in case of unresponsiveness of the tumor (Wuest et al., 2019).

With PS exposure on the cell surface being an universal and early indicator of apoptosis (Martin et al., 1995), application of radionuclide-labeled Annexin V was tested for tumor therapy monitoring with positron emission tomography (PET) or single photon emission

computed tomography (SPECT) (Kuge et al., 2009). In another model, cell death during myocard infarct was visualized by biotin-labeled Annexin V in histology (Kietselaer et al., 2003). However, it was shown that Annexin V is internalized by apoptotic cells in a PS-dependent pathway (Kenis et al., 2004). This feature is not known to be shared by MFG-E8. In addition, it is a Ca^{2+}-independent and more sensitive probe with a binding affinity linear to the membrane PS content as described above, making it an interesting alternative to Annexin V. Side-by-side comparison of both PS-detecting probes modified with the chelator hydrazinonicotinamide (HYNIC) and radionuclide technetium-99m (^{99m}Tc) were undertaken in mice and pigs concerning their biodistribution (Falborg et al., 2010, Poulsen et al., 2013). It was found that Annexin V mostly accumulated in the kidneys whereas MFG-E8 preferentially localized to the liver. The authors argued this being possibly a result from Kupffer cells in the liver binding via $\alpha_v\beta_3$ integrins to the MFG-E8 RGD motif. A recombinant MFG-E8 variant featuring an inactive RGE motif or an EGF-like domain deletion could solve this problem in future approaches. ^{99m}Tc-MFG-E8 showed four times faster plasma clearance than ^{99m}Tc-Annexin V with a lower dosage estimated for humans of 5.8 versus 8.8 µSv/MBq for ^{99m}Tc-Annexin V (Poulsen et al., 2013). These studies proved MFG-E8-based *in vivo* imaging of cell death as a promising approach for tumor therapy monitoring.

3.5 Aim of this thesis

MFG-E8 is a promising molecule amongst PS-binding proteins due to its high-affinity and Ca^{2+}-independent binding. Possible applications range from a detection tool for cell death and vesicles in research with implications in various fields, optimization of analysis processes by removal of dead cells from cell suspensions and imaging strategies in human tumor therapy diagnostics. Research only focused on the full-length molecule or C2 domain but no studies were performed with the isolated C1 and C2 domain. Therefore, characterization of MFG-E8 was one aim of this work for better understanding of the molecule in order to generate variants with enhanced binding properties. So far, MFG-E8 was purified from HEK 293T cells as an EGFP fusion protein and successfully used as a cell death and vesicle detection tool in the laboratory. However, for flow cytometry approaches flexibility of the fluorophore is advantageous favoring a system with easily exchangeable fluorophores, a circumstance which was also addressed in this work. Finally, application of MFG-E8 *in vivo* requires substantial amounts of protein for reliable downstream analysis of stained cells. To aid this, a bacterial expression system for large-scale and cost-efficient production was developed.

4 Materials and methods

Notes

If not indicated otherwise, companies are situated in Germany.
Chemicals were purchased mostly from Carl Roth (Karlsruhe), Thermo Scientific (Waltham, Massachusetts, USA), Sigma-Aldrich (St. Louis, Missouri, USA).
Buffers and solutions were prepared with double distilled H_2O.

Software and statistics

DNA construct design and determination of oligonucleotide T_m was performed with ApE (A plasmid editor, freeware by M. Wayne Davis).
Analysis of flow cytometry data performed with FlowJo v10 (Becton Dickinson; Franklin Lakes, New Jersey, USA). For imaging flow cytometry, compensation was performed by Jan Kranich with IDEAS Version 6.2 (Luminex; Austin, Texas, USA).
Statistical analysis was performed and graphs created with GraphPad Prism 7 (GraphPad Software, Inc.; San Diego, California, USA).
All error bars represent the mean with standard deviation (SD). Significance was analyzed with a student's t-test with
*: p = 0.01 - 0.05; **: p = 0.001 - 0.01; ***: p = 0.0001 - 0.001; ****: p < 0.0001
This thesis was written on a MacBook Pro (2.5 GHz Intel Core i5, 16 GB 1600 MHz DDR3, Intel HD Graphics 4000 1536 MB) using the Microsoft Office 2016 package.

4.1 Buffers and media

PBS	137 mM NaCl
	2.7 mM KCl
	10 mM Na_2HPO_4
	2 mM KH_2PO_4
	pH 7.4

4.1 Buffers and media

OSB	25 mM HEPES
	500 mM NaCl
	8 % glycerol
	18 mM L-arginine
	3.5 mM L-leucine
	5.7 mM L-glutamic acid
	pH 7.4 if not indicated otherwise

OSB is based on (Kooijmans et al., 2018) and was prepared without BSA

FACS buffer	PBS
	2 % (v/v) FCS (Pan Biotech; Aidenbach, Germany)
ACK	8.29 g NH_4Cl
	1 g $KHCO_3$
	37.2 mg Na_2EDTA
	H_2O ad 1 l
	pH 7.4
TAE buffer (50x)	242 g Tris
	57.1 ml 100% (v/v) acetic acid
	100 ml 0.5 M EDTA (pH 8.0)
	H_2O ad 1 l
SDS loading buffer (5x)	250 mM Tris-HCl, pH 6.8
	500 mM DTT (omitted from non-reducing buffer)
	10 % SDS
	0.5 % bromophenolblue
	50 % glycerol
SDS PAGE running buffer (5x)	75 g Tris
	360 g glycine
	25 g SDS
	H_2O ad 5 l

Coomassie G-250 “Blue Silver”	0.12 % Coomassie G-250 (AppliChem; Darmstadt)
	10 % ammonium sulfate
	10 % phosphoric acid
	20% methanol

The preparation of the Coomassie G-250 “Blue Silver” formulation is based on (Candiano et al., 2004).

Western blot transfer buffer	25 mM Tris
	192 mM glycine
	0.002% SDS
	20% MeOH

LB medium	25 g complete powder (Carl Roth)
	H_2O ad 1 l

4.2 Molecular biology

4.2.1 Polymerase chain reaction (PCR)

For cloning:

PCRs for cloning were performed with Platinum Pfx DNA polymerase with 3’ to 5’ proofreading exonuclease activity (Thermo Scientific) according to the manufacturer’s instructions (1x amplification buffer, 1 mM $MgSO_4$, 0.3 µM primer, 1 U polymerase) in 100 µl volume. 10 ng plasmid DNA was used as template and a dNTP mix from Genaxxon (Ulm, Germany) with 0.3 mM each.

Primers for restriction enzyme-mediated cloning were extended at the 5’ end by the recognition sequences for the respective restriction enzymes and a minimum of six additional nucleotides. Primers for generation of products for Gibson Assembly were extended by at least 20 nucleotides with overlap to the neighboring fragment. The overlap was calculated to have a T_m of at least 50°C.

4.2 Molecular Biology

PCR programs depending on initial T_m of primer pairs:

A) T_m < 68°C
1) 94°C 5 min
2) 94°C 15 sec
3) <68°C 30 sec
4) 68°C 1 min / kb
5) 4°C hold

Cycle 32x through 2-4

B) T_m > 68°C
1) 94°C 5 min
2) 94°C 15 sec
3) 68°C 1 min / kb
4) 4°C hold

Cycle 32x through 2-3

C) T_m < 68°C, then > 68°C
1) 94°C 5 min
2) 94°C 15 sec
3) <68°C 30 sec
4) 68°C 1 min / kb
5) 94°C 15 sec
6) 68°C 1 min / kb
7) 4°C hold

Cycle 7x through 2-4
and 25x through 5-6

A) was mostly applied for restriction enzyme-mediated cloning and B) as well as C) for Gibson Assembly, owed to the longer non-complementary primer regions.

For colony PCR:
Successful ligation of inserts in linearized vectors as well as their orientation was tested by colony PCR using MyTaq DNA polymerase and MyTaq reaction buffer red (Bioline; London, UK) according to manufacturer's instructions in a reaction volume of 15 µl. Primer pairs were chosen to bind in the insert and vector backbone, respectively.
A small sample of the bacterial colonies each was transferred from the selective plate to PCR tube and pre-mixed PCR master mix added.

<u>PCR program:</u>

1) 95°C 1 min
2) 95°C 15 sec
3) x°C 15 sec (depending on T_m of primer pair)
4) 72°C 10-20 sec (depending on product length)
5) 4°C hold

Cycle 25x through 2-4

All PCR reaction were performed in a Biometra T3 thermocycler.
PCR success was evaluated by loading of samples on a 1% agarose gel with ethidium bromide, analysis and documentation with a Gel Doc XR+ Molecular Imager (BioRad; Hercules, California, USA).

4.2 Molecular Biology

For cloning, PCR products were purified using the GeneJET PCR purification kit (Thermo Scientific) and concentration determined with SimpliNano (GE Healthcare; Chicago, Illinois, USA).

4.2.2 Restriction hydrolysis

Vector and insert (either PCR product or plasmid for subcloning) were incubated in a restriction hydrolysis mix based on restriction enzymes and respective buffers from NEB (New England Biolabs; Ipswich, Massachusetts, USA). Restriction hydrolysis was performed according to manufacturer's instructions for at least 8 h.
A maximum of 20 µg vector DNA was contained in a restriction hydrolysis mix of 80 µl. Success of the reaction was verified by agarose gel electrophoresis.
For subcloning, the insert was separated from the vector backbone by agarose gel electrophoresis using a 1% agarose gel supplemented with ethidium bromide. Documentation and excision of the desired DNA fragments with a scalpel was performed on the UV table of a Gel Doc XR+ Molecular Imager (BioRad; Hercules, California, USA). Purification of the DNA from the agarose gel done using GeneJET Gel Extraction Kit (Thermo Scientific).

4.2.3 Molecular cloning

Cloning was performed by two approaches:
Classical restriction enzyme-mediated cloning and Gibson Assembly.
All DNA concentration measurements were performed with SimpliNano (GE Healthcare; Chicago, Illinois, USA).

Restriction enzyme-mediated:
50 ng linearized vector backbone was combined with 150 ng insert, 400 U T4 DNA ligase (NEB; Ipswich, Massachusetts, USA), 1x T4 ligase buffer and autoclaved ddH_2O in 10 µl total volume. Reaction for at least 1 h at room temperature.

Gibson Assembly:
Buffers, components and parameters of the reaction were used as previously published for one-step iso assembly of overlapping dsDNA (Gibson, 2011).
Enzymes used: T5 Exonuclease, Phusion HF DNA polymerase and Taq DNA ligase (all NEB; Ipswich, Massachusetts, USA).
For the reaction, 0.02 pmol linearized vector backbone (by restriction hydrolysis) and 0.2 pmol of the respective inserts were filled up with autoclaved ddH_2O to 2.5 µl and 7.5 µl Gibson

Assembly master mix added. For volumes exceeding 2.5 µl, the reaction was scaled up accordingly. Reaction for 1 h at 50°C in Biometra T3 thermocycler, cooled down to 4°C.

After reaction, the ligation mixes were either transformed directly or stored at -20°C.

4.2.4 Oligonucleotides, sequences and vectors

All oligonucleotides were purchased from Eurofins (Luxembourg) and Integrated DNA Technologies (IDT) (Coralville, Iowa, USA).
Verification of DNA sequences by sequencing with respective primers was also done using the services from Eurofins.
Sequences for full length hMFG-E8-EGFP, mMFG-E8-EGFP and hC2_isoform3 were synthesized by Eurofins, codon-optimized for mammalian expression.
Sequence for Sortase A was synthesized by Eurofins, codon-optimized for bacterial expression.
The Flag tag was the common tag for proteins produced in mammalian cells with the peptide sequence DYKDDDDK

Vectors and origin:

Name	Source	Description
pD2523 pD2527 pD2528	purchased from DNA2.0 / ATUM	
pET15b	EMD Millipore, gift by Felix Müller-Planitz	
pET26b	EMD Millipore, gift by Dejana Mokranjac	
pET28PP	EMD Millipore, gift by Karl-Peter Hopfner	pET28a, modified with sequence for HRV-3C protease cleavage site after N-terminal His_6 tag
pET28a	EMD Millipore, gift by Dejana Mokranjac	
pET28a-His_6-TEV	gift from Andreas Ladurner	expression plasmid for His_6-TEV

4.2 Molecular Biology

pGEX-4T-1	GE Healthcare, gift by Dejana Mokranjac	source for GST sequence
pETM11 -SenP2	EMBL	source for SenP2 sequence
pETM11-SUMO3-GFP	EMBL	source for SUMO3 sequence
pFMP241	gift by Felix Müller-Planitz	source for sfGFP
pFMP311	gift by Felix Müller-Planitz	source for TrxA
pFMP314	gift by Felix Müller-Planitz	source for DsbA

Cloned constructs:
Note: For each construct, the unique identifier pTK# and the construct structure is given (vector backbone + insert). Domain deletions are marked with a “d”, for example a construct lacking the C1 domain will be “dC1”.
Template and primers for PCR as well as a short description of the cloning procedure is given, if necessary.

pTK2 - pD2523-hMFG-E8-EGFP-Flag
Template: hMFG-E8 sequence (Eurofins)
Cut from sequence delivered by Eurofins with EcoRI and inserted in linearized pD2523

pTK14 - pD2523-hER_SS-hMFG-E8_dEGF_dC1-C2-EGFP-Flag
Template: hMFG-E8_dEGF_dC1-C2-EGFP sequence (Eurofins)
Cut from sequence delivered by Eurofins with EcoRI and inserted in linearized pD2523

pTK30 - pETM11-SUMO3-hMFG-E8_dEGF_dC1-C2
Template: hMFG-E8 sequence (Eurofins)
Primers fw: CAACAGACCGGTGGAAATGGTTGCGCCAACCC
rv: GGCCGCAAGCTTTTAACAGCCAAGCAGCTCCAGC
PCR product cut with with Age I / Hind III (restriction sites underlined) and ligated in appropriately linearized pETM11-SUMO3 vector

4.2 Molecular Biology

pTK32 - pET28PP-SortaseA_aa26-206
Template: Sortase A sequence (Eurofins)
Primers fw: GCAACTACCATATGAAACCGCATATTGACAACTACC
rv: CGTTAACTAAGCTTTTACTTCACCTCGGTTGCA
PCR product cut with NdeI / HindIII (restriction sites underlined) and ligated in appropriately linearized pET28PP vector

pTK33 - pD2523-hMFG-E8_C1-15aaIgG3-C2-EGFP-Flag
Template: pTK2 (IgG3 linker aa sequence: LKTPLGDTTHT)
Primers fw1: CCACACCCAAGCTGTCTAGAGAATTCTTTTCCCGCGTCCC
rv1: GTTGTGTCTCCCAGAGGTGTCTTGAGGCATCCCAGCAGCTCAAAC
fw2: CACCTCTGGGAGACACAACTCACACCGAACTCAATGGTTGCGCCAAC
rv2: TCCCTATACATGGTGGCGGCTCTAGAttaCTTATCGTCGTCGTCCTTG
PCRs with primer pair 1 and 2 on pTK2, Gibson Assembly in pD2523 cut with XbaI

pTK53 - pD2523-mER_SS-hMFG-E8_dEGF_dC1-C2-EGFP-Flag
Template: pTK2 and pD2523-mMFG-E8-EGFP-Flag
Primers fw1: CCACACCCAAGCTGTCTAGAGAATTCTTTTCCCGCGTCCC
rv1: CGCAGCGGCTGGCAAACAAGCCGGAAGC
fw2: CCAGCCGCTGCGCCAACCCTCTGGG
rv2: TCCCTATACATGGTGGCGGCTCTAGAttaCTTATCGTCGTCGTCCTTG
PCRs with primer pair 1 on pD2523-mMFG-E8-EGFP and with pair 2 on pTK2.
Gibson Assembly in pD2523 cut with XbaI

pTK55 - pD2523-mER_SS-hMFG-E8_dEGF-C1_dC2-EGFP-Flag
Template: pTK2 and pD2523-mMFG-E8-EGFP-Flag
Primers fw1: CCACACCCAAGCTGTCTAGAGAATTCTTTTCCCGCGTCCC
rv1: GACGCAGCGGCTGGCAAACAAGCCGGAAGC
fw2: GTTTGCCAGCCGCTGCGTCGAGCCTCTGGGTA
rv2: CTCCACCGCCGCATCCCAGCAGCTCAAACC
fw3: GCTGGGATGCGGCGGTGGAGGGTCTGGCG
rv3: TCCCTATACATGGTGGCGGCTCTAGAttaCTTATCGTCGTCGTCCTTG
PCRs with primer pair 1 on pD2523-mMFG-E8-EGFP, pair 2 on pTK2 and pair 3 on pTK2.
Gibson Assembly in pD2523 cut with XbaI

4.2 Molecular Biology

pTK64 - pD2523-hMFG-E8_C1-15aaGSlinker-C2-EGFP-Flag

Template: pTK2

Primers fw1: CCACACCCAAGCTGTCTAGAGAATTCTTTTCCCGCGTCCC

rv1: AGACCCGGAGCCGCTTCCACTACCTGACCCGCATCCCAGCAGCTCAAAC

fw2: AAGCGGCTCCGGGTCTGGTAGCGGCTCTGGATGCGCCAACCCTCTGGG

rv2: TCCCTATACATGGTGGCGGCTCTAGAttaCTTATCGTCGTCGTCCTTG

PCRs with primer pair 1 and 2 on pTK2

Gibson Assembly in pD2523 cut with XbaI

pTK65 - pD2523-hMFG-E8_C1-15aaGPlinker-C2-EGFP-Flag

Template: pTK2

Primers fw1: CCACACCCAAGCTGTCTAGAGAATTCTTTTCCCGCGTCCC

rv1: TGGGCCGGGACCGGGTCCTGGCCCAGGACCGCATCCCAGCAGCTCAAAC

fw2: CCCGGTCCCGGCCCAGGACCTGGTCCAGGATGCGCCAACCCTCTGGG

rv2: TCCCTATACATGGTGGCGGCTCTAGATTACTTATCGTCGTCGTCCTTG

PCRs with primer pair 1 and 2 on pTK2

Gibson Assembly in pD2523 cut with XbaI

pTK66 - pD2523-hMFG-E8_C1-15aaAPlinker-C2-EGFP-Flag

Template: pTK2

Primers fw1: CCACACCCAAGCTGTCTAGAGAATTCTTTTCCCGCGTCCC

rv1:TGGAGCAGGTGCGGGAGCTGGTGCAGGAGCGCATCCCAGCAGCTCAAAC

fw2: CCCGCACCTGCTCCAGCACCTGCTCCAGCATGCGCCAACCCTCTGGG

rv2: TCCCTATACATGGTGGCGGCTCTAGATTACTTATCGTCGTCGTCCTTG

PCRs with primer pair 1 and 2 on pTK2

Gibson Assembly in pD2523 cut with XbaI

pTK70 - pET26b-mMFG-E8_dEGF1_dEGF2_dPT_dC1-C2-His6

Template: mMFG-E8-EGFP-Flag

Primers fw: TGTTTAACTTTAAGAAGGAGATATA<u>CATATG</u>AAGTCTGGGTGTAGTGAGC CTCTCGGGCTC

rv: CTCAGTGGTGGTGGTGGTGGTG<u>CTCGAG</u>ACACCCCAGGAGCTCCAGC

PCR product cut with NdeI / XhoI (restriction sites underlined) and ligated in appropriately linearized vector

4.2 Molecular Biology

pTK71 - pET26b-hMFG-E8_dEGF_dC1-C2-His6
Template: pTK2
Primers fw: TTGTTTAACTTTAAGAAGGAGATATACATATGAAGTCTGGGTGCGCCAA
CCCTCTGGGG
rv: TCTCAGTGGTGGTGGTGGTGGTGCTCGAGACAGCCAAGCAGCTCGAGCC
PCR product cut with NdeI / XhoI (restriction sites underlined) and ligated in appropriately linearized vector

pTK76 - pET26b-mMFG-E8_dEGF1_dEGF2_dPT-C1C2-LPETG-His6
Template: pD2523-mMFG-E8-EGFP-Flag
Primers fw: GTTTAACTTTAAGAAGGAGATATACATATGAAGTCTGGGTGCAGTACAC
AGCTGGGAATGG
rv: AGTGGTGGTGGTGGTGGTGCTCGAGGCTCCCTCCAGTTTCGGGCAGA
CTTCCACACCCCAGGAGCTCCAGC
PCR product cut with NdeI / XhoI (restriction sites underlined) and ligated in appropriately linearized vector

pTK77 - pET26b-GST-Senp2
Template: pGEX-4T-1 and pETM11-Senp2
Primers fw1: TTCCCCTCTAGAAATAATTTTGTTTAACTTTAAGAAGGAGATATACATATGT
CCCCTATACTAGGTTATTGGAAAATTAAGGGCC
rv1: CGTAATCGCTCATGCTGCCTTTTGGAGGATGGTCGCCACCAC
fw2: CCATCCTCCAAAAGGCAGCATGAGCGATTACGACATCCCC
rv2: GTGGTGGTGGTGGTGGTGCTCGAGTCACAGCAGTTGTTGATGCAGG
PCRs with primer pair 1 on pGEX-4T-1 and pair 2 on pETM11-Senp2
Gibson Assembly in pET26b cut with NdeI / XhoI

pTK78 - pET26b-GST-SUMO3-mMFG-E8_dEGF1_dEGF2_dPT_dC1-C2-LPETG-His6
Note: This construct was not used for expression in this work but for subcloning of the insert in pTK82
Template: pGEX-4T-1, pETM11-SUMO3-GFP, pD2523-mMFG-E8-EGFP-Flag
Primers fw1: TTCCCCTCTAGAAATAATTTTGTTTAACTTTAAGAAGGAGATATACATATGT
CCCCTATACTAGGTTATTGGAAAATTAAGGGCC
rv1: CATACCAGAGCTGCCTTTTGGAGGATGGTCGCCACCAC
fw2: GACCATCCTCCAAAAGGCAGCTCTGGTATGGGCAACGATCACATTAACC
rv2: GCCCGAGAGGCTCACTACAGGATCCACCGGTCTGTTGC
fw3: CCAGCAACAGACCGGTGGATCCTGTAGTGAGCCTCTCGGGCTC

rv3: AGTGGTGGTGGTGGTGGTGCTCGAGGCTCCCTCCAGTTTCGGGCAGACT
TCCACACCCCAGGAGCTCCAGC

PCRs with primer pair 1 on pGEX-4T-1, pair 2 on pETM11-SUMO3-GFP and pair 3 on pD2523-mMFG-E8-EGFP-Flag.

Gibson Assembly in pET26b cut with NdeI / XhoI

pTK79 - pD2523-hMFG-E8_C1-4aaGSlinker-C2-EGFP-Flag

Template: pTK2

Primers fw1: CTCTGGGGAGAGACCACACCCAAGCTGTCTAGAGAATTCTTTTCCCGCG
TCCC

rv1: GGCGCAGCTGCCGGACCCGCATCCCAGCAGCTCAAAC

fw2: GGGATGCGGGTCCGGCAGCTGCGCCAACCCTCTGGGG

rv2: GCTCAAGCTTCCCTATACATGGTGGCGGCTCTAGATTACTTATCGTCG
TCGTCCTTGTAATC

PCRs with primer pair 1 and pair 2 on pTK2, Gibson Assembly in pD2523 cut with XbaI

pTK80 - pD2523-hMFG-E8_C1-7aaGSlinker-C2-EGFP-Flag

Template: pTK2

Primers fw1: CTCTGGGGAGAGACCACACCCAAGCTGTCTAGAGAATTCTTTTCCC
GCGTCCC

rv1: GCAGCCGCTTCCTCTACCGGACCCGCATCCCAGCAGCTCAAAC

fw1: TGCGGGTCCGGTAGAGGAAGCGGCTGCGCCAACCCTCTGGGG

rv1: GCTCAAGCTTCCCTATACATGGTGGCGGCTCTAGATTACTTATCGTC
GTCGTCCTTGTAATC

PCRs with primer pair 1 and pair 2 on pTK2, Gibson Assembly in pD2523 cut with XbaI

pTK81 - pD2523-hMFG-E8_C1-29aaGSlinker-C2-EGFP-Flag

Template: pTK64

Primers fw1: CTCTGGGGAGAGACCACACCCAAGCTGTCTAGAGAATTCTTTTCCCG
CGTCCC

rv1: GAACCTGATCCGGACCCAGAGCCACTACCTGATCCGGAGCCGCTTC
CACTACC

fw2: GTAGTGGCTCTGGGTCCGGATCAGGTTCCGGCTCTGGGTCTGGTAG
CGGCTCTG

rv2: GCTCAAGCTTCCCTATACATGGTGGCGGCTCTAGATTACTTATCGTCG
TCGTCCTTGTAATC

PCRs with primer pair 1 and pair 2 on pTK64, Gibson Assembly in pD2523 cut with XbaI

pTK82 - pGEX-4T1-SUMO3-mMFG-E8_dEGF1_dEGF2_dPT_dC1-C2-LPETG-His6
Template: pTK78
Primers fw: CGGATCTGGTTCCGCGTGGATCCCCGGAATTCATGGGCAACGATCA
CATTAACCTG
rv: GATGCGGCCGCTCGAGTCGACCCGGGAATTCTCAGTGGTGGTGGTG
GTGG
PCR with primer pair on pTK78, Gibson Assembly in pGEX-4T-1 cut with EcoRI

pTK83 - pET26b-mMFG-E8_dEGF1_dEGF2_dPT-C1_dC2-His6
Template: pD2523-mMFG-E8-EGFP-Flag
Primers fw: TTGTTTAACTTTAAGAAGGAGATATACATATGAAGTCTGGGTGCAGTA
CACAGCTGGGAATG
rv: CAGTGGTGGTGGTGGTGGTGCTCGAGACACCCCAGAAGCTCGAAACG
PCR with primer pair on pD2523-mMFG-E8-EGFP-Flag
Gibson Assembly in pET26b cut with NdeI / XhoI

pTK85 - pGEX-4T1-SUMO3-mMFG-E8_dEGF1_dEGF2_dPT_C1-dC2-LPETG-His6
Template: pETM11-SUMO3-GFP, pD2523-mMFG-E8-EGFP-Flag
Primers fw1: CGGATCTGGTTCCGCGTGGATCCCCGGAATTCATGGGCAACGATCAC
ATTAACCTG
rv1: AGCTGTGTACTGCAGGATCCACCGGTCTGTTGC
fw2: GCATTAGCATAGACCATTAGTAGCAATTGACGGCCGGATGCAGTACA
CAGCTGGGAATG
rv2: TGGTGGTGGTGCTCGAGGCTCCCTCCAGTTTCGGGCAGACTTCCACA
CCCCAGAAGCTCGAAACG
fw3: ACAGACCGGTGGATCCTGCAGTACACAGCTGGGAATGGAG
rv3: GATGCGGCCGCTCGAGTCGACCCGGGAATTCTCAGTGGTGGTGGTGG
TGGTGCTCGAGGC
PCRs with primer pair 1 on pETM11-SUMO3, primer pair 2 on pD2523-mMFG-E8-EGFP-Flag and primer pair 3 on the product from pair 2.
Gibson Assembly of PCR product 1 and 3 in pGEX-4T-1 cut with EcoRI

pTK93 - pD2523-hMFG-E8_C1-43aaGSlinker-C2-EGFP-Flag
Template: pTK81
Primers fw1: CTCTGGGGAGAGACCACACCCAAGCTGTCTAGAGAATTCTTTTCCC
GCGTCCC
rv1: CAGAGCCGCTACCGGATCCGGACCCGCTACCAGACCCAGAGCCAC

TACCTGATC
fw2: CGGGTCCGGATCCGGTAGCGGCTCTGGAAGTGGCTCCGGATCAG
GTTCCGGC
rv2: GCTCAAGCTTCCCTATACATGGTGGCGGCTCTAGATTACTTATCGTC
GTCGTCCTTGTAATC
PCRs with primer pair 1 and 2 on pTK81, Gibson Assembly in pD2523 cut with XbaI

pTK94 - pD2523-hMFG-E8_C1-59aaGSlinker-C2-EGFP-Flag
Template: pTK93
Primers fw1: CTCTGGGGAGAGACCACACCCAAGCTGTCTAGAGAATTCTTTTCCC
GCGTCCC
rv1: CACTTCCGGAACCTGACCCTGATCCGGAGCCGCTACCGGATCCGG
ACCCGCTAC
fw2: CGGATCAGGGTCAGGTTCCGGAAGTGGCTCTGGATCTGGTAGCGG
CTCTGGAAGTGG
rv2: GCTCAAGCTTCCCTATACATGGTGGCGGCTCTAGATTACTTATCGTC
GTCGTCCTTGTAATC

pTK95 - pET15b-His6-SUMO3
Template: pETM11-SUMO3-GFP
Primers fw: GAGATATACCATGGGCAGCAGCCATCATCATCATCATCACAGC
AGCGGCATGGGCAACGATCACATTAACCTG
rv: CAGCTTCCTTTCGGGCTTTGTTAGCAGCCGGATCCACCGGTCTGTTGC
PCR with primer pair on pETM11-SUMO3-GFP, Gibson Assembly of PCR product in pET15b cut with NcoI / BamHI

pTK106 - pET15b-His6-SUMO3-sfGFP-hMFG-E8_dEGF-C1-15aaIgG3linker-C2
Note: This construct was not used for expression in this work but for subcloning of the insert in pTK116 and pTK165
Template: pTK33
Primers fw: TGGCGGAGGCGGAAGTGGCGGCGGCTCGAGTGAGACTAAATGCGT
CGAGCCTC
rv: TTGTTAGCAGCCGGATCCACCGGTCTCGAGTTAACAGCCAAGCAGC
TCCAG
PCRs with primer pair on pTK33, Gibson Assembly of PCR product in pET15b-His6-SUMO3-sfGFP cut with XhoI

4.2 Molecular Biology

pTK108 - pET15b-His6-SUMO3-EGFP
Template: mMFG-E8-EGFP
Primers fw: ACACCATTGACGTGTTCCAGCAACAGACCGGTGGAATGGTGTCTA
AAGGAGAGGAACTC
rv: CGGGCTTTGTTAGCAGCCGGATCCACCGGTTTACTTATAAAGTTCA
TCCATGCCAAGAG
PCR with primer pair on mMFG-E8-EGFP, Gibson Assembly of PCR product in pTK95 cut with AgeI

pTK116 - pET15b-Flag-TEVcs-sfGFP-hMFG-E8_dEGF_C1-15aaIgG3linker-C2-TEVcs-His6
Note: “TEVcs“ stands for TEV cleavage site with the aa sequence ENLYFQG
Template: pTK106
Primers fw1: GGCAGCGACTATAAAGATGACGATGACAAAGAAAATCTGTACTTTCAG
GGTATGCGTAAAGGAGAAGAACTTTTCAC
rv1: ATGGTGATGGCTGCTGCCCTGAAAATAAAGATTCTCCTCGAGACAGCC
AAGCAGCTCCAG
fw2: ATTTTGTTTAACTTTAAGAAGGAGATATACCATGGGCAGCGACTATAAA
GATGACGATGA
rv2: TCCTTTCGGGCTTTGTTAGCAGCCGGATCCTTAGTGATGATGATGGTGA
TGGCTGCTGCC
PCRs with primer pair 1 on pTK106 and with primer pair 2 on PCR product from pair 1.
Gibson Assembly of PCR product 2 in pET15b cut with NcoI / BamHI

pTK131 - pD2523-mMFG-E8_C1-15aaIgG3-C2-EGFP-Flag
Template: pD2523-mMFG-E8-EGFP-Flag
Primers fw1: TGGGGAGAGACCACACCCAAGCTGTCTAGAGGTACCGAATTCTTTTCC
CGCGTCCCG
rv1: TGAGTTGTGTCTCCCAGAGGTGTCTTGAGACACCCCAGAAGCTCGAAACG
fw2: AGACACCTCTGGGAGACACAACTCACACCGAACTCCATGGCTGTAGT
GAGCCTCTCGGGC
rv2: GCTCAAGCTTCCCTATACATGGTGGCGGCTCTAGATTACTTATCGTCGTC
GTCCTTGTAATC
PCRs with primer pair 1 and 2 on pD2523-mMFG-E8-EGFP-Flag
Gibson Assembly of products in pD2523 cut with XbaI

pTK132 - pGEX-4T1-SUMO3-mMFG-E8_dEGF1_dEGF2_dPT-C1_dC2-10aaGS-LPETG-TEV-His6

Note: This construct was not used for expression in this work but served as backbone for pTK133

Template: pET15b-GST-SUMO3-mMFG-E8_dEGF1_dEGF_dPT-C1_dC2-10aaGS-LPETG-TEV-His10-13aa-His6 (pTK126)

Primers fw: CGGATCTGGTTCCGCGTGGATCCCCGGAATTCATGGGCAACGATCACA TTAACCTG

rv: ATGCGGCCGCTCGAGTCGACCCGGGAATTCTTAGTGATGATGATGGTG ATGGCTGC

PCR with primer pair on pTK126, Gibson Assembly of product in pGEX-4T-1 cut with EcoRI

pTK133 - pGEX-4T-1-SUMO3-hMFG-E8_dEGF_dC1-C2_iso3-10aaGS-LPETG-TEVcs-His6

Note: “TEVcs“ stands for TEV cleavage site with the aa sequence ENLYFQG

Template: hC2_iso3 synthesized by Eurofins

Primers fw: GTTCCAGCAACAGACCGGTGGATCCTGCGCCAACCCTCTGGGG

rv: CGCCGCCACCGCTCCCGCCACCGGTACAGCCAAGCAGCTCGAGCC

PCR on hC2_iso3, Gibson Assembly of product in pTK132 cut with AgeI

pTK135 - pET15b-hMFG-E8_dEGF_dC1-C2_isoform3-LPETG-His6

Note: This construct was not used for expression in this work but served as backbone for pTK136, pTK137 and pTK138

Template: hC2_iso3 synthesized by Eurofins

Primers fw1: TGGAGCGACCAGCAGGTACCGAGAATCTTTATTTTCAGGGCTGCGCC AACCCTCTGGGGC

rv1: TGGTGGTGGTGGCTCCCTCCAGTTTCGGGCAGACCGGTACAGCCAAG CAGCTCGAGCCTC

fw2: TTTGTTTAACTTTAAGAAGGAGATATACCATGGAACTGGAGCGACCAGC AGGTACC

rv2: TCCTTTCGGGCTTTGTTAGCAGCCGGATCCTTAGTGGTGGTGGTGGTG GTGGCTCCCTC

PCR with primer pair 1 on hC2_iso3 and with primer pair 2 on product from pair 1

Gibson Assembly of product from pair 2 in pET15b cut with NcoI / BamHI

pTK136 - pET15b-TrxA-TEVcs-hMFG-E8_dEGF_dC1-C2_iso3-LPETG-His6

Note: “TEVcs“ stands for TEV cleavage site with the aa sequence ENLYFQG

Template: pFMP311

Primers fw: TTTGTTTAACTTTAAGAAGGAGATATACCATGAGCGATAAAATTATTC
ACCTGACTGAC
rv: CCTGAAAATAAAGATTCTCGGTACCACCACTGCCAGATCCGG
PCR on pFMP311, Gibson Assembly of product in pTK135 cut with NcoI / KpnI

pTK137 - pET15b-DsbA(leaderless)-TEVcs-hMFG-E8_dEGF_dC1-C2_iso3-LPETG-His6
Note: “TEVcs“ stands for TEV cleavage site with the aa sequence ENLYFQG
Template: pFMP314
Primers fw: TGTTTAACTTTAAGAAGGAGATATACCATGAAAGCGCAGTATGAAGATGG
rv: CCTGAAAATAAAGATTCTCGGTACCACCACTAGTTGATCCTTTTTTCTCG
PCR on pFMP314, Gibson Assembly of product in pTK135 cut with NcoI / KpnI

pTK138 - pET15b-DsbC(leaderless)-TEVcs-hMFG-E8_dEGF_dC1-C2_iso3-LPETG-His6
Note: “TEVcs“ stands for TEV cleavage site with the aa sequence ENLYFQG
Template: BL21(DE3) genomic DNA
Primers fw: ATTTTGTTTAACTTTAAGAAGGAGATATACCATGAAAGATGACGCGGCAA
TTCAACAAACGTTAGC
rv: CCTGAAAATAAAGATTCTCGGTACCACCACTAGTTGATCCTTTACCGCTG
GTCATTTTTTGGTGTTCGTC
PCR on BL21(DE3) cells, Gibson Assembly of product in pTK135 cut with NcoI / KpnI

pTK150 - pET15b-DsbC(leaderless)-linker_TEVcs_linker-hMFG-E8_C1-15aaIgG3linker-C2-LPETG-His6
Note: This construct was not used for expression in this work but served as backbone for pTK165
Template: pET15b-DsbC(leaderless)-TEVcs-hMFG-E8_C1-15aaIgG3linker-C2-LPETG-His6 (pTK146)
Primers fw1: TTTCAGAGCTCTGGCTCGGGGAGCGGTACCCTCGATATCTGTTCCAA
GAATCCCTGTCAC
rv1: GTGGCTCCCTCCAGTTTCGGGCAGACCGGTACAGCCAAGCAGCTCCAGC
fw2: GGTAAAGGATCAACTAGTGGTGGCGGTGAGAATCTTTATTTTCAGAGCT
CTGGCTCGGGG
rv2: GTGGCTCCCTCCAGTTTCGGGCAGACCGGTACAGCCAAGCAGCTCCAGC
PCR with primer pair 1 on pTK146 and with primer pair 2 on product from pair 1.
Gibson Assembly of product from pair 2 in pTK138 cut with KpnI / AgeI

4.2 Molecular Biology

pTK165 - pET15b-DsbC(leaderless)-linker_TEVcs_linker-hMFG-E8_C1-15aaIgG3linker-C2-sfGFP-LPETG-His6
Note: “TEVcs“ stands for TEV cleavage site with the aa sequence ENLYFQS
Template: pTK106
Primers fw: TTGAGGCTGGAGCTGCTTGGCTGTACCGGTGGCGGTGGAGGGTCTGG CGGAGGTGGGATGCGTAAAGGAGAAGAACTTTTCACTG
rv: GTGGCTCCCTCCAGTTTCGGGCAGACCGGTTTTGTATAGTTCATCCATG CCATGTGT
PCR on pTK106, Gibson Assembly of product in pTK150 cut with AgeI

pTK168 - pET15b-DsbC(leaderless)-linker_TEVcs_linker-sfGFP-hMFG-E8_C1-15aaIgG3linker-C2-LPETG-His6
Note: “TEVcs“ stands for TEV cleavage site with the aa sequence ENLYFQS
Template: pTK165
Primers fw1: TTTCAGAGCTCTGGCTCGGGGAGCGGTACCATGCGTAAAGGAGAAGA ACTTTTCAC
rv1: GGTACCGCTCCCGCCGCCGCCACTCCCACCTTTGTATAGTTCATCCAT GCCATGTGT
fw2: TTTCAGAGCTCTGGCTCGGGGAGCGGTACCATGCGTAAAGGAGAAGAA CTTTTCAC
rv2: TTCTTGGAACAGATATCGAGGGTACCGCTCCCGCCGCCGCCAC
PCR with primer pair 1 on pTK165 and with primer pair 2 on product from pair 1.
Gibson Assembly of product from pair 2 in pTK150 cut with KpnI

4.2.5 Bacteria genotypes

Used for molecular cloning:

Stratagene SoloPack Gold (Agilent Technologies; Santa Clara, California, USA)
Tetr∆(mcrA)183 ∆(mcrCB-hsdSMR-mrr)173 endA1 supE44 thi-1 recA1 gyrA96 relA1 lac Hte [F´ proAB lacIqZ∆M15 Tn10 (Tetr) Amy Camr]

Used for protein production:

Novagen BL21 (DE3) (Merck Millipore; Burlington, Massachusetts, USA)
F^- *ompT gal dcm lon hsdS*$_B$($r_B^-m_B^-$) λ(DE3 [*lacI lacUV5-T7p07 ind1 sam7 nin5*]) [*malB*$^+$]$_{K-12}$(λ^S)

4.2 Molecular Biology

Novagen Origami B (DE3) (Merck Millipore; Burlington, Massachusetts, USA)
F^- *ompT hsd*S_B(r_B^- m_B^-) *gal dcm lacY1 ahpC* (DE3) *gor522*:: Tn*10 trxB* (Kan^R, Tet^R)

4.2.6 Preparation of chemically competent bacteria

RF I		RF II	
2.25% (v/v)	glycerin	2.25 % (v/v)	glycerin
100 mM	KCl	10 mM	KCl
50 mM	$MnCl_2$	10 mM	MOPS
30 mM	$C_2H_3KO_2$	75 mM	$CaCl_2$
10 mM	$CaCl_2$		
Adjust pH 5.8 with 0.2 mM acetic acid		Adjust pH 6.8 with 1 N NaOH	
Sterile filter buffers and store at 4°C			

Inoculated 5 – 8 ml LB medium without antibiotics with bacteria for overnight culture.
The next day, added 1 ml overnight culture to 100 ml LB, supplemented with 1 ml 1 M $MgCl_2$ and cultured cells again shaking at 37°C.
After 2 h measured OD_{600}. At 0.4 – 0.6, divided culture in two 50 ml tubes and placed 10 min on ice. Spun cells 4000 x g, 15 min, 4°C and resuspended each pellet in 5 ml RF I. Filled up to 20 ml with RF I and placed 15 min on ice. Spun cells 4000 x g, 15 min, 4°C, resuspended each pellet in 4 ml RF II and pooled. Placed on ice for 15 min, mixed carefully and aliquoted to 100 µl in 1.5 ml reaction tubes. Snap-froze aliquots in liquid nitrogen and stored at -80°C.

4.2.7 Transformation of chemically competent bacteria

Aliquots of 50 µl chemically competent bacteria were thawed on ice and 5 µl ligation mix or purified plasmid for transformation added. Mixing was performed by flicking the tube carefully and the cells placed on ice for 30 min. Afterwards, they were heat shocked in a Thermomixer compact (Eppendorf; Hamburg, Germany) for 30 sec at 42°C. Reaction tube with cells was placed on ice for 2 min and 800 µl LB medium added. Regeneration of bacteria for at least 1 h shaking at 37°C, 900 rpm (Thermomixer compact). Plated 50 µl of the transformation mix on one half of a selective LB agar plate, spun the cells 4000 x g, 5 min and plated the pellet on the other half. Placed selective plate overnight at 37°C in a bacterial incubator (Binder; Tuttlingen, Germany).

4.2 Molecular Biology

4.2.8 Phenol-Chloroform extraction of plasmid DNA from bacteria

Alkaline lysis solution I	Alkaline lysis solution II	Alkaline lysis solution III
50 mM glucose	0.2 N NaOH	60 ml 5 M potassium acetate
25 mM Tris-HCl, pH 8.0	1% SDS	11.5 ml glacial acetic acid
10 mM EDTA, pH 8.0	always prepare fresh	28.5 ml H_2O
store at 4°C		store at 4°C

STE
10 mM Tris-HCl, pH 8.0
0.1 M NaCl
1 mM EDTA, pH 8.0

Inoculated 6 x 5 ml LB medium containing respective antibiotics (100 µg/ml Ampicillin or 50 µg/ml Kanamycin) in 14 ml Falcon polypropylene round-bottom tubes (Corning; Corning, New York, USA) with bacteria from glycerol stocks and grew culture shaking overnight at 37°C and 180 rpm (Innova 44 Incubator shaker; New Brunswick Scientific; Edison, New Jersey, USA).

The next day, spun culture 10 min, 4000 x g to pellet cells.
Resuspended cell pellets in 900 µl STE each, combined 2-3 pellets in one 2 ml reaction tube. Pelleted cells again, 1 min, 14 000 x g, removed all liquid.
Resuspended cells in 200 µl ALS I, vortexed thoroughly. Added 400 µl ALS II, mixed thoroughly by inverting the reaction tube and incubated for 3 min at room temperature. Added 300 µl ALS III, mixed by inverting the reaction tube and placed tubes 3 - 5 min on ice. Spun tubes 10 min, 16 000 x g and transferred SN to fresh 2 ml reaction tubes. Added 3 µl RNase A (stock 100 mg/ml; Macherey-Nagel; Düren, Germany) and incubated for 10 min at 57°C. Subsequently added 30 µl Proteinase K (stock 10 mg/ml; Sigma-Aldrich) and incubated for another 14 min at 57°C.
Added 900 µl Phenol:Chloroform (Phenol:Chloroform:Isoamyl Alcohol 25:24:1, saturated with 10 mM Tris, pH 8.0, 1 mM EDTA; Sigma-Aldrich), mixed properly and spun 10 min, 16 000 x g. Transferred upper aequeous phase to fresh tube and added 450 µl Chloroform. Spun 10 min, 16 000 x g, again transferred upper aequeous phase to fresh tube and added 900 µl ethanol. Incubated at least 5 min at room temperature, spun 4°C, 15 min, 20 000 x g, remove liquid, washed pellet with 200 µl 70% ethanol and spun again 4°C, 10 min, 20 000 x g. Removed liquid, dried pellet at room temperature until it appeared rather transparent and residual ethanol was gone. Resuspended pellet in 150 µl TE buffer by shaking in Eppendorf Thermomixer. Combined the volumes of the same construct, determined DNA concentration

(SimpliNano; GE Healthcare; Chicago, Illinois, USA) and adjusted concentration to 1 µg/µl. Stored purified DNA at -20°C.

4.2.9 anti-GFP ELISA for determination of recombinant protein concentration

Coating buffer	Blocking / sample buffer
1.58 g Na_2CO_3 + 2.94 g $NaHCO_3$	1x Casein blocking buffer in water
H_2O ad 500 ml	+ 0.1% Tween-20
(= 0.1 M sodium carbonate, pH 9.6)	(Sigma-Aldrich)

ELISA wash buffer	Stop solution
PBS + 0.1% Tween-20	0.5 M H_2SO_4

HRP substrate
TMB 2-Component Microwell
Peroxidase Substrate kit
(Seracare; Milford, Massachusetts, USA)

Note: Volume for all steps was 100 µl unless specified otherwise, all incubation steps were performed at room temperature and Finnpipette Multipette was used (Thermo Scientific).
A 96 well Maxisorp Immuno plate (Thermo Scientific) was coated with 400 ng/ml anti-GFP (ab1218, clone 9F9.F9, Abcam; Cambridge, UK) in coating buffer overnight at 4°C. The next day, the plate was emptied and washed 6 times by immersing in wash buffer, flicked over sink and tapped on paper towels.
Blocking with blocking buffer for 2 h. Prepared sample by dilution of concentrated HEK SN 10x in sample buffer for the top row. Discarded blocking buffer in the plate, added 150 µl sample to the top row and performed 1:3 dilution series. Prepared dilution series of recombinant EGFP (self-produced) starting with 100 ng/ml as standard. Incubated the plate for 2 h. Washed plate 6 times subsequently and added biotin-labelled polyclonal anti-GFP (ab6658, Abcam; Cambridge, UK) 1:20000 in sample buffer to each well. Incubation for 1 h, washed plate 6 times afterwards. Added Pierce High Sensitivity Streptavidin-HRP (Thermo Scientific) 1:10000 in sample buffer, incubation for 1 h. Washed plate 4 times with wash buffer and 2 times with PBS. Added HRP substrate solution to each well and stopped reaction with stop solution when appropriate. Measured absorbance at A450 with VersaMax Microplate Reader (Molecular Devices; San José, California, USA). Data were analyzed by a 4-Parameter logistic fit as provided by the software.

4.3 Biochemistry

4.3.1 Preparation of SDS gels for protein analysis

Mix sufficient for four 12% SDS gels

	Separating gel	Stacking gel
ddH_2O	8.25 ml	4.25 ml
Acrylamide (30% solution)	10 ml	1.04 ml
Tris-HCl	6.25 ml	0.79 ml
SDS (10 % solution)	250 µl	62.5 µl
APS (10 % solution)	250 µl	62.5 µl
TEMED	25 µl	6.25 µl

Chemical were purchased from Carl Roth.
For separating gel, 1.5 M Tris-HCl, pH 8.8 was used and for stacking gel 1 M Tris-HCl, pH 6.8 Gels were prepared using glass plates with 1 mm spacer and the gel casting system from Bio-Rad (Hercules, California, USA) using 15 well or 10 well combs for sample pockets.

4.3.2 SDS PAGE (Polyacrylamide gel electrophoresis)

Self-prepared SDS gels were placed in Mini Protean 3 system (Bio-Rad; Hercules, California, USA) and wells rinsed with running buffer to remove residual gel fragments. Protein samples in SDS loading buffer were loaded in the wells with Pageruler Plus Prestained Protein Ladder (Thermo Scientific) used as a reference. Gel run at 80 V with PowerPac HC (Bio-Rad) until samples completely entered the stacking gel, then shifted to 130 V until complete separation of proteins was determined according to the MW standard.
The glass plates were removed, proceeded with the gel either with Coomassie staining (see general buffers) or Western Blot.

Coomassie staining: Fixation of proteins in the gel by shaking in 10 % acetic acid, 30 % methanol for 1 h at room temperature. Washed gel 4 x 15 min with H_2O, added Coomassie G-250 “Blue Silver” staining solution and stained proteins by shaking overnight. The next day, removed staining solution and removed excessive staining by shaking in H_2O.

Western Blot: The SDS gel and an Amersham nitrocellulose blotting membrane (GE Healthcare; Chicago, Illinois, USA) were assembled alongside with two gel blotting papers (Schleicher und Schuell) on each side and suitable sponges in a cassette immersed in transfer buffer. Blotting at 90 V for 90 min with PowerPac HC (Bio-Rad) at 4°C. Blocked membrane

with Casein blocking buffer (Sigma-Aldrich) +0.1% Tween-20 for 2 h shaking at room temperature and incubated overnight shaking at 4°C in anti-GFP(biotin) (1 mg/ml stock; Abcam; Cambridge, UK) 1:10000 in blocking buffer + 0.1% Tween-20. The next day, washed membrane 3x 15 min with PBS + 0.1% Tween-20. Added Pierce High Sensitivity Streptavidin-HRP (1.1 mg/ml stock; Thermo Scientific) 1:10000 in blocking buffer + 0.1% Tween-20 and incubated shaking at room temperature for 1 h. Washed membrane again 3 x 15 min with PBS + 0.1 % Tween-20, added Western Lightning Plus-ECL substrate solution (PerkinElmer; Waltham, Massachusetts, USA) and analysed the chemiluminescence signal with the Sapphire Biomolecular Imager system (Azure Biosystems; Dublin, California, USA).

4.3.3 Cultivation of bacterial cells

Working concentrations for antibiotics:
Ampicillin – 100 µg/ml, Kanamycin – 50 µg/ml, Tetracyclin – 10 µg/ml
Bacteria were cultured at 37°C in LB medium (powder by Carl Roth) in liquid culture or in petri dishes on LB-Agar (LB medium supplemented with 2% (w/v) agar).

4.3.4 Bacterial expression cultures

For Origami B (DE3), overnight cultures were shaken in LB+Amp/Kan/Tet at 37°C and 170 rpm in an Innova 44 Incubator Shaker (New Brunswick Scientific; Edison, New Jersey, USA). The next day, cultures were spun 4000 x g, 10 min and the pellet transferred to a higher volume of fresh medium in an Erlenmeyer flask. Cells were cultured at 120 rpm and OD_{600} determined using a BioPhotometer (Eppendorf; Hamburg) until it reached a value of 2-3. Cells were spun again and the cell pellet transferred to double the volume (e.g. 1 l LB in 2 l Erlenmeyer flask with baffles). Bacteria were grown again for 1 h at 100 rpm, the culture cooled down to 25°C and a sample equivalent of 0.4 OD taken in a reagent tube. Pelleted cells were resuspended in 60 µl 1x SDS sample buffer for the sample “before induction”. Protein expression was induced by addition of 1 mM IPTG. Induced cultures were left overnight shaking for 16 h. The next day, the sample “after induction” was taken see above, cells from the cultures harvested by centrifugation, the cell pellet snap-frozen in liquid nitrogen and stored at -80°C for further processing.

Expression cultures from the BL21 (DE3) strain were handled similarly, except that the main expression culture was directly inoculated with 1/100 of its volume with overnight culture. Cells were grown until OD_{600} = 0.7 and protein expression induced by addition of 0.2 – 0.5 mM IPTG.

4.3 Biochemistry

4.3.5 Lysis of bacterial cells by sonication

Cell pellets were thawed and resuspended in the appropriate lysis buffer at 10 ml / g wet cell weight (if possible supplemented with 1x cOmplete protease inhibitor mix (Roche; Basel, Switzerland).
For small volume (2-4 ml, e.g. test lysis), lysis was performed using a Branson sonicator 150. Lysis in 50 ml tube in an ice-cooled water bath, output: 10, continuous pulse for at least 6 cycles, each 2 min, with at least 1:30 min break in between lysis cycles to allow the lysate to cool down. Lysate was spun 20 000 x g, 30 min, 4°C to pellet insoluble material. Supernatant was taken off and the pellet resuspended in an equivalent volume of 10% SDS. An equivalent of 0.4 OD was taken from the supernatant and the solubilized pellet in 1x SDS sample buffer (60 µl total volume).

For larger volumes (up to 50 ml, e.g. protein purification), lysis was performed using a Branson sonifier cell disruptor B15 with a ½ `` tip, output: 7, 40% duty cycle in a 100 ml metal beaker cooled in a water bath see above. At least 5 lysis cycles for 7 min each with 2 min breaks until the appearance of the liquid changed from turbid to vivid and opalescent. Processing see above, the supernatant was further used in affinity chromatography.

4.3.6 Lysis of bacterial cells for analytical purposes

Solubility of single domains in a simple buffer system – His_6-SUMO3-hC2 (pTK30), mC2-His_6 (pTK70), hC2-His_6 (pTK71), mC1-His_6 (pTK83), mC1C2-His_6 (pTK76)
Buffers in all cases: 20 mM $NaPO_4$, 500 mM NaCl, but with pH 6.5 for pTK30, pH 7.3 for pTK70, pTK71, pTK76 and pTK83

Lysis of BL21 (DE3) and Origami B (DE3) cells expressing the GST-SUMO3-mC1-LPETG-His_6 (pTK85) and GST-SUMO3-mC2-LPETG-His_6 (pTK82) construct was performed in 50 mM HEPES, 400 mM NaCl, 10% glycerol, pH 7.6

Comparison tags GST-SUMO (pTK133), TrxA (pTK136), DsbA (pTK137), DsbC (pTK138)
Expression in Origami B (DE3). Buffers used for lysis: OSB in all cases, but with pH 7.4 for pTK133 / 136 and with pH 8.2 for pTK137 / 138

hMFG-E8 variants – N terminal and C terminal sfGFP (pTK165 / pTK168 construct)
Expression in Origami B (DE3). Cells were lysed in OSB + 20 mM imidazole.

4.3 Biochemistry

For lysate supernatant after centrifugation, fluorescence was determined with NanoDrop ND-1000 Spectrophotometer (peqlab; Erlangen) at 488 nm. Densitometry of the respective protein bands and lanes from the Coomassie-stained SDS gel was performed with ImageJ.

4.3.7 Protein purification from bacterial lysates

General notes:

All purified proteins were spun 30 000 x g, 30 min, 4°C to remove aggregates, protein concentration determined by spectrophotometry (NanoDrop ND-1000; peqlab; Erlangen) using the respective molar extinction coefficient as given by the ExPASy ProtParam online tool (https://web.expasy.org/protparam/). For impure preparations, the setting 1 Abs = 1 mg/ml was applied. Protein was snap-frozen in aliquots in liquid nitrogen and stored at -80°C. Aliquots were only thawed for a maximum of 3 times. All purification steps were surveilled on a Coomassie-stained SDS gel and the final product integrity and purity verified.

General procedure for Ni^{2+}-NTA affinity chromatography

Cleared supernatant from lysate centrifugation was added to washed Protino Ni^{2+}-NTA agarose beads (Macherey-Nagel; Düren) and rotated for at least 1 h at 4°C. Beads were separated from the supernatant using a 14 ml or 35 ml Protino gravity flow chromatography column (Macherey-Nagel; Düren). Beads were washed with at least 10 column volumes (CV) of wash buffer and lysis buffer, respectively and if needed a sample of 20 µl beads boiled in 75 µl 1x SDS sample buffer (analyzed 7.5 µl on SDS gel for the equivalent of 2 µl beads). Elution of protein from the beads using 5-10 CV elution buffer in 4-5 fractions. Incubation for 4 min after each addition of fresh buffer. Sample of elution fractions: SDS sample buffer with 1 µl eluate / CV in respective fraction, analyzed 2.5 µl equivalent of the elution fraction on SDS gel. Pooled all protein-containing fractions as determined by spectrophotometry (NanoDrop ND-1000; peqlab; Erlangen). High imidazole from elution buffer was either removed by dialysis using SnakeSkin dialysis tubing 10K MWCO (Thermo Scientific), by ultrafiltration using protein concentrators like VIVASPIN 20 PES (Sartorius; Göttingen) or size exclusion chromatography (see respective section).

His_6-Sortase A (pTK32 construct)

Protein was produced in BL21 (DE3) and purification performed according to instructions given in (Guimaraes et al., 2013). Lysis buffer did not contain DNase or lysozyme and lysis was performed by sonication. SEC column used: HiLoad 26/600 Superdex 200 pg (GE Lifesciences; Chicago, Illinois, USA), purified protein was concentrated to 25 mg/ml.

4.3 Biochemistry

EGFP (from His_6-SUMO3-EGFP, pTK108 construct)

Lysis buffer	Wash buffer	Elution buffer	Dialysis buffer	
50 mM	50 mM	50 mM	50 mM	$NaPO_4$
300 mM	300 mM	300 mM	300 mM	NaCl
5 mM	20 mM	250 mM	-	imidazole
10% (v/v)	-	-	-	glycerol

All buffers were adjusted to pH 7.4 at 4°C

EGFP was produced in BL21 (DE3).

Imidazole from elution was removed by dialysis overnight with concomitant proteolytic cleavage of the His_6-SUMO3 tag by addition of His_6-Senp2 (R&D systems; Minneapolis, Minnesota, USA). The next day, protease, His_6-SUMO3 tag, uncleaved His_6-SUMO3-EGFP and potential impurities were removed by a second Ni^{2+}-NTA affinity chromatography, the flow-through concentrated, spun 30 000 x g, 30 min, 4°C and stored in aliquots at -80°C. Before usage as standard for α-GFP-ELISA or in the DTNB assay for measurement of free thiols, final polishing of the EGFP solution was performed in small scale by SEC using a Superdex 200 Increase 10/300 GL column pre-equilibrated with dialysis buffer.

His_6-TEV

Lysis buffer	Elution buffer	SEC buffer	
25 mM	25 mM	25 mM	HEPES
300 mM	300 mM	300 mM	NaCl
10 % (v/v)	10 % (v/v)	8 % (v/v)	glycerol
10 mM	200 mM	-	imidazole
0.5 mM	1 mM	2 mM	DTT
-	-	2 mM	EDTA

pH was adjusted to 7.5 at 4°C in all cases.

Wash buffer is lysis buffer + 0.1 % Triton X-100.

His_6-TEV was produced in BL21 (DE3). Purification according to general procedure, Ni^{2+}-NTA beads with associated protein were washed with 10 CV wash buffer and 10 CV lysis buffer before elution. Pooled elution fractions were concentrated to 5 ml and loaded on HiLoad 26/600 Superdex 200 pg column, pre-equilibrated with SEC buffer for overnight run. The next day, peak fractions were pooled, concentrated to 6.49 mg/ml and the same volume 100% glycerol added for cryoprotection. Prepared aliquots and stored at -80°C.

4.3 Biochemistry

mC1 / mC2 (from GST-SUMO3-mC1/mC2-LPETG-His_6, pTK85 / pTK82 construct)

Lysis buffer

20 mM HEPES

300 mM imidazole

20 mM imidazole

pH 7.4 at 4°C

Wash buffer was prepared by supplementing lysis buffer with 0.1 % Triton X-100

Proteins were produced in Origami B (DE3). After association of protein from the lysate supernatant with the beads, they were washed with 10 CV wash buffer and 10 CV lysis buffer. For on-bead-cleavage of the GST-SUMO3 tag, 4 ml beads were rotated in 7 CV lysis buffer and 250 µg GST-Senp2 protease for 1.5 h at room temperature in a gravity flow chromatography column. Afterwards, column was drained and the process repeated with fresh protease for another 1.5 h. Beads were washed with 10 CV wash buffer, 10 CV OSB, 10 CV OSB + 0.1 % BSA (fatty acid free) and stored at 4°C. The next day, beads were washed with 10 CV OSB and protein eluted with 10 CV OSB + 200 mM imidazole in 4 fractions. Protein-containing fractions were pooled and slowly filled up with an equivalent volume of OSB to decrease the imidazole concentration. Protein solution was concentrated to 5 ml and loaded on a HiLoad 26/600 Superdex 200 pg column (GE Lifesciences; Chicago, Illinois, USA), pre-equilibrated with OSB. Protein-containing fractions were pooled and protein concentrated up to 5 mg/ml. Prepared aliquots and stored at -80°C.

hMFG-E8 variant - for experiment unspecific association with beads (pTK116 construct)

Lysis buffer

20 mM	HEPES
300 mM	NaCl
5 mM	imidazole

pH 7.5

Protein was produced in Origami B (DE3). After association of protein with the Ni^{2+}-NTA beads, beads were washed with lysis buffer and 2 CV lysis buffer + 50 mM EDTA added. Repeated this treatment twice. After taking samples of beads and flow-through, added 2 CV lysis buffer + 250 mM imidazole and took samples again.

4.3 Biochemistry

hMFG-E8 variant – influence of CHAPS (pTK168 construct)

SEC buffer

200 mM L-arginine

137 mM succinate

pH 5.0

Protein produced in Origami B (DE3). Lysed cells in OSB + 20 mM imidazole. Split supernatant from lysate centrifugation in two portions, added CHAPS from a 10x stock in lysis buffer to 2 % (w/v) final concentration to one part and only lysis buffer to the other and incubated rotating at 4°C for 2 h. Afterwards, added washed Ni^2-NTA beads to the lysate supernatant -/+ CHAPS and rotated at 4°C for 1 h. Rest see general description. Elution with OSB + 200 mM imidazole, pH 7.4. Pooled protein-containing fractions each and removed imidazole by ultrafiltration filling up the protein solution with OSB. Final concentration and centrifugation, stored in aliquots at -80°C.

Protein purification from bacterial lysates by GST affinity chromatography

GST-Senp2 (pTK77 construct)

Lysis buffer	Elution buffer	Storage buffer	
20 mM	20 mM	20 mM	Tris
350 mM	350 mM	150 mM	NaCl
1 mM	1 mM	1 mM	DTT
-	10 mM	-	glutathione (reduced)
-	-	20 % (v/v)	glycerol
pH 7.6	pH 7.6	pH 8.0	

Wash buffer was prepared by supplementing lysis buffer with 0.1 % Triton X-100

Supernatant from centrifugation of bacterial lysate was incubated with washed glutathione sepharose 4B (GE Lifesciences; Chicago, Illinois, USA) for 2 h rotating at 4°C. Beads were washed with 30 CV wash buffer and 20 CV lysis buffer in a gravity flow chromatography column. Elution of proteins with 4 CV elution buffer, incubated for 10 min after each addition of fresh buffer. Dialyzed pooled protein-containing fractions with storage buffer overnight. The next day, concentrated dialysate, spun 30 000 x g, 30 min, 4°C and stored in aliquots at -80°C.

4.3.8 Purification of secreted MFG-E8-EGFP variants from HEK293T production

HEK293T stable with the respective constructs in the vector backbones pD2527 and pD2528 were selected using the respective antibiotics Hygromycin B (Thermo Scientific) and Blasticidin

(InvivoGen; San Diego, California, USA). Cells were adapted to serum-free medium (ExCell293; Sigma-Aldrich). Purification performed by Jan Kranich and Agnieszka Foltyn-Arfa Kia as described previously (Trautz et al., 2017).

4.3.9 Size exclusion chromatography of protein solutions

Size exclusion chromatography was performed using a ÄKTA pure 25 L1 (GE Lifesciences; Chicago, Illinois, USA) with the following columns:

Superdex 200 Increase 10/300 GL (0.5 ml loop used)
Parameters: Pre-column pressure limit 5 MPa; Flow rate throughout all steps 0.5 ml/min; equilibration until the total volume is 3 ml; inject sample in loop; empty loop with 1 ml; isocratic elution - volume 35.0 ml; fractionation using fraction collector with fixed fractionation volume of 0.5 ml; start fractionation after 4 ml

HiLoad 26/600 Superdex 200 pg (5 ml loop used)
Parameters: Pre-column pressure limit 0.5 MPa; Flow rate throughout all steps 2.0 ml/min; equilibration until the total volume is 20 ml; inject sample in loop; empty loop with 10 ml; isocratic elution - volume 360.0 ml; fractionation using fraction collector with fixed fractionation volume of 2.5 ml; start fractionation after 60 ml

Columns were equilibrated with at least 1 CV of the respective SEC buffer and the loop rinsed with the same buffer before application of protein. After each run, columns were washed with ddH_2O and for long-term storage columns were equilibrated with 20 % ethanol. All liquids used in SEC columns were filtered (0.2 µm) and degassed prior to usage.

4.3.10 DTNB assay for determination of free thiols

All proteins were diluted to yield 80 µM in final sample and concentration verified by spectrophotometry (NanoDrop ND-1000; peqlab; Erlangen). Dilution 1:1 with denaturation buffer (100 mM Tris, 2% SDS, 2 mM EDTA, pH 7.4), denaturation for 15 min at 75°C to expose free cysteine residues. Standard curve was performed with serial dilution of L-cysteine hydrochloride monohydrate (Sigma-Aldrich) in comparable buffer. Added to 5,5'-Dithiobis (2-nitrobenzoic acid (DTNB) (Sigma-Aldrich) solution, 3.2 mM final concentration in assay. Determined A_{410} with VersaMax microplate reader (Molecular Devices; San José, California, USA).

4.3 Biochemistry

4.3.11 Thermal shift assay

Purified mC1 and mC2 was diluted to a concentration yielding 10 µM in final sample, concentration verified via spectrophotometry (NanoDrop ND-1000; peqlab; Erlangen and combined with 1x thermal shift dye (Protein thermal shift dye kit, Thermo Scientific) and the respective buffer in MicroAmp EnduraPlates (Thermo Scientific). Assay was performed with QuantStudio 3 (Thermo Scientific) with increase of the temperature from 25°C to 99°C with 0.05 °C / sec. The values for the melting curve's first derivative were normalized (lowest value set to 0, highest to 1) and each T_m determined from the minimum of the respective melting curve.

4.3.12 Sortase reaction

Reaction buffers:

Standard buffer		OSB-based
50 mM	Tris	OSB, supplemented with 10 mM $CaCl_2$
150 mM	NaCl	pH 7.5 at room temperature
10 mM	$CaCl_2$	prepared as 5x stock
pH 7.5 at room temperature		
prepared as 10x stock		
Preparation based on		
(Guimaraes et al., 2013)		

Peptides were purchased from Genscript Biotech (Piscataway Township, New Jersey, USA).
Sequences (N -> C-terminus):
Fluorescent peptide GGGK(FITC)
Biotin-containing peptide GGGENLYFQGK(biotin)

Procedure:
50 µM target protein was combined with 50 µM Sortase A, 1 mM peptide and 1x reaction buffer in an appropriate volume. Incubation of reaction for at least 1 h at 25°C. Reaction was stopped by addition of 3 parts Sortase stop buffer (OSB + 7 mM EDTA + 2x protease inhibitor, pH 7.4 at 4°C) to 1 part Sortase reaction. Incubated for 20 min on ice. Concentrated stopped Sortase reaction with VIVASPIN 20, 10 kDa MWCO, PES (Sartorius; Göttingen) to < 5 ml and loaded on HiLoad 26/600 Superdex 200 pg, pre-equilibrated with OSB for SEC. Pooled respective fraction, concentrated to at least 3 mg/ml and stored biotinylated proteins in aliquots at -80°C. In-gel fluorescence readout of proteins conjugated with the FITC-containing peptide was

performed with a Typhoon FLA9500 laser imaging system (GE Lifesciences; Chicago, Illinois, USA).

4.3.13 Multimer assembly

The stoichiometric ratio of mC1-biotin / mC2-biotin and Avidin variants was calculated based on protein concentrations obtained by spectrophotometry (NanoDrop ND-1000; peqlab; Erlangen) using the respective molar extinction coefficient for mC1-biotin / mC2-biotin or concentrations as provided by the manufacturer for Avidin. Four accessible biotin binding sites per molecule were assumed. For complete assembly, biotinylated monomers were used in at least 4.5 x molar excess to Avidin. The mix was incubated for at least 10 min on ice for assembly. For dilutions, if necessary, either OSB or FACS buffer (for cell stainings) was used. Long-term storage after centrifugation 30 000 x g, 30 min, 4°C and snap-freezing in aliquots at -80°C.

Avidin variants for multimer assembly were Strepavidin(FITC) and Streptavidin(AlexaFluor647) (both BioLegend; San Diego, California, USA), Streptavidin (NEB; Ipswich, Massachusetts, USA)

4.3.14 mC1 multimer solubility assay

Arg/Glu buffer	Dilution buffer	
25 mM	25 mM	HEPES
115 mM	115 mM	NaCl
2 % (v/v)	2 % (v/v)	glycerol
150 mM	-	L-arginine
150 mM	-	L-glutamic acid

Assembled a batch of multimer using SA(FITC) (BioLegend; San Diego, California, USA) and divided into smaller portions. Mixed 1 part of multimer solution with 2.4 parts of the respective buffer with varying concentration of components NaCl, glycerol and Arg/Glu. Took one sample as “input” sample in OSB and one for centrifugation to assay solubility in OSB. To vary the Arg/Glu concentration, Arg/Glu buffer was mixed with dilution buffer in different ratios. Spun the samples at 40 000 x g, 30 min, 4°C, took 15 µl of the soluble supernatant and mixed with 7.5 µl 2x SDS sample buffer (reducing). Loaded 500 ng SA(FITC) equivalent per sample on an SDS gel. Analysis of in-gel fluorescence with Typhoon FLA9500 laser imaging system (GE Lifesciences; Chicago, Illinois, USA), staining of proteins in gel with Coomassie “Blue Silver” formulation.

4.3 Biochemistry

4.3.15 mC1 multimer application *in vivo*

Injection buffer

20 mM	HEPES
2 % (v/v)	glycerol
200 mM	L-arginine
200 mM	L-glutamic acid

mC1 multimer (AlexaFluor 647) was diluted with injection buffer to reach at least 100 mM Arg/Glu and supplemented with NaCl to a final concentration of 150 mM. Spun 30 000 x g, 30 min, 4°C to remove aggregates and 20 µg injected intravenously per mouse (C57BL6 genetic background). For comparison, mMFG-E8-EGFP (self-produced) was diluted in OSB -NaCl to reach 150 mM NaCl and 100 µg injected per mouse. Mice were sacrificed 30 min after injection. If needed, mice were irradiated 13 h before experiment using the Multirad 225 system (RPS system; Byfleet, Surrey, UK) with a 0.5 mm Cu filter, 160 mV, 20 mA, level 2 for 15 min. Total irradiation dose: 9 Gy.

<u>For imaging flow cytometry using ImageStream Mark II (Luminex; Austin, Texas, USA):</u>
Single cell suspensions were prepared and erythrocyte lysis performed (see respective sections). Up to 5 x 10^6 cells were stained per condition in 200 µl volume. Prior to addition of antibody mix, an Fc receptor block was performed for 10 min on ice with TruStain fcX α-mouse CD16/32 (#101320, BioLegend; San Diego, California, USA).
Staining reagents (diluted in FACS buffer):
Live/dead fixable violet dead cell stain #L34955 and α-CD11b (APC-Cy7) #47-0112-82 (Thermo Scientific)
α-TCRß (PE) #109208 and α-CD19 (PE-Cy7) #115520 (BioLegend)
pAb a-GFP (FITC) (ab6662, Abcam) to enhance EGFP signal suffering from PFA fixation.
Additionally, cells from mice injected with mC1 multimer were counterstained with mMFG-E8-EGFP *in vitro* and vice versa. Staining for 30 min on ice, washed cells twice with 200 µl FACS buffer.
Cells were fixated with 4% (w/v) paraformaldehyde in PBS and washed with FACS buffer.

<u>For histology:</u>
Cryosections from mouse spleen were prepared using a CM 1950 Cryostat (Leica Microsystems; Wetzlar) and dried overnight. Slides were fixated in icecold acetone for 10 min at -20°C. Dried slides for at least 1 h at room temperature in the dark and rehydrated in PBS + 0.25 % BSA for 15 min. Blocked the slides in a humid chamber with 250 µl PBS + 0.25 %

BSA + 1 % mouse serum for 15 min. Added 250 µl of a staining mix with CD21 (PE) #552957 (clone 7G6; BD Biosciences; Franklin Lakes, New Jersey, USA) and 4',6-Diamidino-2-Phenylindole (DAPI) #D1306 (Thermo Scientific), diluted in PBS + 0.25 % BSA + 1 % mouse serum for 30 min at room temperature in a humid chamber. Washed the slides in PBS + 0.25 % BSA for 3 min. Added Fluoromount-G (Thermo Scientific) mounting medium, covered the slides with a coverslip and dried overnight at 4°C. Analysis with an Olympus BX41 fluorescence microscope, 10x magnification.

4.4 Cell biology

4.4.1 Cultivation of mammalian cells

HEK293T cells were cultured in a humid atmosphere of 37°C and 5 % CO_2 in a Galaxy 170S incubator (Eppendorf; Hamburg, Germany). Medium used: gibco DMEM (1x) GlutaMAX-I (Thermo Scientific, Waltham, Massachusetts, USA), supplemented with 8% FCS (Pan Biotech; Aidenbach, Germany) and 1% Pen/Strep (Thermo Scientific).
Cells were cultured in 75 cm^2 or 175 cm^2 cell culture flasks (greiner bio-one; Kremsmünster, Austria) and split two times a week using 2 mM EDTA (disodium salt solution; Sigma-Aldrich) in PBS (Dulbecco's Phosphate Buffered Saline; Sigma-Aldrich) for detachment of the adherent cells.

Shaking cultures for fermenter production of proteins were grown in ExCell 293 serum-free medium (Sigma-Aldrich), supplemented with 1 % L-glutamine (Thermo Scientific), 1 % Pen/Strep (Thermo Scientific) and 20 mM HEPES (1 M stock solution, pH 7.0 – 7.6, sterile filtered; Sigma-Aldrich) in Corning Erlenmeyer baffled cell culture flasks (Sigma-Aldrich) placed on a shaker in the incubator.

Sterile handling of cells was performed in a Safety cabinet FlowSafe B-[MaxPro]3-160 (Berner International GmbH; Elmshorn, Germany).
All liquids were warmed to 37°C before usage.

4.4 Cell biology

4.4.2 Transfection of HEK293T cells

<u>2x HBS</u>	2.5 M $CaCl_2$ in H_2O, filtered 0.2 µm
50 mM HEPES	
1.5 mM $Na_2HPO_4 \bullet 2\ H_2O$	100 mM chloroquine in H_2O, filtered 0.2 µm
280 mM NaCl	
pH 6.95	purified H_2O "Ampuwa Spüllösung"
filtered 0.2 µm	(Fresenius Kabi; Bad Homburg, Germany)

All reagents were brought to room temperature prior to transfection.
The day before transfection, HEK293T cells were seed into 150 x 20 cell culture Nunc dishes (Thermo Scientific) at 4 x 10^6 cells / plate. 1 h before transfection, medium was refreshed (DMEM GlutaMAX +8% FCS +1% Pen/Strep, Thermo Scientific).
Transfection mix per plate: 105 µl purified vector DNA (1 µg/µl) was added to 819 µl H_2O in 15 ml tube (greiner bio-one; Kremsmünster, Austria), vortexed shortly and 126 µl 2.5 M $CaCl_2$ added. 1050 µl 2x HBS was added dropwise while vortexing and the mix incubated at room temperature for 3-4 min. Meanwhile, 5.25 µl chloroquine was added to medium (25 µM final concentration). Dropwise addition of transfection mix to the cell culture medium and distributed uniformly. Cells were placed in cell culture incubator overnight, checked on $CaPO_4$ crystals with a microscope the next day and the cells washed after 16 h 2x with PBS to remove excess crystals. 21 ml / dish serum-free medium for secretion of the recombinant proteins was added (ExCell 293 (Sigma), supplemented with 1% L-glutamine (Thermo Scientific), 1% Pen/Strep (Thermo Scientific) and 20 mM HEPES (Sigma)). Cells secreted proteins for 3 days in SN until harvest.

Stable transfections were performed accordingly in smaller 100 x 20 Nunc dishes (Thermo Scientific) with transfection mix scaled down appropriately. Medium was changed to 10 ml DMEM GlutaMAX, 8% FCS, 1% Pen/Strep (see above). Stable cells were selected with 100 µg/ml Hygromycin B (Thermo Scientific) for the pD2527 vector backbone and 6 µg/ml Blasticidin for pD2528.

4.4.3 Processing and preparation of concentrated supernatant from HEK293T

Cells secreted recombinant proteins in ExCell 293 medium (Sigma) for 3 days. Successful transfection of the cells with EGFP constructs was analyzed by fluorescence microscopy. SN from cell culture dishes was harvested, similar constructs pooled and spun 4°C, 10 min, 4200 g to remove cells. SN was again spun 4°C, 30 min, 30 000 g to remove debris. After filtering

with Minisart NML hydrophilic 0.2 µm syringe filter (Sartorius; Göttingen, Germany), Albumin fraction V (Carl Roth) from a 5% stock in PBS was added at 0.01% or 0.1%. SN was concentrated 10x with Amicon Ultra-15 Ultracel-10K (Merck Millipore; Burlington, Massachusetts, USA) (predominantly used in master thesis of Larissa Köppel) or Vivaspin 20 10,000 MWCO PES (Sartorius; Göttingen, Germany). Final Albumin concentration was either 0.1% or 1%. Concentrated SN was again spun 4°C, 30 min, 30 000 g to remove aggregates, aliquots snap-frozen in liquid nitrogen and stored at -80°C.

Concentration of recombinant proteins in concentrated SN was determined for each batch with three independent ELISA measurements and calculation of the mean value.

4.4.4 Counting of cells

Cell numbers from cell culture or for experiments were determined using a CASY TT cell counter (OMNI Life Sciences; Bremen, Germany), 150 µm capillary, 400 µl sample volume, 1 x 10^3 sample dilution

Parameters for

	HEK293T	mouse thymocytes / splenocytes
X-Axis	30 µm	15 µm
Cycles	3	2
Eval.Cursor	8.63 – 30 µm	5.14 – 15 µm
Norm.Cursor	1.05 – 30 µm	1.01 – 15 µm
Debris	Off	On
Aggr.Correct	Auto	Off

4.4.5 Staining of cells for flow cytometry

All volumes used in the staining procedure were 100 µl. Centrifugation in Heraeus Multifuge X3R (Thermo Scientific) 4°C, 300 x g, 3-5 min. Staining in a Mikrotest plate 96 well, R (Sarstedt, Nürnbrecht, Germany)

Cells were stained with 1:2000 dilution of eBioscience fixable viability dye eFluor780 in PBS for 10 min on ice. In case of live/dead staining with PI, this step was omitted and PI from the Annexin V (FITC) apoptosis staining / detection kit (Abcam; Cambridge, UK) added to the cell suspension prior to analysis according to the manufacturer's instructions. FACS buffer was added, cells spun and stained with purified proteins or concentrated SN from transient HEK transfections diluted in FACS buffer for 30 min on ice.

Note: Aliquots from concentrated HEK293T SN were thawed for a maximum of 2 times.

FACS buffer was again added, cells spun and washed two times.
Subsequently, cells were filtered through a 40 µm mesh and transferred to Falcon 5 ml round bottom polystyrene test tube (Corning; Corning, New York, USA) for flow cytometry at FacsCANTO II (BD Biosciences; Franklin Lakes, New Jersey, USA) or SafeSeal 1.5 ml reaction tube (Sarstedt; Nürnbrecht, Germany) for imaging flow cytometry analysis at ImageStream Mark II (Luminex; Austin, Texas, USA). Per condition, 5 x 10^5 or 1 x 10^6 cells were stained for flow cytometry.

4.4.6 mC1 multimer staining with Annexin V (FITC) and mMFG-E8-EGFP

Thymocytes treated with Staurosporine or left untreated were stained with mC1 multimer (AF647), mMFG-E8-EGFP (self-produced) and Annexin V-FITC (Annexin V-FITC apoptosis staining / detection kit; ab14085; Abcam; Cambridge, UK) either alone or in combination. Staining procedure as described, used Ca^{2+}-containing Annexin V binding buffer from the kit or FACS buffer without Ca^{2+}.

4.4.7 Depletion of dead cells from cell suspensions

Coupling of antibody to magnetic beads:
140 µg α-Streptavidin antibody (clone 3A20.2, BioLegend; San Diego, California, USA) was coupled to 650 µl Dynabeads M-450, tosylactivated (Thermo Fisher) according to manufacturer's instructions. Used 0.1 M sodium borate buffer, pH 9.5 as coupling buffer, rotated at 37°C overnight. Deactivation of free tosyl groups was performed with 0.2 M Tris, 0.1 % BSA, pH 8.5 for 4.5 h at 37°C.

Dead cell depletion:
Prepared single cell suspension from mouse spleen (as described in the respective section). Stained 5 x 10^5 cells per condition with fixable viability dye eFluor780 (Thermo Scientific) in PBS and washed with FACS buffer. A Fc receptor block was performed for 10 min on ice with TruStain fcX α-mouse CD16/32 (#101320, BioLegend; San Diego, California, USA). Stained cells with mC1 multimer (FITC) or mMFG-E8-EGFP for 30 min on ice and washed twice with FACS buffer. Left one sample each in well for sample "untreated" and transferred cells from other wells in 2 ml reaction tubes with 200 µl magnetic beads (see above) or FACS buffer ("-beads") and filled up with FACS buffer to a total volume of 600 µl. Rotated slowly at 4°C for 40 min. Spun tubes 300 x g, 5 min, 4°C to collect liquid at the bottom. Resuspended beads and cells and placed tubes in magnetic rack. Transferred liquid to fresh tubes and washed beads

with 2 x 200 µl FACS buffer, liberating trapped particles. Spun liquid 300 x g, 10 min, 4°C, took off SN and resuspended pellet in 200 µl FACS buffer for analysis.

4.4.8 Preparation of cell suspensions from tissue and induction of apoptosis

All centrifugation steps were done in Heraeus Multifuge X3R (Thermo Scientific), 4°C, 300 x g, 5 min.

Mice with C57BL6 or C57BL6 x 129SVJ/X1 genetic background were sacrificed using a CO_2 chamber. Organs were taken and cell suspensions prepared by squeezing the organs between two meshes (mesh size 40 µm for thymus, 100 µm for spleen) in FACS buffer. Cells were pelleted by centrifugation, buffer discarded and cells resuspended in 1 ml ACK buffer for lysis of erythrocytes. Incubation for 5 min at room temperature, added 13 ml FACS buffer and spun cells.

For induction of apoptosis, cells were resuspended in DMEM 1% Pen/Strep -FCS and counted. 30 – 50 x 10^6 cells were incubated for 2 h in 10 ml DMEM 1% Pen/Strep -FCS and 0.2 µg/ml Staurosporine (Sigma-Aldrich) in petri dishes in a cell culture incubator at 37°C and 5 % CO_2. Cells were collected again, washed 2x with 7 ml FACS buffer and stored in FACS buffer overnight on ice at 4°C.

5 Results

5.1 Using a mammalian expression system for MFG-E8 variant binding studies

5.1.1 hMFG-E8 single domains are efficiently secreted by HEK cells using the murine ER signal sequence

In the literature, studies with MFG-E8 were restricted to full-length or C2 only of the murine or bovine homologue and rather focused on structural analyses of C2, its membrane-binding motif as well as biophysical and biochemical characterization of the binding event (Ye et al., 2013, Reddy Nanga et al., 2007, Shao et al., 2008, Lin et al., 2007). Single domain binding studies with C1 have not been published so far and work with the human homologue focused on expression, purification and general verification of PS- and integrin-binding activity (Castellanos et al., 2016). The approach taken in this work targeted on the comparative analysis of both single PS binding domains and full-length hMFG-E8 originated from a uniform mammalian expression system.

For binding studies of hMFG-E8 single C domains, the ER signal sequence of hMFG-E8 was used for secretion of the constructs into the supernatant of transfected HEK cells with subsequent staining of apoptotic cells and analysis by flow cytometry. Cells were highly fluorescent after transfection whereas in the supernatant only little protein could be detected. This led to the assumption that the 23 aa long ER signal sequence of hMFG-E8 (hER SS) was not correctly annotated in the NCBI database (Reference sequence: NP_005919.2). HEK cells were transfected with the same construct, hC2 domain as EGFP fusion protein featuring the ER SS of either the human or murine MFG-E8 homologue at the N-terminus (Fig. 5.1 A). In direct comparison, the 22 aa mMFG-E8 ER SS showed a drastically different appearance of the transfected HEK cells. The hER SS containing construct was retained inside the cells and distributed throughout the whole cytoplasm whereas the mER SS resulted in fluorescent cells with a more speckled appearance (Fig. 5.1 B).
In addition, the population of live, transfected cells with hER SS showed a drastically higher MFI as compared to the mER SS construct upon analysis by flow cytometry (Fig. 5.1 C). The signal sequence of the mMFG-E8 homologue indeed allowed for more efficient secretion as revealed by ELISA of culture supernatant of transfected cells (Fig. 5.1 D). It is possible that HEK cells require additional aa to make the hER SS functional since full length hMFG-E8 was

secreted successfully. However, for the design of all other constructs in this study the mER SS was employed.

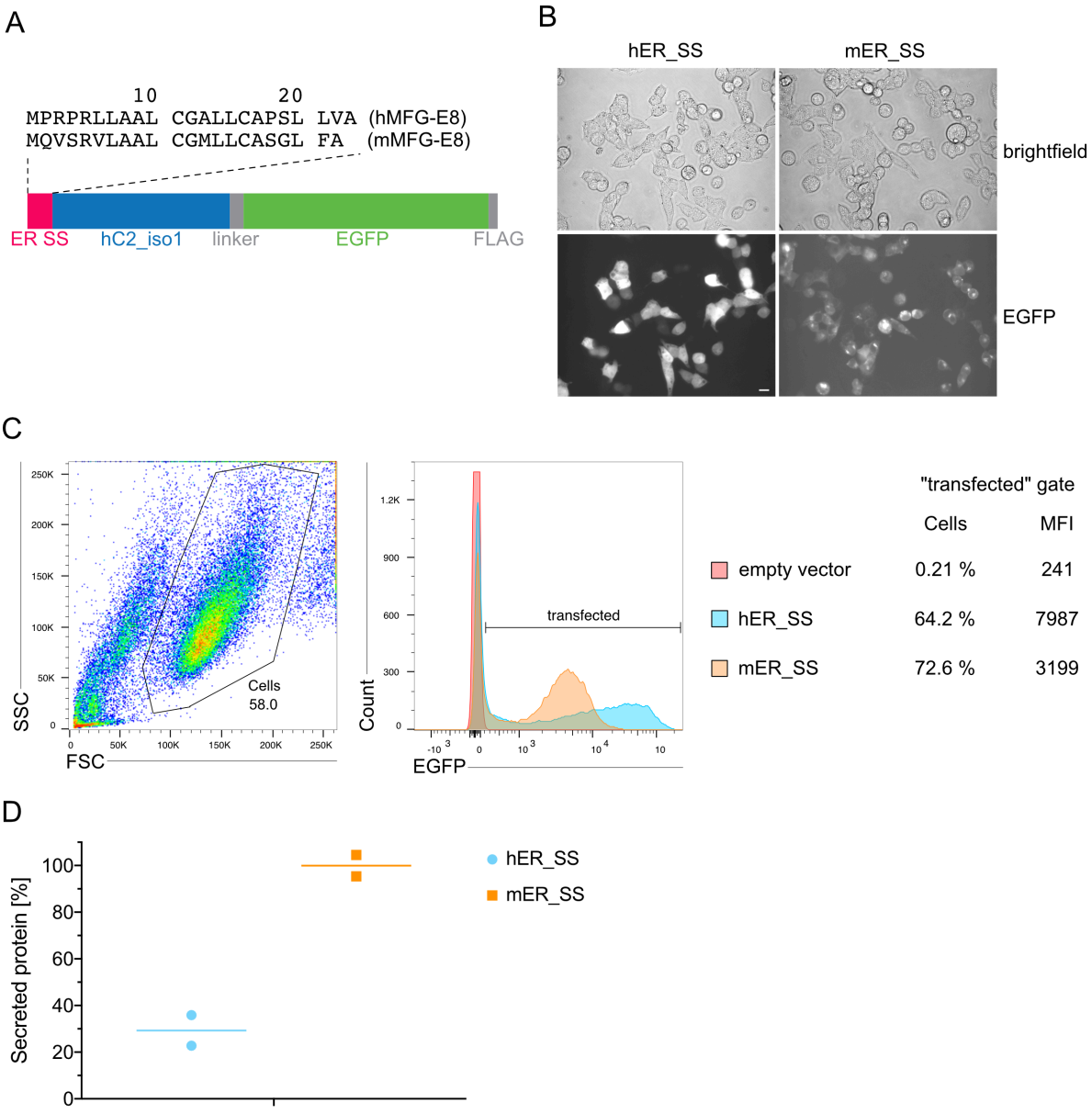

Fig. 5.1: The ER signal sequence of mMFG-E8 but not hMFG-E8 allows for efficient secretion of proteins from HEK cells

(A) The ER signal sequence (ER SS) of hMFG-E8 and mMFG-E8 was fused to the N-terminus of the hC2 domain. A C-terminal EGFP served as a reporter molecule.

(B) Fluorescence microscopy one day post-transfection revealed different effects of hER SS and mER SS on the localization of fluorescent proteins. Scale bar: 5 µm.

(C) Cells from (B) analyzed by flow cytometry. Live cells were gated and the respective population of transfected cells for both constructs compared to cells transfected with empty vector.

(D) Medium from transfected cells was processed three days post-transfection and the secreted protein measured in an anti-GFP ELISA. The mean of two independent experiments is given with the one from the mER SS construct set to 100%.

5.1 Using a mammalian expression system for MFG-E8 variant binding studies

5.1.2 Single domain studies reveal high binding activity for the hMFG-E8 C1 domain

For characterization of the single domain contribution in the binding event of hMFG-E8, full length as well as C1 and C2 as EGFP fusion proteins were created (Fig. 5.2 A). In an anti-GFP western blot the apparent MW of hC1-EGFP matched the expected 47 kDa, whereas hC2-EGFP and hMFG-E8-EGFP showed a higher apparent MW than the calculated 47.19 kDa and 69.97 kDa, respectively. For the latter two proteins a double band was detected (Fig. 5.2 B). In light of the high homology the strong difference between hC1-EGFP and hC2-EGFP might be surprising at first, but could be explained by the occurrence of four N-linked glycosylation sites in hC2. In full-length hMFG-E8, one additional site is present between C1 and C2 domain (Picariello et al., 2008).

The supernatant (SN) from transiently transfected HEK cells was then used in staining of mouse thymocytes with the recombinant proteins. To discriminate between apoptotic and necrotic cells, an amino-reactive live/dead (ld) dye was used. Note, that throughout this work both the apoptotic and necrotic cell population was pre-gated using the FSC/SSC parameters as shown in Fig. 5.2 C.
Only C1 and full length hMFG-E8 showed binding activity, while C2 failed to bind (Fig. 5.2 C). Both, full length and C1 bound to necrotic (ld^+ MFG-$E8^+$) as well as apoptotic (ld^- MFG-$E8^+$) cells (Fig. 5.2 C) and C1 caused a slightly different staining pattern as it revealed an MFG-$E8^{hi}$ and an MFG-$E8^{lo}$ population.
In case of C2, binding activity has been previously published: A comparable bacterially expressed Glutathione S-transferase fusion protein (GST-EGFP-mC2) reached its maximum staining capabilities around 1 µM, but still performed worse than the Annexin V control (Ye et al., 2013). This concentration exceeds the protein amount used for staining in this study by far. It is therefore possible that with higher C2 concentration in the HEK SN a staining could have been detected as well. Taken together, the results are especially stunning since C1 was not shown before in the literature to have binding activity and single domain studies were only performed with C2.

In case of poor protein yields and usage of almost pure concentrated cell culture supernatant for cell staining cells were found to be permeabilized, leading to the ld^- MFG-$E8^{hi}$ population in the hC1 staining panel. Permeabilization was proven when untreated thymocytes were sequentially stained first with amino-reactive live/dead eFluor780 dye, then hC1-EGFP and PI as post-staining live/dead dye prior to analysis. An $eFluor780^-$ PI^+ population of 37.7% revealed the permeabilization of cells upon exposure to high amounts of SN (Supp. Fig. 1).

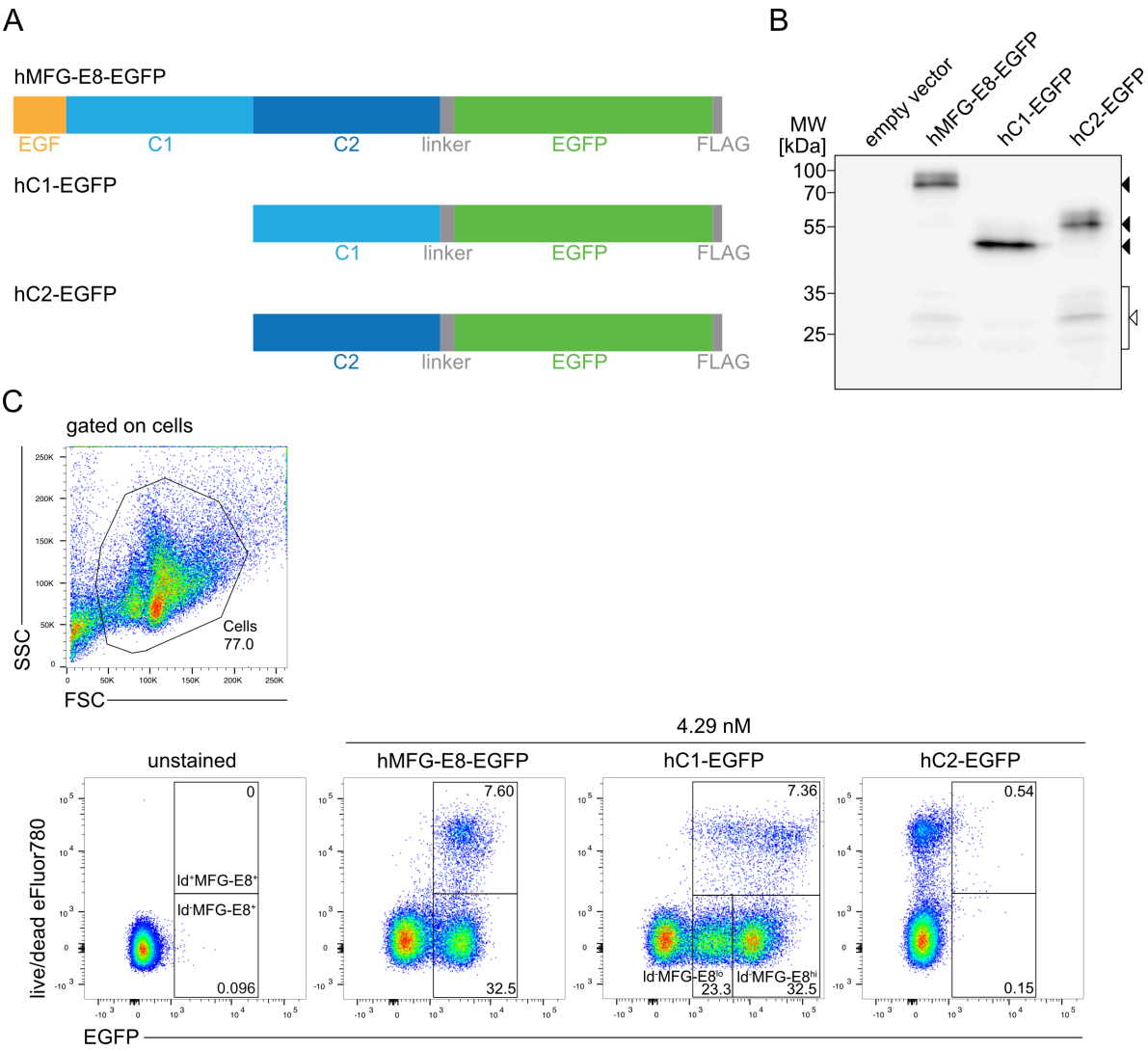

Fig. 5.2: The hMFG-E8 C1 domain shows strong binding to dying cells
(A) Schematic representation of full-length wildtype hMFG-E8 and the respective single PS-binding domains, hC1 and hC2 as EGFP fusion proteins. All protein domains are scaled according to their aa count.
(B) Supernatant from HEK cells transfected with empty vector or the respective constructs was analyzed for the secreted overexpressed proteins by anti-GFP western blot. Black arrowheads indicate the expected bands, the white arrowhead additional low-MW protein bands.
(C) Mouse thymocytes were treated with Staurosporine to induce apoptosis. Staining was performed with live/dead eFluor780 as viability dye and subsequently with equimolar amounts of full-length hMFG-E8 or single C domains.

However, full length variants did not bind this population. Due to simplicity of the assay and screening of only full-length variants in the following paragraphs, experiments were further conducted by staining of cells with proteins in SN from transfected HEK cells as described in this paragraph.

5.1 Using a mammalian expression system for MFG-E8 variant binding studies

5.1.3 A linker extension between C1 and C2 of hMFG-E8 increases binding properties in an *in vitro* assay primarily depending on linker length

Having shown that both, full length hMFG-E8 and hC1 bind to PS^+ cells (Fig. 5.2), we next studied the possibility that MFG-E8 with its two F5/8 type C domains does not rely solely on C2 in the binding event, as stated in the literature (Andersen et al., 2000, Andersen et al., 1997). An interesting additional fact is the preference of MFG-E8 for membranes with high curvature (Shi et al., 2004, Otzen et al., 2012). Furthermore, a relatively short 4 aa linker between C1 and C2 domain is highly conserved in all MFG-E8 homologues (*H. sapiens* NP_005919, *M. musculus* NP_032620, *B. taurus* NP_788783, *R. norvegicus* NP_001035276). With the two PS binding pockets of C1 and C2 most likely facing away from each other as depicted in a model for hMFG-E8 (Oshima et al., 2014) we hypothesized that parallel binding of both domains to relatively flat surfaces like whole cells is rather inefficient.

To provide additional space and potentially facilitate parallel binding of both C domains thus promoting an additive effect, extension of the 4 aa linker by additional 11 aa from the flexible hinge region of human IgG3 was realized (Fig. 5.3 A). In our binding studies wild type hMFG-E8 never matched the performance of mMFG-E8, but interestingly the linker extension (termed hMFG-E8_C1-15aaIgG3-C2) vastly enhanced binding of hMFG-E8 to dying cells, whereas the same modification abolished binding of the murine homologue (Fig. 5.3 B). For apoptotic cells (PI^- MFG-$E8^+$) and necrotic cells / debris (PI^+ MFG-$E8^+$) the modified human homologue showed drastically higher MFI values than the wild type (Fig. 5.3 C).

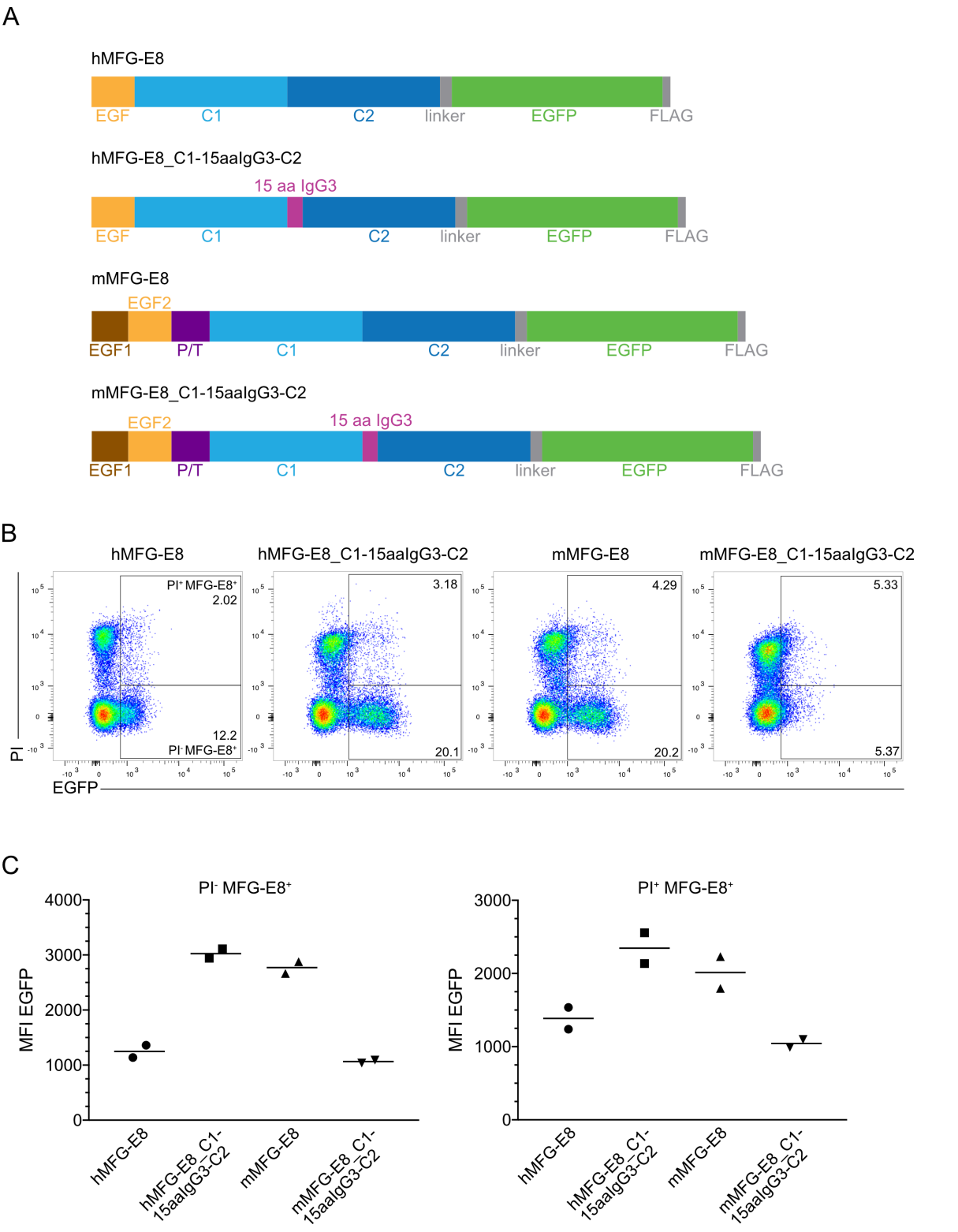

Fig. 5.3: A 15 aa linker separating C1 and C2 domain improves binding properties of hMFG-E8 but not mMFG-E8 in a comparative cell-binding assay

(A) Schematic representation of wild type hMFG-E8 and mMFG-E8 as well as the variants featuring a 11 aa sequence from the human IgG3 hinge region in addition to the natural 4 aa linker between C1 and C2 domain, all as EGFP fusion proteins.

(B) Staining of Staurosporine-treated mouse thymocytes with the protein variants. PI was used as viability dye.

(C) MFI analysis of the quadrants PI^- $MFG\text{-}E8^+$ and PI^+ $MFG\text{-}E8^+$ from (B). Two independent experiments are shown.

5.1 Using a mammalian expression system for MFG-E8 variant binding studies

We next wanted to characterize different linker properties responsible for increased binding of hMFG-E8:

(1) aa composition with concomitant flexibility / rigidity

(2) the length of the linker.

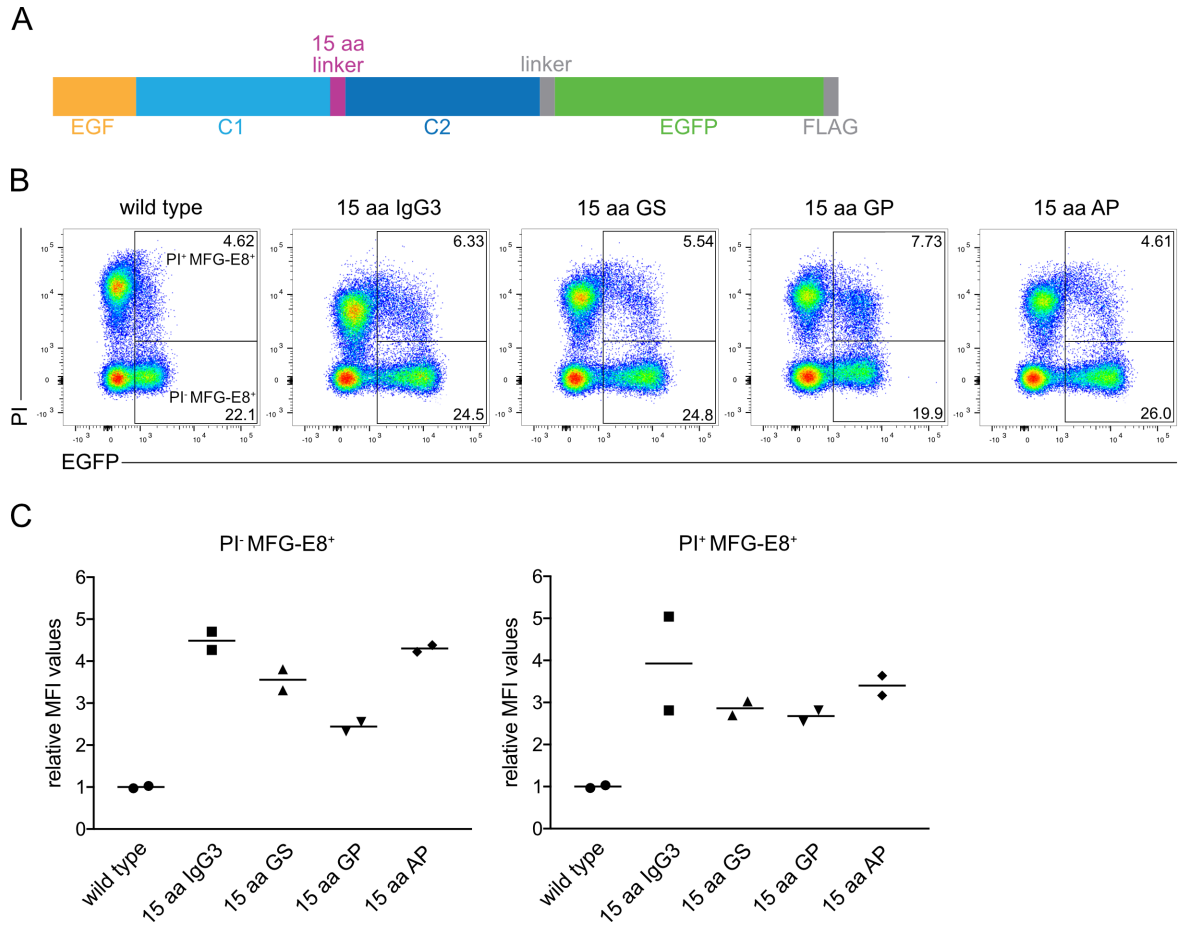

Fig. 5.4: Linker character has a minor influence on hMFG-E8 binding properties in a comparative assay

(A) A 15 aa long uniform linker of the composition GS, GP or AP was integrated between C1 and C2 domain of hMFG-E8.

(B) Staurosporine-treated thymocytes were stained with 15 aa long linker variants of varying character and wild type hMFG-E8 for comparison. PI was used as viability dye.

(C) Analysis of EGFP MFI values from two independent experiments of the gates PI^- $MFG\text{-}E8^+$ and PI^+ $MFG\text{-}E8^+$ as shown in (B). The mean of wild type hMFG-E8 was set to 1. Data shown in (B) and (C) were generated by Larissa Köppel and re-analyzed.

Both possibilities were investigated separately using different protein variants. First, the aa composition of the linker with a fixed length of 15 aa was altered. The IgG3 linker with supposed intermediate flexibility was changed to a glycine-serine sequence with alternating GS residues and concomitant high flexibility as well as two additional linkers glycine-proline (GP) and alanine-proline (AP) supposedly being more rigid due to the presence proline with

low conformational freedom in the peptide backbone (Richardson and Richardson, 1989) (Fig. 5.4 A).

Although the GP linker resulted in a lower MFI of PI^- $MFG\text{-}E8^+$ cells than the other linker variants, all variants with the linker extended to 15 aa performed better than wild type hMFG-E8 in the assay (Fig. 5.4 B and C).

Next, the GS linker was altered in length with the sequence spanning 4 – 59 aa (Fig. 5.5 A). Interestingly, longer linkers provided the variants with improved binding properties (Fig. 5.5 B) with the MFI values peaking for the variant with a 29 aa linker (Fig. 5.5 C).

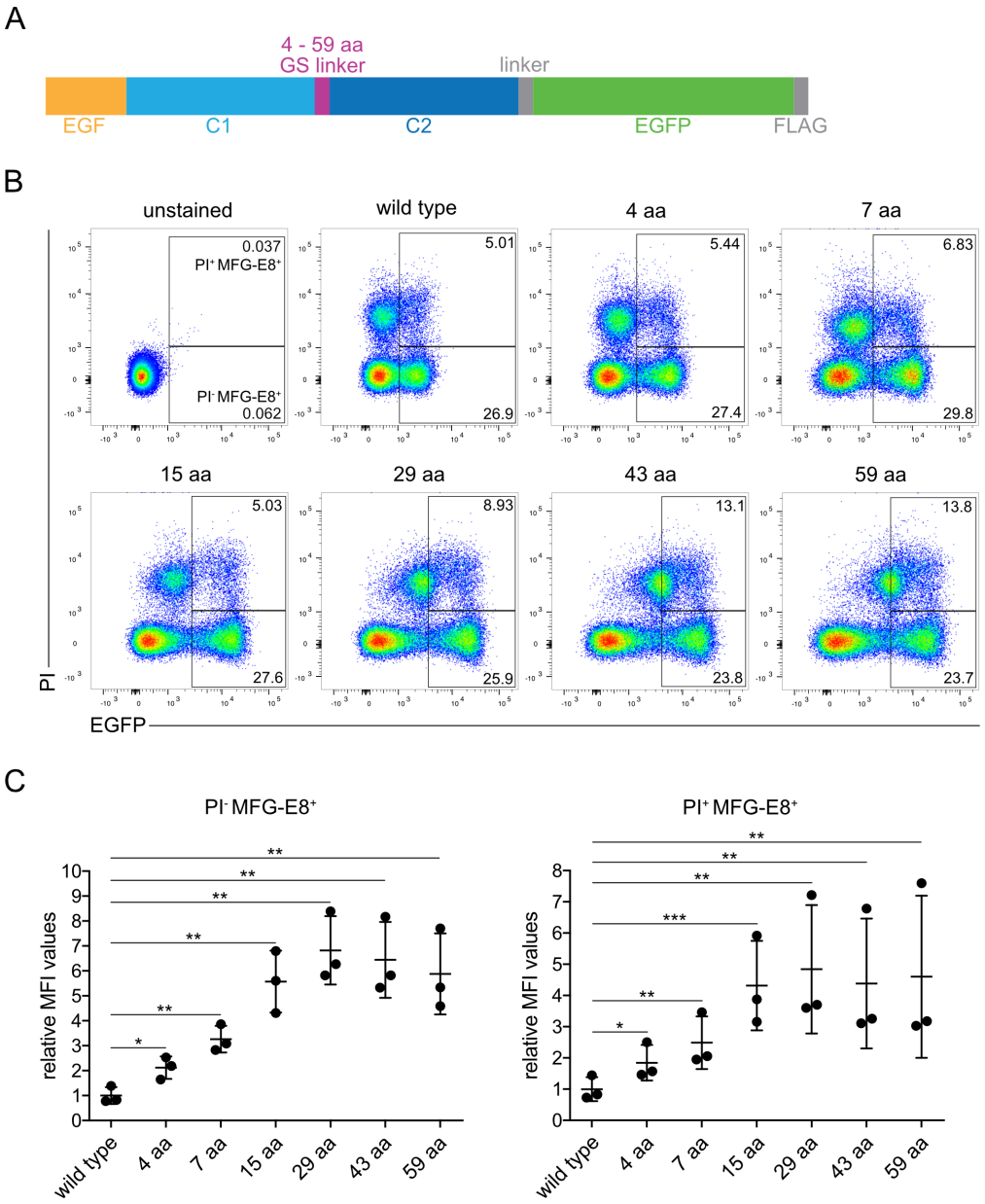

Fig. 5.5: Linker length has a dominant effect on hMFG-E8 binding properties in a comparative assay

(A) The GS linker separating C1 and C2 of hMFG-E8 was varied in length with 4 – 59 aa.

(B) Staining of Staurosporine-treated thymocytes with the constructs and PI as viability dye. The gate was individually adjusted to contain the EGFP positive populations.

(C) Analysis of EGFP MFI values of PI^- $MFG\text{-}E8^+$ and PI^+ $MFG\text{-}E8^+$ cells from three independent experiments as shown in (E). The mean of wild type hMFG-E8 was set to 1. Ratio-paired t-test, two-tailed, threshold $p < 0.05$. Data shown in (B) and (C) were generated by Larissa Köppel and re-analyzed.

However, when the albumin concentration was increased from 0.1% to 1% to stabilize the recombinant proteins, the beneficial effect of the linker was not observed anymore. An hMFG-E8 variant shown previously to have superior binding properties to the wild type protein did not perform as good as it did in the buffer with lower albumin concentration (Supplementary Figure 2).

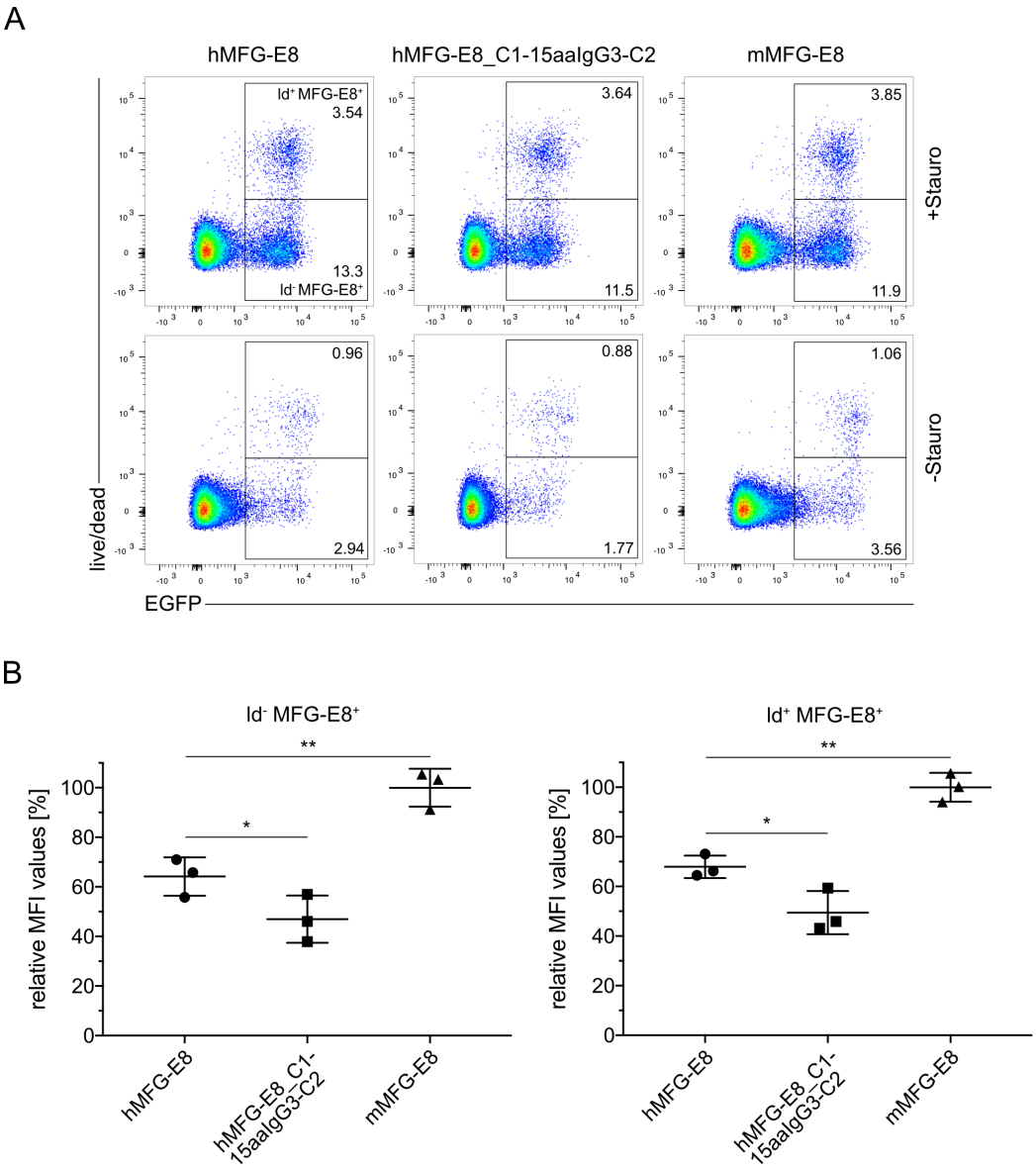

Fig. 5.6: Purified hMFG-E8 performs as well as purified hMFG-E8 with linker
(A) Thymocytes were either treated with Staurosporine for induction of apoptosis or left untreated and stained with equimolar concentrations of wild type hMFG-E8, mMFG-E8 or hMFG-E8 with the 15 aa IgG3 linker separating C1 and C2 domain. All proteins were purified via the C-terminal Flag tag in affinity chromatography under equal conditions. For analysis, gates were adjusted individually to contain only the positive populations. Live/dead dye eFluor780 was used.

(B) MFI values for EGFP from gates as shown in (A) panel +Stauro, separating live/dead$^-$ and live/dead$^+$ populations. Analysis of three independent experiments, the mean of the strongest signal (mMFG-E8) was set to 100% and all other values normalized accordingly. Statistics: Ratio-paired t-test, two-tailed, threshold $p < 0.05$.

In side-by-side comparison of wild type and the 15 aa IgG3 linker modified variant with both 0.1% and 1% Albumin no impact of the Albumin concentration on hMFG-E8 binding properties could be detected (Supp. Fig. 3A). Interestingly, performance of the linker variant again exceeded the wild type protein as already seen before (Supp. Fig. 3B). To shed light on this issue, both variants were produced in large scale in a fermenter, affinity purified via α-Flag affinity chromatography and compared with mMFG-E8 using the same buffer conditions. Test staining revealed mMFG-E8 to outperform hMFG-E8, as observed previously, but this time the IgG3 linker modification appeared to have no beneficial effect on hMFG-E8 (Fig. 5.6 A). This result was consistent over three independent experiments (Fig. 5.6 B). Up to this time, this experiment utilizing affinity purified proteins under the same, standardized buffer conditions, which have been shown to keep MFG-E8 stably in solution most likely mirrors the actual properties correctly. In the binding assays utilizing cell culture SN (Fig. 5.3, 5.4, 5.5) the linker modification could have improved hMFG-E8 stability in the medium and availability for binding. On the other hand enhanced formation of aggregates containing more GFP could have led to higher MFI values of the linker variants in cell culture SN. However, the exact factors leading to the observed superior performance need yet to be determined.

5.2 Bacterial production of full-length hMFG-E8

5.2.1 hMFG-E8 shows unspecific association with agarose beads in affinity chromatography purification

To lay the foundation for cost-effective and large-scale production of full length hMFG-E8 for future biochemical and biophysical analyses as well as diagnostic approaches, expression in *E. coli* was a promising pathway. Throughout several purification attempts of hMFG-E8 and mMFG-E8 single C domains and variants from bacterial lysates it was observed that a major fraction of the protein still remained associated with the agarose beads, especially after elution of GST-coupled proteins of interest (POIs) with free reduced glutathione from the respective beads.

However, this was not observed in the case of imidazole-mediated elution from Ni^{2+}-NTA beads. Ni^{2+} ions are immobilized on agarose beads in a complex with nitrilotriacetic acid linked

to the matrix material. They form the basis for interactions of proteins via polyhistidine stretches with the His_6 tag being most commonly used in purification of recombinant proteins.

In order to reveal the type of interaction with the column material, a hMFG-E8 variant from bacterial lysate was associated with Ni^{2+}-NTA beads and elution steps undertaken with an EDTA-containing buffer, binding all Ni^{2+} ions and resolving all specific interactions. Most of the contaminating endogenous *E. coli* proteins eluted from the beads, leaving an almost pure hMFG-E8 variant still bound to the beads (Fig. 5.7). Only imidazole was capable to remove residual bound protein. This shows that the type of interaction of MFG-E8 with agarose beads is mostly unspecific, only leaving the opportunity for single-step imidazole elution without further testing of other options. Most likely the C domains are responsible for the observed unspecific association as they were also previously identified as promoters of aggregation (Castellanos et al., 2016). For high yield and efficient elution from any agarose bead - based affinity chromatography system protein purification in this work was therefore restricted to immobilized metal affinity chromatography (IMAC) with imidazole elution.

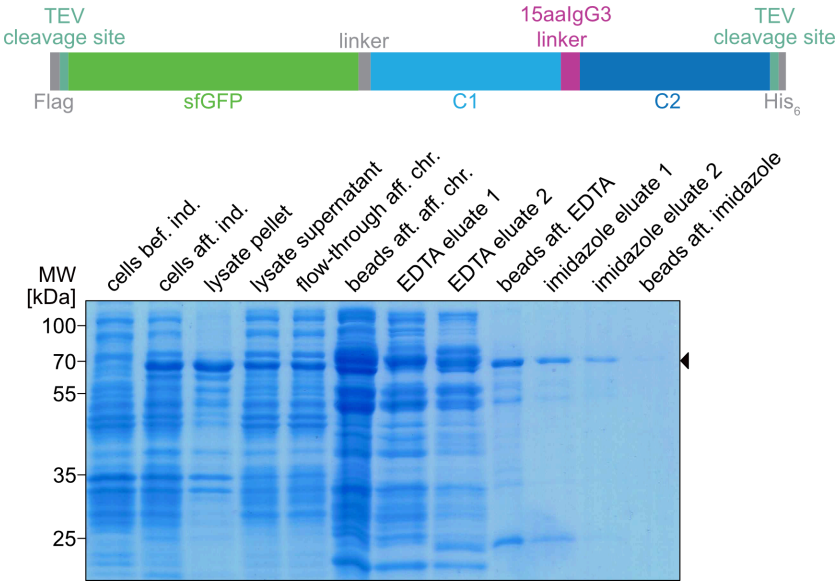

Fig. 5.7: An hMFG-E8 variant shows strong unspecific binding to Ni^{2+}-NTA agarose beads
An hMFG-E8 variant featuring only the two C domains in fusion with an N-terminal sfGFP (upper panel) was produced in Origami B and the soluble lysate supernatant incubated with Ni^{2+}-NTA agarose beads. Samples were taken of the beads after affinity chromatography, two elution steps with an EDTA-containing buffer, beads after that procedure, two subsequent elution steps with an imidazole-containing buffer and a final bead sample after imidazole elution. The target protein is marked by an arrowhead.

5.2 Bacterial production of full-length hMFG-E8

5.2.2 DsbC is a promising tag for soluble expression of hMFG-E8

For the attempted high-yield bacterial production of MFG-E8 single domains as well as probably the full-length protein, different N-terminal tags were tested. GST-SUMO3 proved to be a tag combination for successful soluble expression of MFG-E8 C domains using Origami B (DE3) as the host strain (see 5.3.2). Due to its mainly oxidizing cytoplasm (Prinz et al., 1997), this strain guarantees the establishment and maintenance of disulfide bonds, most likely critical for the structure and for folding of the MFG-E8 C domains. GST is a commonly used tag for affinity chromatography with solubilizing potential. Small-ubiquitin-like modifier (SUMO) shares this feature and opens the possibility of specific tag cleavage by a SUMO protease (Kimple et al., 2013).
As a challenging protein, the difficult-to-express C2 domain, isoform 3 of hMFG-E8 was chosen which is missing 51 aa (NCBI reference sequence: NP_001108086.1). This naturally occurring isoform has been previously selected in the work for this thesis for biochemical and structural investigation. So far, the GST-SUMO3 tag system did not yield soluble protein in the case of hC2 isoform 3.

Fusion tags with chaperone and redox activity, TrxA, DsbA and DsbC without their respective signal peptides were promising candidates for cytoplasmic soluble production. All of them were successfully employed in production of disulfide bridge-rich proteins (Nozach et al., 2013). Of the candidates tested, the thiol disulfide oxidoreductase DsbA and the disulfide isomerase DsbC proved to be very potent fusion partners for soluble expression of hC2 isoform3. Under non-reducing conditions, some of the protein displayed additional disulfide bonds which could result either from faulty establishment or the tags redox centers being trapped in an oxidized state. TrxA strongly increased production as well but led to a completely insoluble product (Fig. 5.8).
The weak induction band for the GST-SUMO3 fusion protein does not necessarily result from the tag choice but could also be owed to the *tac* promoter utilized in this pGEX-4T-1 construct whereas in all other cases the *T7* promoter in the pET15b backbone was applied.

5.2 Bacterial production of full-length hMFG-E8

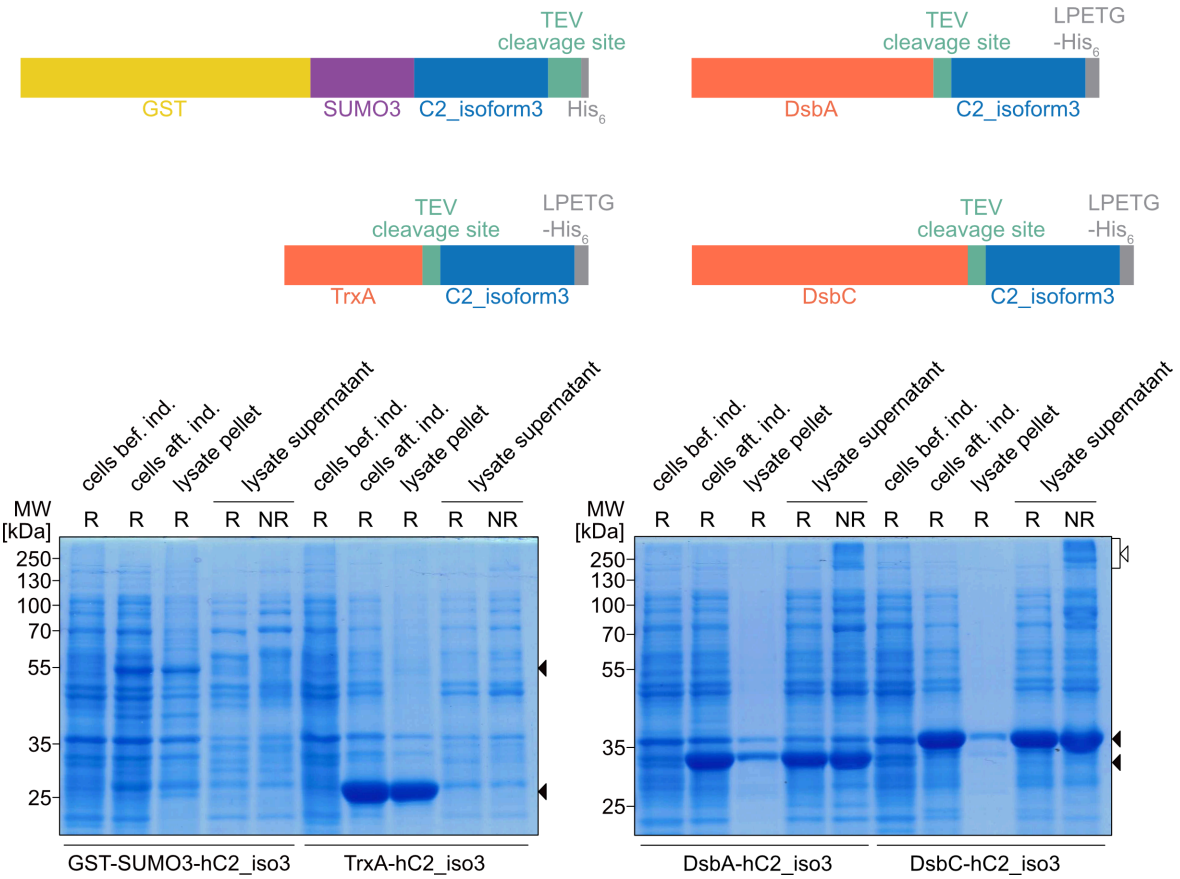

Fig. 5.8: DsbA and DsbC are promising tags for soluble expression of an MFG-E8 C-domain. Four different tags were N-terminally fused to the C2 domain (isoform 3) of hMFG-E8 (upper panel, schematic representation). Constructs were expressed in Origami B (DE3), cells lysed and the lysate separated into the soluble supernatant and insoluble pellet fraction by centrifugation. The respective products are indicated by black arrowheads, both under reducing (R) or non-reducing (NR) conditions. The white arrowhead shows a minor fraction of the soluble product shifted to high molecular weight due to the presence of additional disulfide bonds.

5.2.3 Functional, yet aggregated hMFG-E8 can be purified from *E. coli* with sfGFP showing a positional effect in N-terminal versus C-terminal tag choice

As the chaperone and disulfide bond isomerase DsbC proved to be a potent tag for the difficult-to-express hC2 isoform 3, utilization of this fusion partner in context of full length hMFG-E8_C1-15aaIgG3linker-C2 production was tested. Due to the ease of analysis in the purification procedure and functional assays by flow cytometry a fluorescent tag was applied. Since EGFP was previously published to form disulfide bond-linked oligomers in oxidizing environments such as the mammalian ER or the bacterial periplasm (Aronson et al., 2011) a superfolder (sfGFP) variant was chosen overcoming this obstacle in the oxidizing cytoplasm of Origami B (Prinz et al., 1997). The full length hMFG-E8 variant was successfully purified from Origami B (DE3) lysates via Ni^{2+}-NTA affinity chromatography.

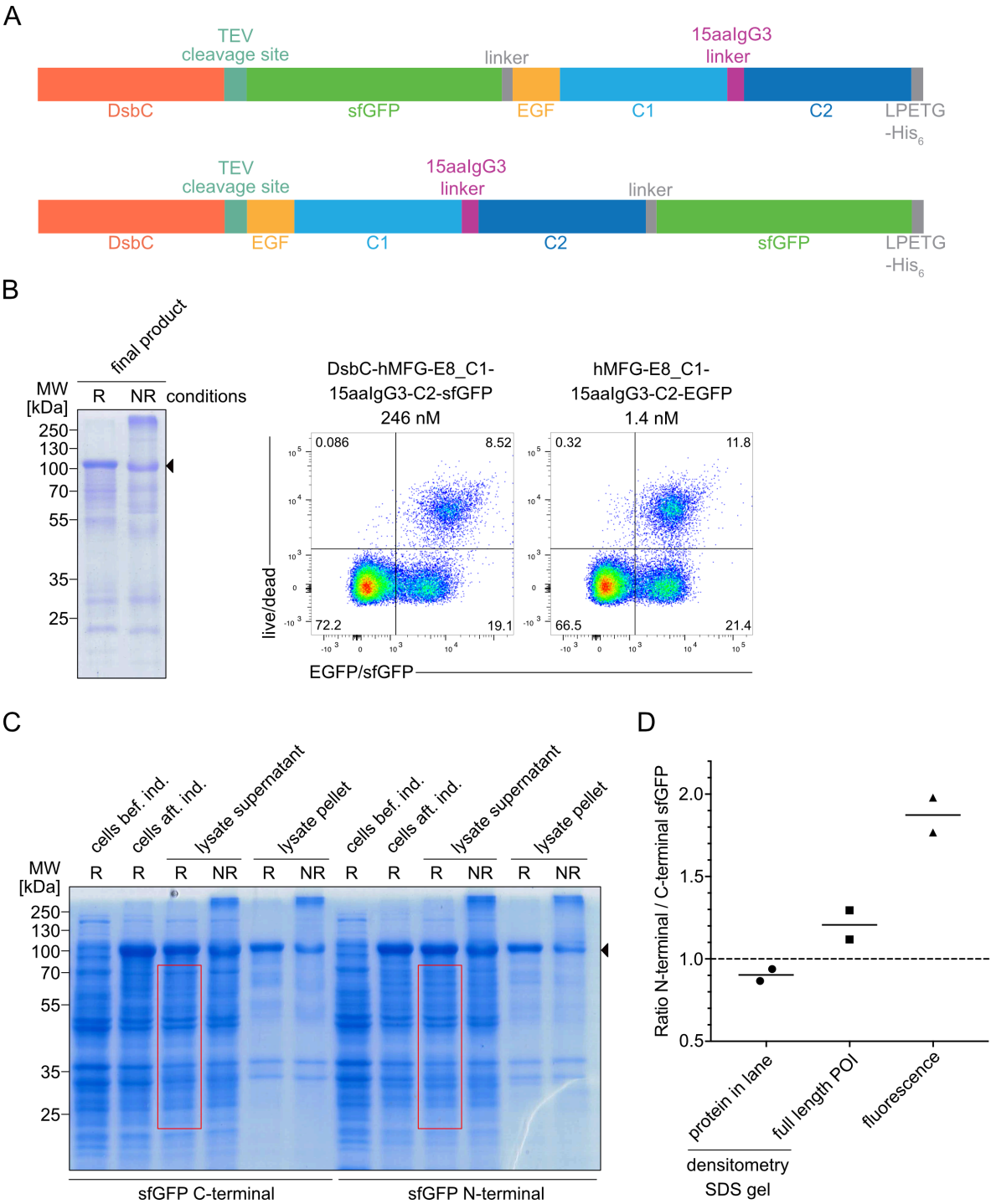

Fig. 5.9: A functional hMFG-E8 variant can be purified from bacterial lysates revealing a positional effect for sfGFP fluorescence

(A) The DsbC tag is followed by hMFG-E8_C1-15aaIgG3linker-C2 either with N-terminal or C-terminal fusion of sfGFP. The TEV cleavage site is embedded between two flexible GS linkers.

(B) The full length hMFG-E8 variant with C-terminal sfGFP was purified from Origami B (DE3), final product is shown under reducing (R) and non-reducing (NR) conditions. The arrowhead marks the full-length protein of interest (POI) (left panel). Staurosporine-treated thymocytes were stained with the bacterially expressed sfGFP or the HEK-expressed EGFP fusion protein, live/dead eFluor780 used as a viability dye (right panel)

(C) Constructs were produced in Origami B (DE3) and samples taken from the cells before induction (bef. ind.), after induction (aft. ind.) as well as from the lysate supernatant or pellet after centrifugation both in sample buffer with reducing (R) or non-reducing (NR) conditions. Red rectangles highlight the area for densitometric analysis of “protein in lane”. Full length POI is marked by the arrowhead

(D) Densitometric analysis of the lane “lysate supernatant, R” with respect to total protein in the lane and full-length POI as well as measured fluorescence of the lysate supernatant. Results are given as a ratio of N-terminal / C-terminal fusion of sfGFP. Analysis of two independent experiments.

The final product still featured a high fraction of contaminating proteins and possibly degradation products. Non-reducing conditions revealed the presence of some oligomers which could result from faulty intermolecular disulfide bonds between the protein of interest and/or linkage of the DsbC redox centers (Fig. 5.9 B, left panel). Staining of apoptotic thymocytes was successful, although a high protein concentration was necessary (Fig. 5.9 B, right panel). Note that protein concentration for the bacterially expressed sfGFP variant was determined by another method than the HEK-produced EGFP variant, Spectrophotometry and ELISA, respectively. For the EGFP fusion protein in HEK SN spectrophotometry was not amenable as quantification method due to the inherent fluorescence of the medium. For the sfGFP fusion protein ELISA could not be used since pure sfGFP was not available as standard and equal recognition like EGFP by the used antibodies was not guaranteed. In addition, all impurities in the protein preparation like degradation products are also measured by the approaches. Alongside with different spectral properties of the used fluorophores only a qualitative but no quantitative statement about the affinity of the bacterially produced protein can be made.

However, positioning sfGFP at the N-terminus of hMFG-E8_C1-15aaIgG3linker-C2 proved to be advantageous compared to C-terminal sfGFP in the bacterial expression constructs. In both cases robust expression could be achieved with a substantial fraction of the protein in the soluble supernatant of the bacterial lysate. sfGFP at the N-terminus led to a slightly increased yield but strikingly to much higher fluorescence than the C-terminal counterpart as determined by densitometry of the SDS PAGE protein bands and spectrophotometric determination of sfGFP fluorescence in the lysate supernatant (Fig. 5.9 C and D). By densitometric analysis of the proteins with lower MW than the full-length product less total protein was found in the lane for N-terminal than for C-terminal sfGFP. Therefore, the higher fluorescence could not be explained by the presence of fluorescent degradation products. It is rather possible that in case of C-terminally positioned sfGFP the already translated hMFG-E8 variant aggregates and interferes with proper folding of sfGFP as well as the maturation of the chromophore. Due to superior fluorescence, the study was continued with the N-terminal sfGFP fusion protein.

5.2 Bacterial production of full-length hMFG-E8

A

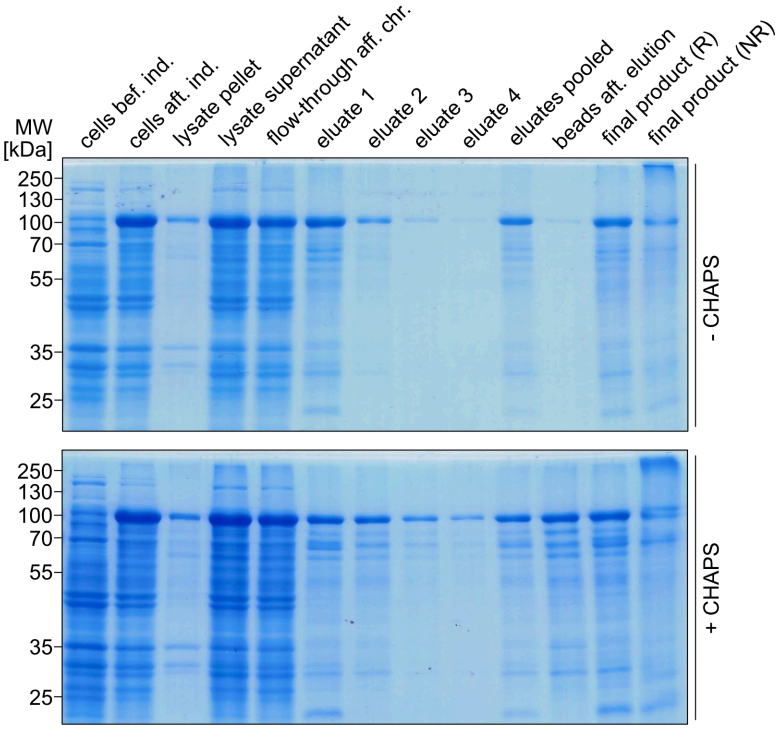

B

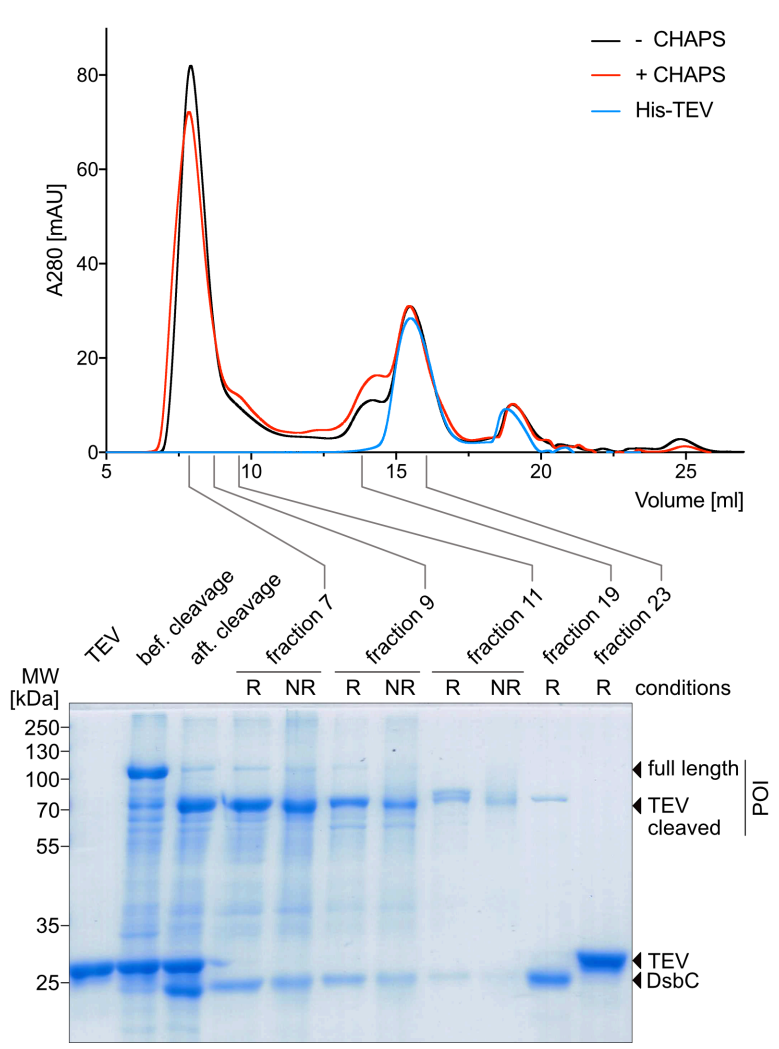

Fig. 5.10: A fluorescent hMFG-E8 variant can only be purified from bacterial lysate in an aggregated state.
(A) Lysate from Origami B cells expressing DsbC-TEV_cleavage_site-sfGFP-hMFG-E8_C1-15aaIgG3_linker-C2-LPETG-His_6 was centrifuged and equal amounts of supernatant and resuspended pellet loaded. Purification was continued either with or without the addition of CHAPS to the supernatant (lower and upper panel), which was subjected to Ni^{2+}-NTA affinity chromatography. Protein was eluted from the beads with an imidazole-containing buffer in four fractions (eluate 1-4) and fractions 1-3 pooled. The imidazole-free final product is shown under reducing (R) and non-reducing conditions (NR).
(B) 1 mg final product see (A) (POI, protein of interest), from conditions -/+ CHAPS was subjected to TEV cleavage to liberate it from the DsbC tag and loaded on a Superdex SD 200 Increase 10/300 GL SEC column, pre-equilibrated with 200 mM L-arginine and 137 mM succinate. Upper panel: Elution profile of both conditions with TEV protease for comparison. Lower panel: SDS gel analysis of TEV cleavage mix before/after cleavage and single fractions from SEC run under reducing (R) and non-reducing (NR) conditions. Only samples from the procedure "- CHAPS" are shown.

To avoid protein aggregation, purification of DsbC-TEV_cleavage_site-sfGFP-hMFG-E8_C1-15aaIgG3_linker-C2-LPETG-His_6 was attempted in the presence of CHAPS. This detergent was previously identified as a potent agent successfully counteracting the aggregation of hMFG-E8 and mMFG-E8 Fc fusion proteins expressed in CHO cells (Castellanos et al., 2016). Supernatant from bacterial lysate was split after centrifugation and 2% CHAPS added to one half. After a two-hour incubation at 4°C purification commenced with Ni^{2+}-NTA agarose beads. Only a minor fraction of the target protein bound to the beads, most of it was still found in the flow-through. This is most likely owed to highly unspecific binding to the beads with the protein occupying more space than in case of specific His_6 tag-mediated association. Subsequent wash and elution buffers did not contain detergent.

Interestingly, association of CHAPS-treated protein with the beads appeared to be stronger and largely withstood imidazole elution as a significant portion was still found on the beads after elution (Fig. 5.10 A). Analysis of the final product showed multiple bands from lower MW contaminating proteins, possibly products of degradation or premature translational stops. The DsbC tag was removed by TEV cleavage in the presence of the reducing agent DTT and the aggregation status tested in analytical SEC. CHAPS did not appear to have a beneficial effect since the target protein mostly eluted in the aggregate peak (see fractions 7, 9 and 11, Fig. 5.10 B), independent of the purification procedure. In these fractions also DsbC co-eluted, putatively associated with the aggregates due to its chaperone activity. Remarkably, the band pattern in SDS PAGE analysis was comparable under reducing and non-reducing conditions, indicating DTT-mediated resolution of faulty disulfide bonds and possibly correction by DsbC.

5.3 Purified C domains can be site-specifically modified in a Sortase reaction

5.3.1 A standard *E. coli* expression strain only allows for soluble expression of the mC2 domain

HEK-expressed single MFG-E8 domains as EGFP fusion proteins yielded the surprising result of a high binding activity for hC1, whereas hC2 underperformed in the assay (Fig. 5.2). This laid the foundation for future biochemical and biophysical analyses as well as binding studies to get further insight into the molecular characteristics of MFG-E8 C-domains and develop effective PS-binding probes. The demand for a high-yield expression system led to the utilization of *E. coli* as a promising host for production. So far, the bovine and murine MFG-E8 C2 domain and variants thereof were produced and purified from *E. coli* lysates (Shao et al., 2008, Ye et al., 2013, Reddy Nanga et al., 2007).

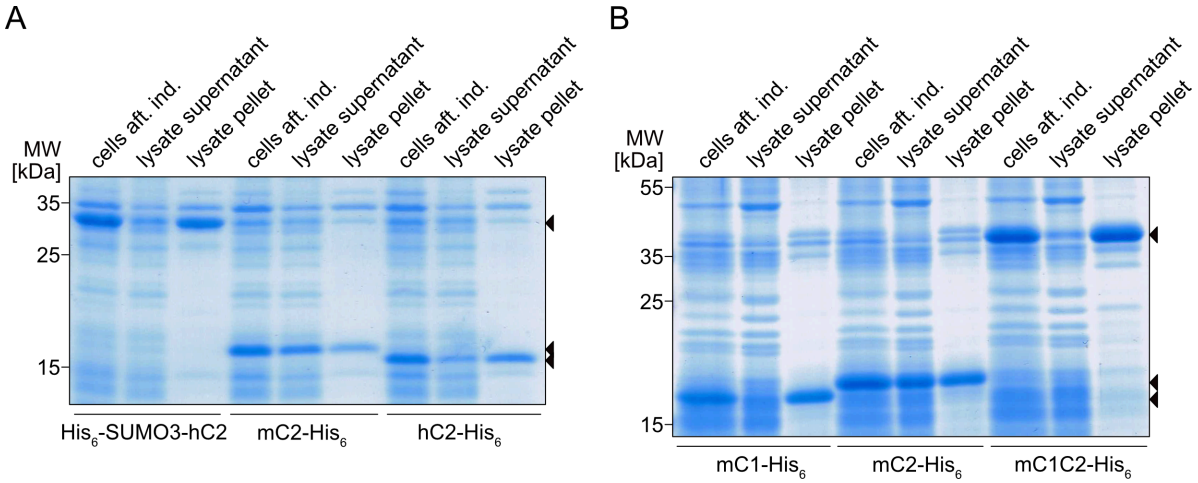

Fig. 5.11: Soluble expression of hC2 and mC1 domain is difficult in a standard bacterial expression strain
(A) BL21 (DE3) bacterial cells expressing the single mC2 / hC2 domain with C-terminal His_6 tag or the hC2 with an N-terminal His_6-SUMO3 tag were lysed in a simple buffer system (20 mM $NaPO_4$, 500 mM NaCl), the lysate was spun and equivalent amounts of the supernatant / pellet fractions analyzed by SDS PAGE followed by Coomassie staining. Black arrowheads indicate the recombinant protein bands. (B) BL21 (DE3) cells expressing either the mC1 / mC2 or the natural mC1C2 fusion protein with C-terminal His_6 tag were processed as done in (A).

In a simple $NaPO_4$ / NaCl buffer system for bacterial lysis, solubility was higher for the mC2 single domain than for hC2. Even SUMO, well known for enhancing protein expression and solubility (Marblestone et al., 2006) merely resulted in a stronger induction band but not higher yield of soluble protein (Fig. 5.11 A). A comparative analysis of mMFG-E8 C domain solubility in the standard expression strain BL21 (DE3) yielded almost completely insoluble mC1 and

mC1C2 domains with the majority of the overexpressed protein found in the pellet fraction (Fig. 5.11 B). A similar observation was made previously describing the human C1 domain as problematic in terms of low yields and significant aggregation upon expression in mammalian cells (Castellanos et al., 2016).

5.3.2 The Origami B (DE3) expression strain is a promising host for mMFG-E8 C domain production and purification

However, in order to harness the expected superior binding abilities of C1 we searched for a suitable expression and purification procedure. An important feature of the SUMO3 tag is the specific cleavage by the Senp2 protease with high catalytic efficiency leaving the target protein with its natural N-terminus (Marblestone et al., 2006). To aid purification, initially a GST moiety was chosen as an additional tag (Fig. 5.12 A). Specific association to beads with immobilized reduced glutathione and mild elution conditions are advantages in this setup (Harper and Speicher, 2011). The system was successfully employed in production of fairly pure mC2 single domain, though with low yield (work with Filip Zubic, data not shown).

A main characteristic of the C domains is the occurrence of disulfide bonds. Whereas the cytoplasm of all cells features a reducing environment, a special genetically modified *E. coli* expression strain termed Origami has these conditions shifted to an oxidizing cytoplasm favoring the establishment of disulfide bridges in proteins upon cytoplasmic expression (Prinz et al., 1997). Indeed, the ratio of soluble to insoluble protein was elevated for both mC1 and mC2 in Origami (Fig. 5.12 B). Interestingly, the GST-SUMO3 tag also yielded soluble protein for both C domains in BL21. The apparent solubilizing powers of the tag system in combination with the promising Origami expression strain allowed subsequent purification.

For high yield Ni^{2+}-NTA agarose beads were the choice for affinity chromatography. After immobilization of the target protein on the beads, the GST-SUMO3 tag was cleaved off by the SUMO protease Senp2. Even after excessive washing the tag was still found in the eluate which was not due to faulty disulfide bonds as demonstrated by non-reducing conditions (Fig. 5.12 C, left panel). Contaminating proteins were removed in a final SEC polishing step (Fig. 5.12 C, right panel) yielding approx. 7 mg pure mC1 protein per liter of culture medium. mC2 domain was purified according to the same protocol.

5.3 Purified C domains can be site-specifically modified in a Sortase reaction

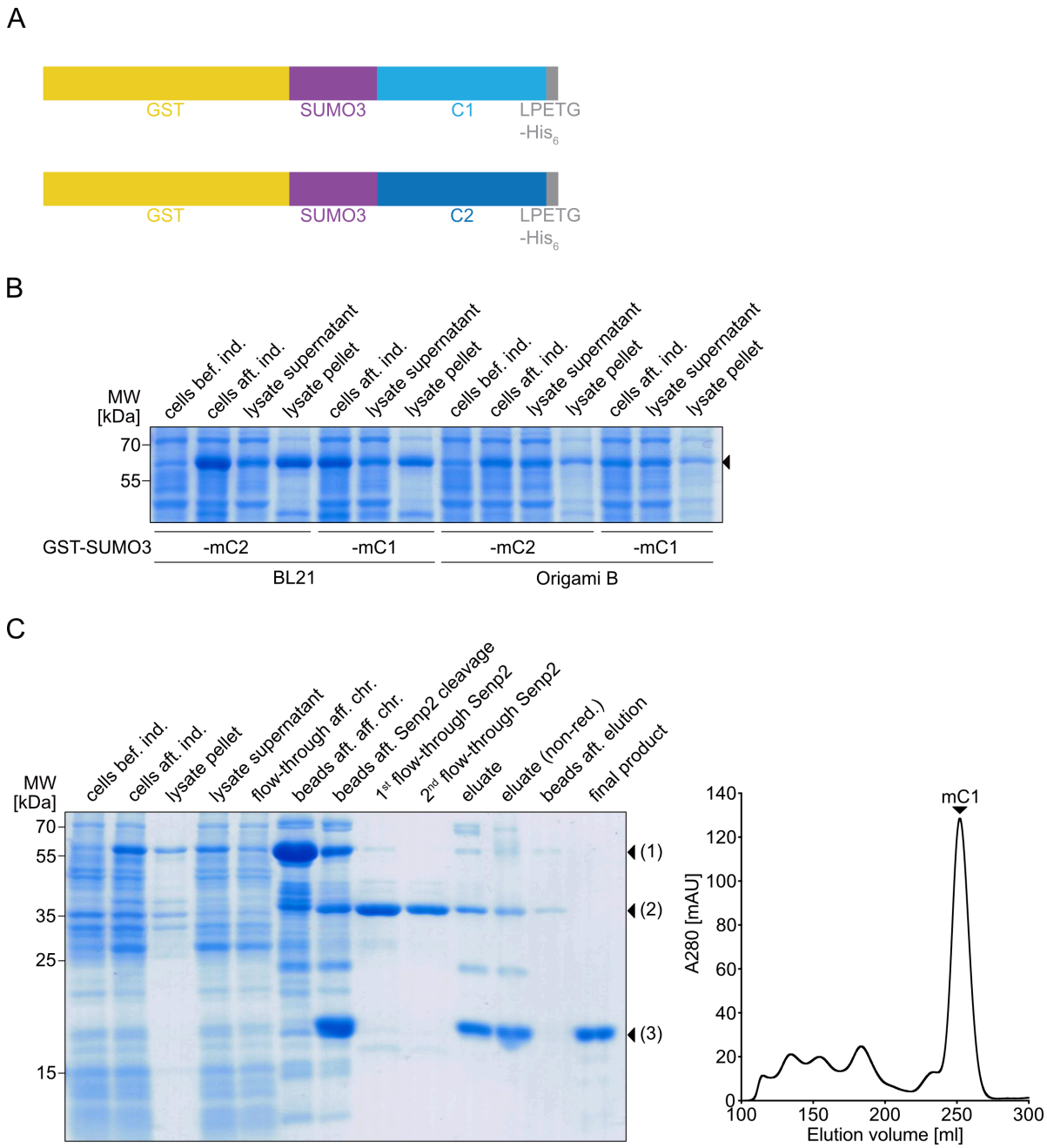

Fig. 5.12: A GST-SUMO3 fusion construct allows for soluble expression and successful purification of MFG-E8 single C domains from bacterial lysates

(A) Schematic representation of the utilized constructs, protein domains are drawn to scale according to their aa count. A combination of the GST-SUMO3 tags is followed C-terminally by the mC1 or mC2 domain with an additional LPETG-His_6 motif to enhance the options for modification and purification.

(B) Fusion proteins as displayed in (A) were produced in the *E. coli* expression strains BL21 (DE3) and Origami B (DE3) in parallel and cells lysed in 50 mM HEPES, 400 mM NaCl, 10% glycerol, pH 7.6. Equivalent amounts of the supernatant and pellet fraction after lysate centrifugation were analysed by SDS PAGE and Coomassie staining.

(C) GST-SUMO3-mC1 (1) was expressed in Origami B (DE3) and the lysate supernatant incubated with Ni^{2+}-NTA agarose beads. Most of the target protein bound to the beads (see flow-through affinity chromatography), where the tag was cleaved with Senp2 protease in two rounds. Most of the GST-SUMO3 tag (2) was found in the flow-through (1^{st} and 2^{nd}), mC1 (3) alongside with contaminating proteins was eluted with an imidazole-containing buffer. The final product was obtained by application of the pooled eluate fractions on a HiLoad 26/600 Superdex 200 pg SEC column and pooling of the respective peak fractions (SEC elution profile on the right side, mC1 peak indicated by black arrowhead).

5.3 Purified C domains can be site-specifically modified in a Sortase reaction

5.3.3 Purified mMFG-E8 C domains can be modified with chemical groups in a Sortase reaction

The purified single C domains featured an LPETG sequence at their C-terminus which is the recognition site for enzymatic modification using Sortase A from *Staphylococcus aureus*. Any (poly)peptide with an N-terminal triglycine motif will be attached to the C domain in the reaction, leaving room for versatile functionalization approaches by attachment of e.g. fluorophore or biotin coupled peptides (Fig. 5.13 A).

In this study, a pentamutant Sortase A was used with drastically enhanced catalytic activity (Chen et al., 2011). The Sortase reaction was set up with a standard buffer system (Guimaraes et al., 2013) at first but due to the aggregation propensity of the MFG-E8 C domains a custom-made Sortase reaction buffer based on the already published "optimized stabilizing buffer" (OSB) (Kooijmans et al., 2018) was tested for feasibility. No apparent differences were visible using linkage of a fluorescent FITC-conjugated peptide as a readout. The reaction could also be followed in the time course by downshift of mC1 in an SDS gel upon loss of its His_6 tag (Fig. 5.13 B). Using equimolar amounts of Sortase A and substrate protein, the reaction was completed after 40 min. In order to enhance the binding properties of the MFG-E8 single C domains an approach was planned to increase the avidity by linkage of a biotin-containing peptide with subsequent Streptavidin-mediated multimerization, a concept which proved to be successful in the generation of MHC "tetramers" for the detection of antigen-specific T cells (Altman et al., 1996).

Sortase reactions were set up to label purified mC1 and mC2 with a biotin-containing peptide and the resulting product was further purified by SEC. Although being similar in size, presumably structure and also hydrodynamic volume, mC2 eluted later from the SEC column than mC1 did (Fig. 5.13 C). This delayed elution property of C2 might be due to unspecific interactions with the column material. In addition, side products of the Sortase reactions could be observed for both C domains, one in the mC2 reaction also not eluting according to its expected hydrodynamic volume which speaks for a mC2 moiety being involved (Fig. 5.13 C). In conclusion, increase of fluorescence upon labeling with a fluorescent peptide and general downshift of the mC1 / mC2 domains in the SDS gel after loss of the C-terminal His_6 tag show successful and quantitative peptide labeling and demonstrate the versatility of the Sortase reaction.

5.3 Purified C domains can be site-specifically modified in a Sortase reaction

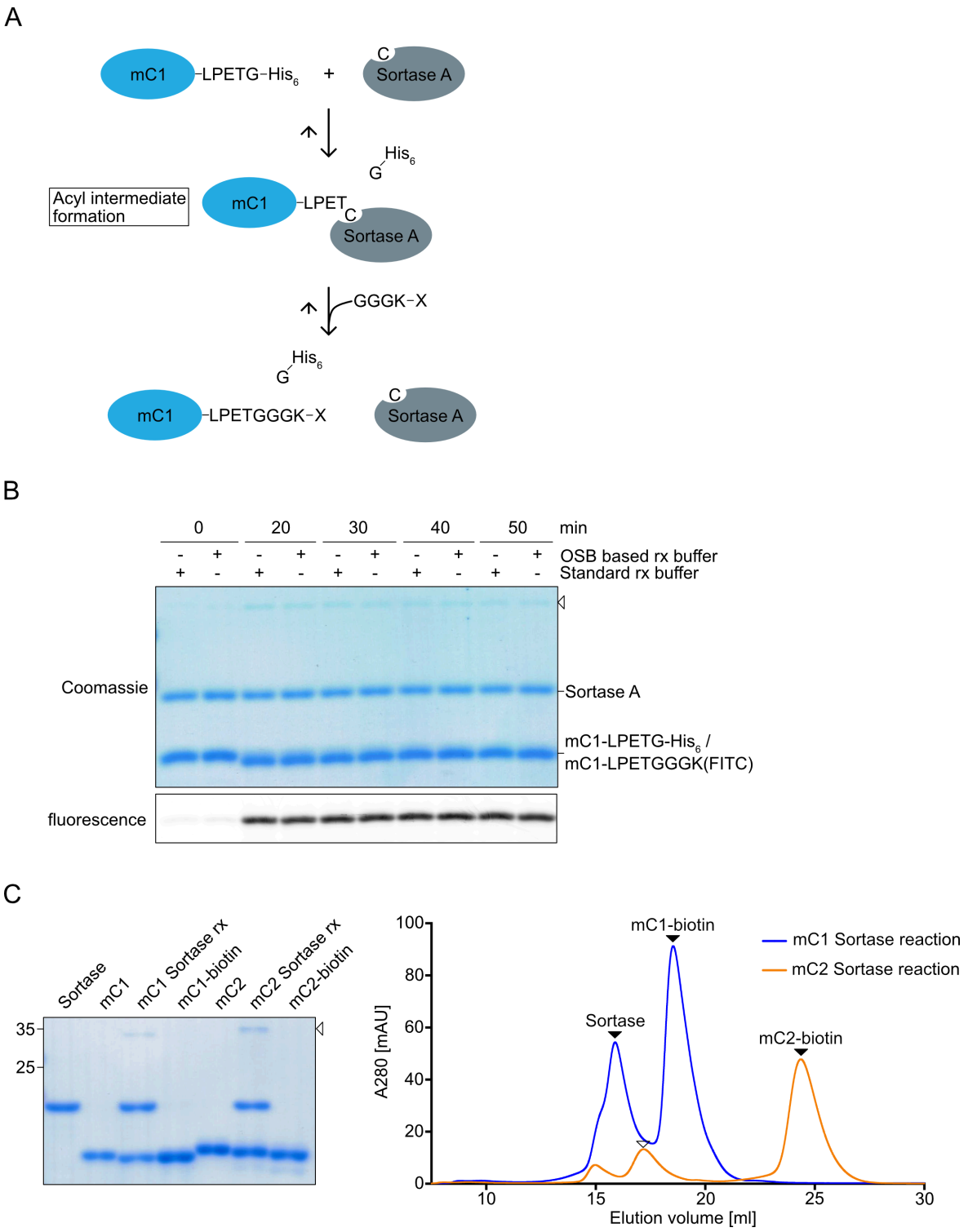

Fig. 5.13: Purified MFG-E8 C domains can be modified in a Sortase reaction with peptides carrying functional chemical groups

(A) The active-site cysteine of Sortase A cleaves the peptide bond between threonine and glycine in the LPETG Sortase recognition motif of mC1, forming an acyl intermediate and releasing the C-terminal glycine alongside with the His_6 tag. The triglycine motif of a peptide probe serves as a nucleophile to resolve the acyl intermediate and attach any desired functional component (X) to mC1. Unidirectionality of this reversible reaction is promoted by large excess of nucleophile.

(B) Sortase reaction mix was prepared with either standard reaction buffer or OSB-based reaction buffer. A GGGK(FITC) peptide was used as a nucleophile to follow the labelling reaction by analysis of in-gel fluorescence. Samples were taken at the indicated time points and reaction stopped by boiling in SDS sample buffer. The band for one side-reaction product is indicated by a white arrowhead.

(C) Samples from purified mMFG-E8 single C domains, Sortase reaction mix and final products conjugated with biotin-containing peptide after SEC purification. SEC elution profile of the Sortase reactions, the respective peaks are labelled with black arrowheads (right panel). The white arrowhead marks the same mC2 reaction side product as on the SDS gel.

5.4 Multimerized mMFG-E8 C domains can be used as PS detection tools

5.4.1 mC1 and mC2 show different biochemical properties

Streptavidin (SA) is a homotetrameric protein originated from the bacterium *Streptomyces avidinii* with each of its subunits harboring one high-affinity binding site for biotin (Weber et al., 1989). Using this unique feature, it is possible to combine several biotinylated proteins into a highly stable protein complex with e.g. increased avidity of binding domains. Since in the present case fluorophore-labeled SA variants were used with conjugated fluorophores possibly blocking single biotin-binding sites, the assembled protein complex will be referred to as “multimer” instead of the highest possible order “tetramer”.

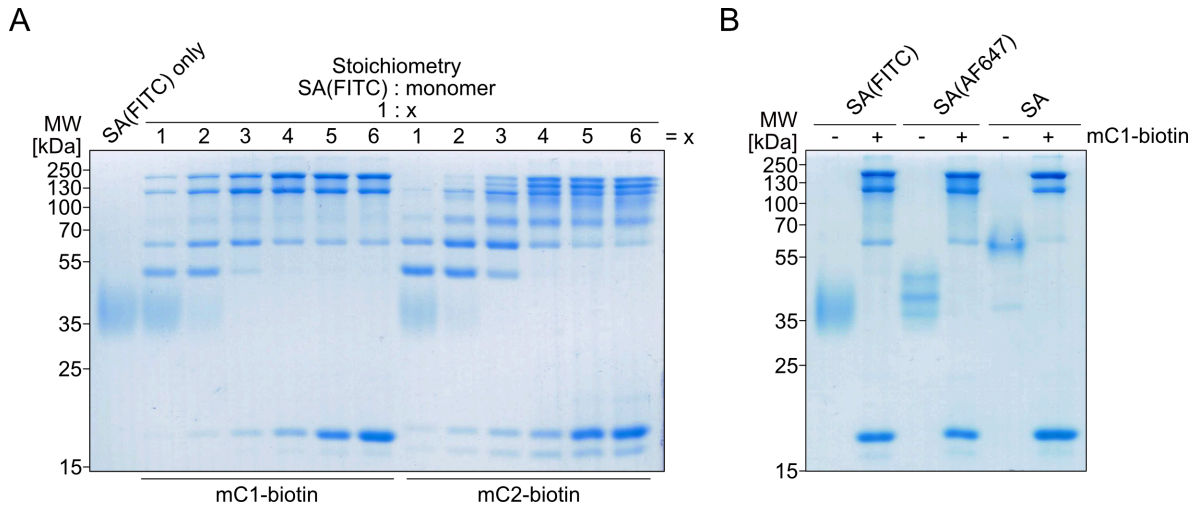

Fig. 5.14: mC1 and mC2 multimers show a distinct band pattern on an SDS gel independent of the used Streptavidin variant
(A) mC1-biotin and mC2-biotin were titrated in increasing stoichiometric ratios to Streptavidin(FITC) for multimer assembly, samples taken in reducing SDS sample buffer and analyzed by SDS PAGE without previous boiling to preserve multimer integrity.
(B) Three different Streptavidin variants, either unlabeled or conjugated to FITC and Alexa Fluor 647 fluorophores were used in multimer assembly with excess mC1-biotin and samples treated as done in (A).

5.4 Multimerized mMFG-E8 C domains can be used as PS detection tools

SDS PAGE analysis of mC1-biotin and mC2-biotin multimers revealed a characteristic band pattern each. Even excess monomer did not change this band pattern, incomplete multimerization can therefore be excluded as an explanation (Fig. 5.14 A). The second component, the used SA variant is also not responsible for this phenomenon, since SA with different labels or unlabeled SA produced the same result (Fig. 5.14 B). It is very likely that the prominent band pattern is just a result from the sample preparation procedure with the samples not being boiled prior to SDS gel analysis, which usually leads to proper protein unfolding and homogenous association with SDS. However, complete multimerization of the biotinylated monomers using SA was seen at a stoichiometric ratio of SA : monomer of at least 1 : 4, just as expected in theory.

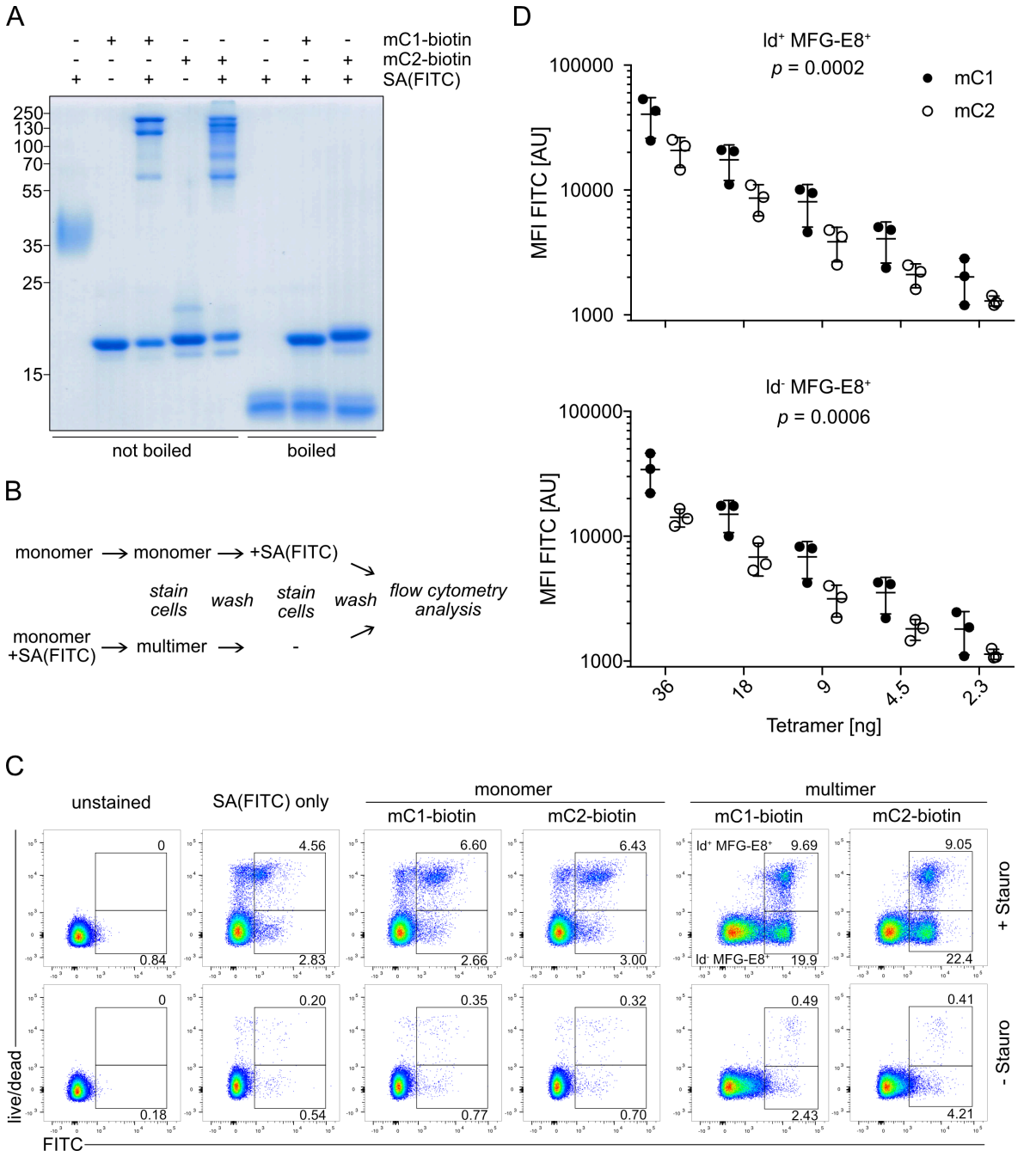

5.4 Multimerized mMFG-E8 C domains can be used as PS detection tools

Fig. 5.15: mC1 multimers show binding properties superior to mC2 multimers
(A) An equal amount of biotinylated single domains was either premixed with SA(FITC) for multimer assembly or left as monomers. Samples were taken and the multimeric status assayed on an SDS gel. All lanes contain the same amount of monomers and only two protein species each are involved in the assembly as shown by the boiled samples.
(B) Monomer was either used directly or pre-assembled as multimer to stain thymocytes. Excess protein was removed by a washing step and cell-associated monomer stained with SA(FITC). After a second washing step, cells were analyzed by flow cytometry.
(C) Mouse thymocytes were either treated with Staurosporine or left untreated and stained as shown in (B). For multimer analysis, the gates were adjusted individually to contain the positive populations. Monomers were gated according to the unstained control. Live/dead eFluor780 was used as viability dye.
(D) MFI analysis of a titration series using the gates as shown in (C). For reasons of simplicity, full tetramerization was assumed in the calculation of the amount of protein used for staining. Ratio paired t-test, two-tailed in triplicates over all titration steps (5 pairs of triplicates).

As multimer assembly was found to be successful and complete the binding activity and performance of the bacterially produced MFG-E8 PS binding domains were to be tested next. The same amount of biotinylated mC1 and mC2 domain was either pre-assembled with SA(FITC) to yield multimers or left in their monomeric state. SDS PAGE analysis revealed complete multimer assembly (Fig. 5.15 A). Monomers and multimers were added to cells and bound monomers additionally stained with SA(FITC) for analysis by flow cytometry (Fig. 5.15 B). Multimers showed strong binding activity and vastly outperformed the respective monomers due to their increased avidity as expected. Binding of monomers was only slightly above background staining of SA(FITC) and seemed to be stronger for the $Id^+MFG\text{-}E8^+$ population than $Id^-MFG\text{-}E8^+$ (Fig. 5.15 C). MFI analysis showed the mC1 multimers to perform significantly better than their mC2 counterparts by almost a factor of 2 over a wide titration range (Fig. 5.15 D). Whether this effect results from the inherent binding properties of both domains or only mirrors their binding activity in multimer context cannot be finally stated. Further experiments with purified multimers will be necessary to finally conclude on these differences.

The finding of mC1 and mC2 multimers displaying differences in binding activity raised interest in biochemical characterization of the two separate PS binding domains. Although C1 and C2 of MFG-E8 are highly homologous, they can furthermore be distinguished by two molecular characteristics. Both feature disulfide bonds spanning from their very N- to the C-terminus most likely providing them with enhanced stability in the context of MFG-E8 as an extracellular protein. mC1 harbors one additional disulfide bond close to the C-terminus. The presence of these disulfide bonds was already proven for the bovine MFG-E8 homologue using mass spectrometry (Hvarregaard et al., 1996).
Strikingly, in the same region an asparagine residue is highly conserved in the C2 domain (Fig. 5.16 A). In another report, just this residue was found to be present in a distorted conformation

within the polypeptide backbone placing it in the disallowed region within a Ramachandran plot (Shao et al., 2008). The authors hypothesized about a role of the asparagine residue serving as a switch for conformational change upon membrane binding as it was already observed for the C2 domains of blood coagulation factor V and VIII. In a 5,5'-Dithiobis-2-nitrobenzoeacid (DTNB) assay probing for free thiols, the bacterially produced mC1 and mC2 domain were found to be fully oxidized whereas free thiols in EGFP produced under reducing conditions were accurately determined (Fig. 5.16 B). Interestingly, mC1 proved to be significantly less stable than mC2 in a thermal shift assay using two buffer conditions, OSB which was the main buffer system in this work and standard PBS (Fig. 5.16 C). This was surprising since it seemed likely for the second disulfide bond to provide mC1 with additional stability. With these findings at hand it is tempting to speculate about a critical impact of these molecular features on mC1 and mC2 binding activity.

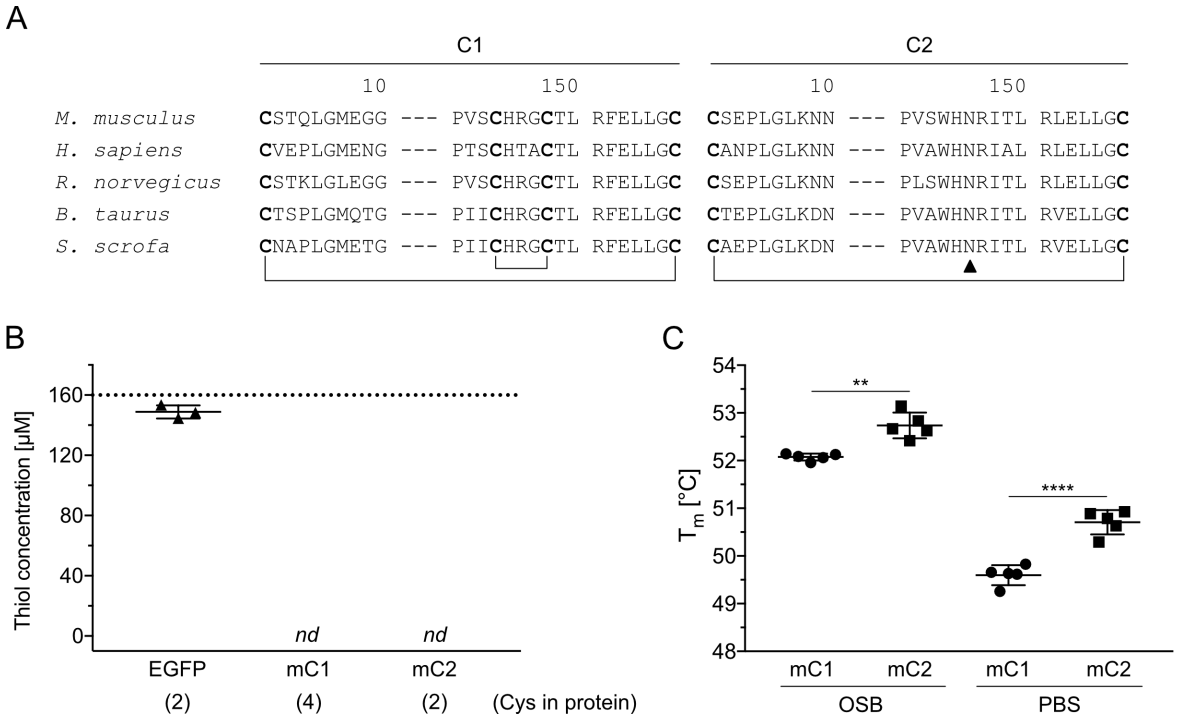

Fig. 5.16: mC1 features an additional disulfide bond not providing enhanced stability compared to mC2

(A) Alignment of MFG-E8 C1 and C2 domains from sequenced vertebrate homologues. N- and C-termini are linked by a disulfide bond, C1 features an additional one. C2 is characterized by a conserved asparagine residue in the same area (black arrowhead).

(B) Free thiol groups in 80 µM denatured protein each were determined in a chromogenic DTNB assay using a cysteine standard curve. The number of cysteine residues per protein is given in brackets, the dotted line marks the theoretically expected value for two free thiols as accurately measured for EGFP. Oxidized cysteine residues in mC1 and mC2 could not be detected (*nd*).

(C) In a thermal shift assay, mC2 is significantly more stable than mC1 in both OSB and PBS. Values for the minima of normalized curves from the first derivative representing T_m are shown. Pooled data from five experiments (ratio paired t test, two-tailed), each data point originates from the mean of three technical replicates.

5.4 Multimerized mMFG-E8 C domains can be used as PS detection tools

5.4.2 The mC1 multimer is a Ca^{2+}- independent alternative to Annexin V

However, the superior binding properties of mC1 multimers led to the decision to focus on them in continuation of the project. A common, already established tool for the detection of cell death is Annexin V (Vermes et al., 1995). The main ligand for Annexin V is PS, although PE can support the binding event. Importantly, binding is dependent on Ca^{2+} and most effective with concentrations > 3 mM (Stuart et al., 1998). It was therefore important to verify whether the mC1 multimers stain cell populations comparable to Annexin V.

Mouse thymocytes were again treated with Staurosporine and single- as well as double stainings with both reagents performed using a Ca^{2+}-containing buffer. Indeed, both mC1 multimer and Annexin V recognized the same populations and the staining was strongly increased after Staurosporine treatment, indicating that the staining was specific for dying cells (Fig. 5.17 A). When using standard FACS buffer without considerable amounts of Ca^{2+} ions, only the multimer staining prevailed, while Annexin V failed to bind. Binding specificity of the multimer proved to be also comparable to full length HEK-produced and purified mMFG-E8-EGFP (Fig. 5.17 B). These results opened the possibilities for usage of the mC1 multimer in various buffer systems as a replacement for Annexin V and an inexpensive alternative to HEK-produced mMFG-E8, most importantly without the dependence on Ca^{2+} ions.

5.4 Multimerized mMFG-E8 C domains can be used as PS detection tools

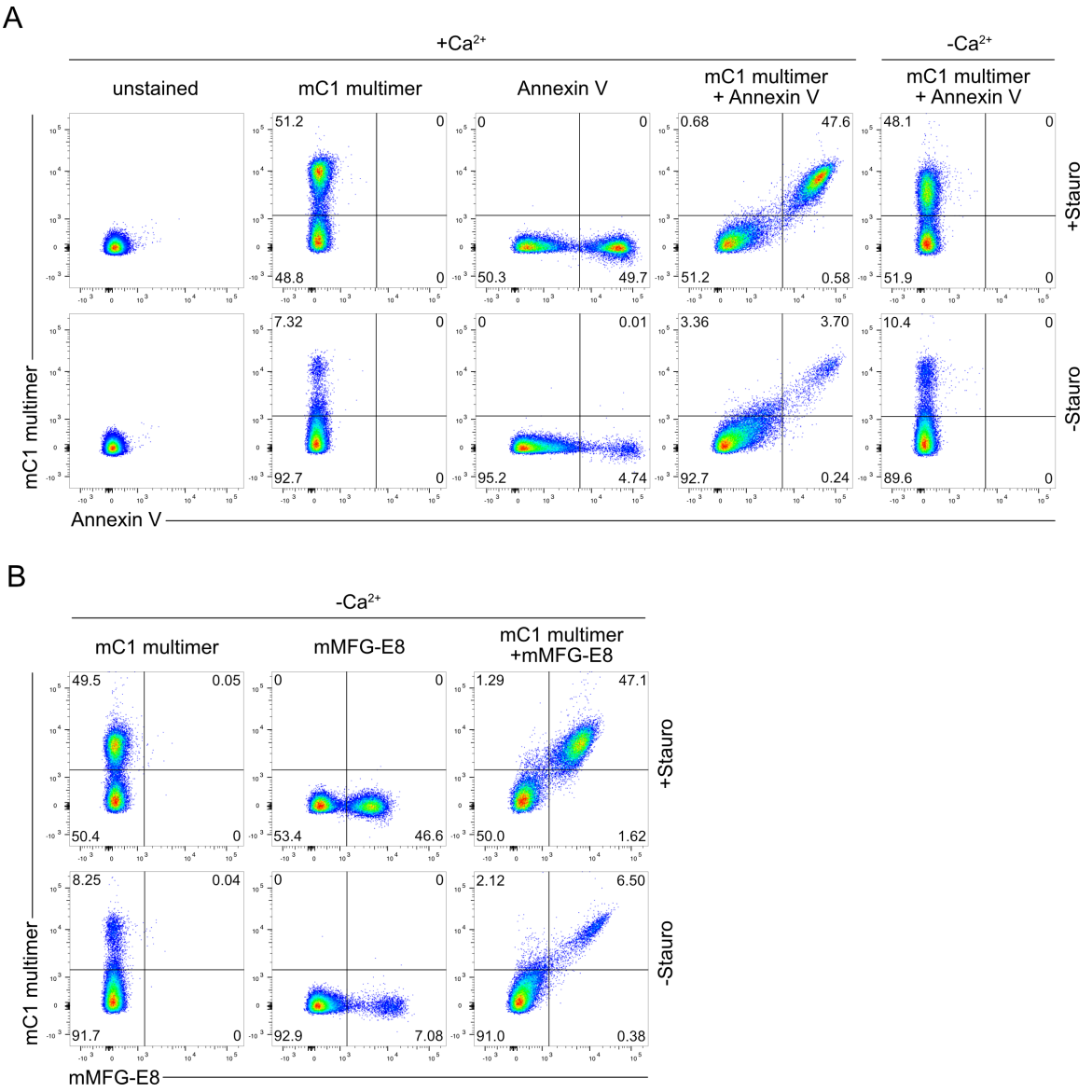

Fig. 5.17: mC1 multimers recognize the same cell populations as Annexin V and full length mMFG-E8-EGFP in a Ca^{2+} - independent fashion

(A) Mouse thymocytes, treated with Staurosporine or left untreated were either stained with mC1 multimer (AF647) or Annexin V (FITC) alone or in combination using a commercial Annexin V binding buffer (+Ca^{2+}) or standard FACS buffer (-Ca^{2+}). For analysis, cells were gated using FSC/SSC as shown in Fig. 5.2.

(B) Staining and analysis performed with mMFG-E8-EGFP and mC1 multimer (AF647) as done in (A) but only in standard FACS buffer.

5.4 Multimerized mMFG-E8 C domains can be used as PS detection tools

5.4.3 The mC1 multimer can be used for dead cell removal *in vitro*

With any buffer restrictions relieved from the system, a possible application of the mC1 multimers was the removal of PS-positive particles such as necrotic and apoptotic cells or debris from cell suspensions. Especially said cells interfere with e.g. RNA sequencing approaches due to a high amount of structurally compromised RNA and need to be excluded from the analysis (Szabo et al., 2019, Carter et al., 2018, Chen et al., 2019, Ilicic et al., 2016). Furthermore, they are difficult to remove, only accomplishable by time-consuming FACS sorting which is not available to every laboratory. Dead cell depletion kits are commercially available and rely on Annexin V binding with the Ca^{2+} binding buffer potentially interfering with downstream analysis of the cells.

To test the applicability of mC1 multimers in a dead cell depletion assay, mouse splenocytes were prepared. These cells naturally feature a high amount of removable particles posing a suitable challenge for the assay. Cells were stained with multimer or HEK-produced mMFG-E8-EGFP as a control. Specific depletion was attempted by incubation of the cells with magnetic beads, covalently coupled to anti-Streptavidin antibody targeting the respective epitopes on the multimer. Samples were also taken from cells without the addition of beads as an additional control (Fig. 5.18 A).
Analysis was performed by categorization of different populations: (I) $Id^{+}MFG\text{-}E8^{+}$ for necrotic cells and debris, (II) $Id^{-}MFG\text{-}E8^{hi}$ for apoptotic cells, (III) $Id^{-}MFG\text{-}E8^{lo}$ for cells in an early apoptotic stage. Whereas the latter population remained largely unaffected, significant specific multimer-mediated depletion was proven regarding populations (I) and (II) (Fig. 5.18 B).
The percentage of live cells was improved from 77% before depletion to 93% (Fig. 5.18 C) and 70% of the cell input was recovered (Fig. 5.18 D).
The usage of mC1 multimer for specific depletion of debris, necrotic and apoptotic cells therefore proved to be a powerful, buffer-independent tool to increase the percentage of live cells in a cell suspension for downstream approaches.

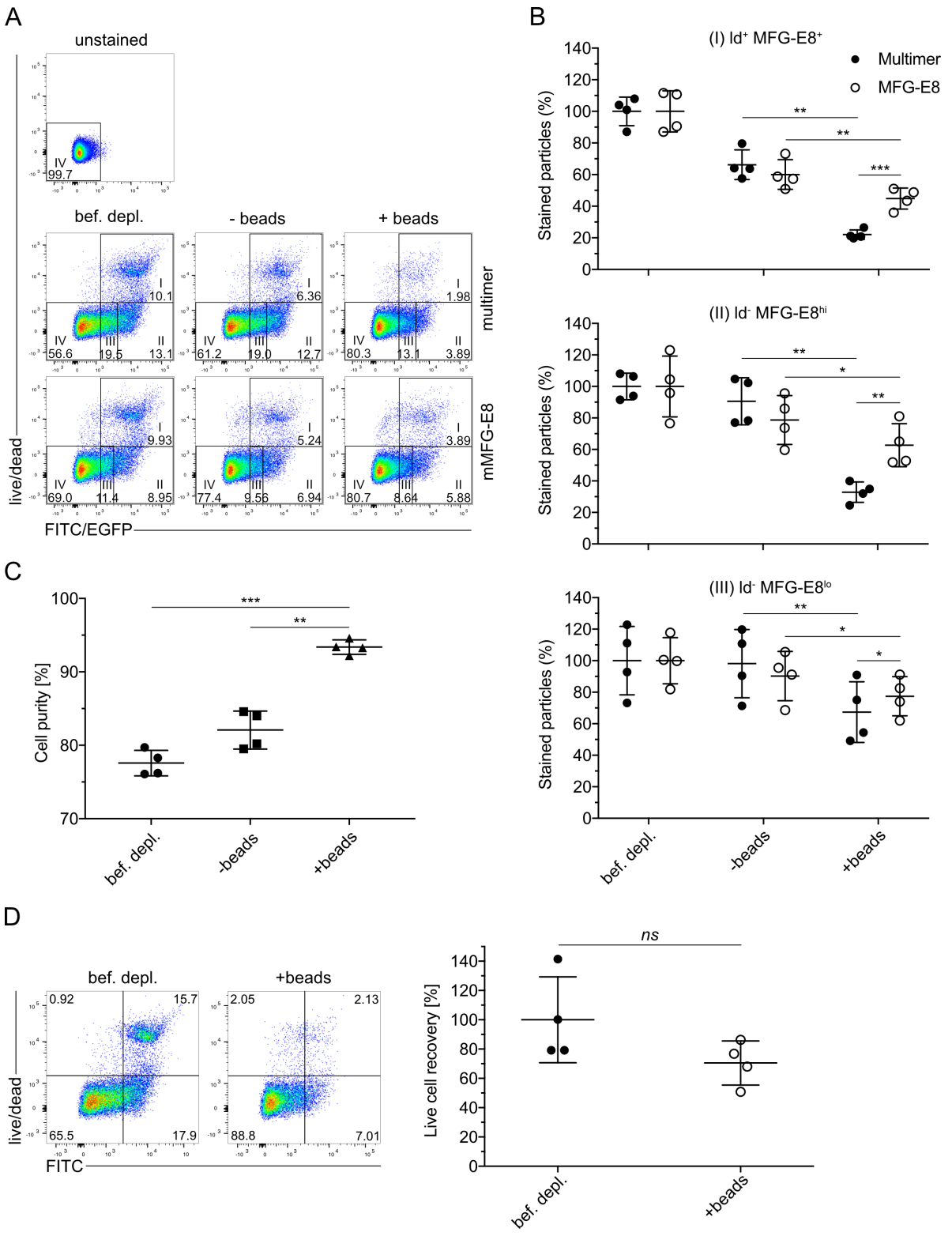

Fig. 5.18: mC1 multimers can be used for efficient depletion of dead cells and debris from a cell suspension

(A) Mouse splenocytes were prepared and stained with live/dead eFluor780 and either mC1 multimer (FITC) or mMFG-E8-EGFP. Cells were either left untreated (bef. depl.), added to α-Streptavidin coated beads for depletion of PS positive particles (+beads) or underwent the procedure without addition of beads (-beads).

(B) Analysis of depletion for multimer- and MFG-E8-coated particles using the gates I, II and III as shown in (A). Four independent experiments, statistical significance $p < 0.05$; ratio paired t test, two-tailed.

(C) Analysis of live cells and increase of cell purity from the multimer coating approach using the gate IV as shown in (A). Four independent experiments, statistical significance $p < 0.05$; ratio paired t test, two-tailed.
(D) Analysis of total cell recovery using flow cytometry. Samples of multimer-coated cells were taken before depletion and after addition of beads and events counted using a constant flow rate and recording time. Prior to analysis, autofluorescent particles were gated out. Four independent experiments, statistical significance $p < 0.05$; ratio paired t test, two-tailed.

The Ca^{2+} independence of MFG-E8 and the mC1 multimer is a valuable asset not only in free choice of the buffer system but also for possible applications *in vivo*. Since physiological Ca^{2+} concentrations are quite low with values of 0.94 – 1.33 mM as determined in human serum (Moore, 1970) only a few experiments *in vivo* were performed using Annexin V in the mouse model (Guo et al., 2009, Blankenberg et al., 1998, Yang et al., 2006).

5.4.4 mC1 multimers are applicable *in vivo* for staining of dying cells and vesicles

In order to employ the comparatively cost-effective and versatile mC1 multimer platform *in vivo*, first tests were performed. Upon preparation for injection, shifting the multimer from OSB-related high salt conditions to physiological salt concentrations, significant precipitation was observed. Therefore, an assay was set up to test different buffer conditions for prevention of multimer precipitation. Soluble and insoluble fraction was separated by centrifugation and the supernatant analyzed by SDS PAGE, Coomassie staining of proteins and in-gel fluorescence of the SA moiety. Multimer precipitation was indeed owed to the decrease in salt concentration and not due to lower glycerol concentration (Fig. 5.19 A). In the experimental setup, also the presence of protein from FCS in FACS buffer did not inhibit multimer precipitation. This does not necessarily speak against usage of FACS buffer for *in vitro* stainings in general, since multimer concentrations were high in that assay for subsequent analysis via SDS PAGE, possibly critically promoting precipitation (Fig. 5.19 A).

Since for *in vivo* application a certain concentration of multimer was necessary, agents suppressing aggregation were crucial and found by the example of formulations used for monoclonal antibodies. An equimolar mixture of the aa L-arginine and L-glutamic acid proved to be a powerful suppressor of aggregation and vastly enhanced stability for long-term storage (Golovanov et al., 2004, Kheddo et al., 2014). A similar concentration-dependent effect could be proven for mC1 multimer. Whereas high salt in OSB kept the multimer soluble after centrifugation (compare “input” with lane 1), 100 mM Arg/Glu was equally effective with physiological concentrations of NaCl (Fig. 5.19 B). With only aa involved in the formulation of the buffer, it was regarded as safe for injection.

5.4 Multimerized mMFG-E8 C domains can be used as PS detection tools

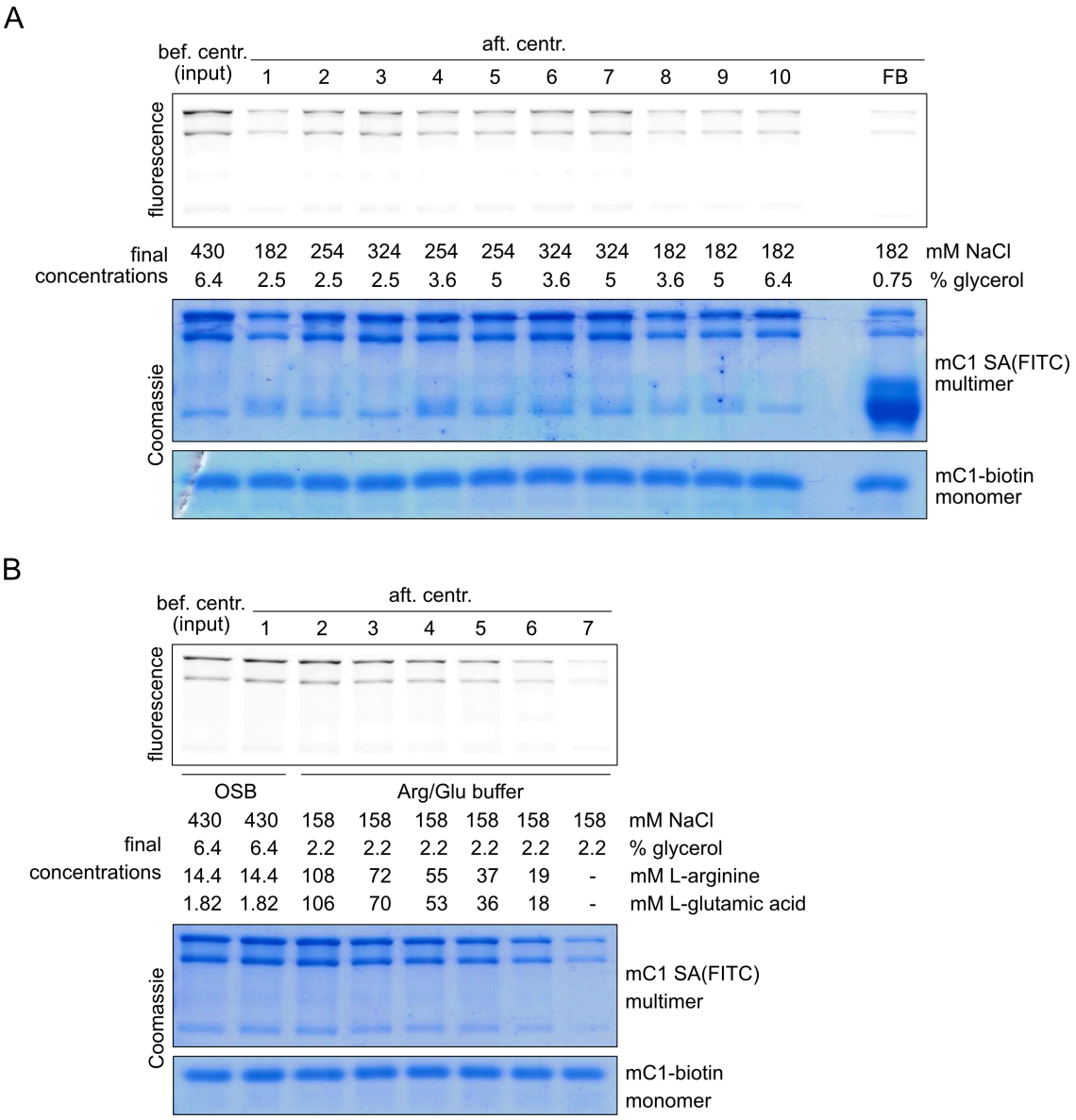

Fig. 5.19: The requirement for high salt to inhibit mC1 multimer aggregation can be substituted with an equimolar mix of arginine and glutamate
(A) A stock of mC1 multimer with OSB as starting buffer was prepared and aliquots mixed with buffers containing different concentrations of NaCl and glycerol or FACS buffer (FB = PBS 2% FCS). Final concentrations are given. Samples were centrifuged to pellet aggregated protein and supernatant with the soluble fraction analyzed on an SDS gel using Coomassie stain and readout of in-gel fluorescence of the SA(FITC) moiety.
(B) Same procedure as done in (A), but glycerol levels were kept constant and NaCl at a physiological level whereas the concentration of Arg/Glu was varied.

To test functionality as well as specificity of the mC1 multimer *in vivo*, mice were injected either with the reagent or the fluorescent SA(AF647), saturated with biotin to block its respective binding sites. Minimal background was detected for the negative control (SA only) whereas internal fluorescence of the multimer revealed PS-positive structures in the spleen in histological samples (Fig. 5.20).

5.4 Multimerized mMFG-E8 C domains can be used as PS detection tools

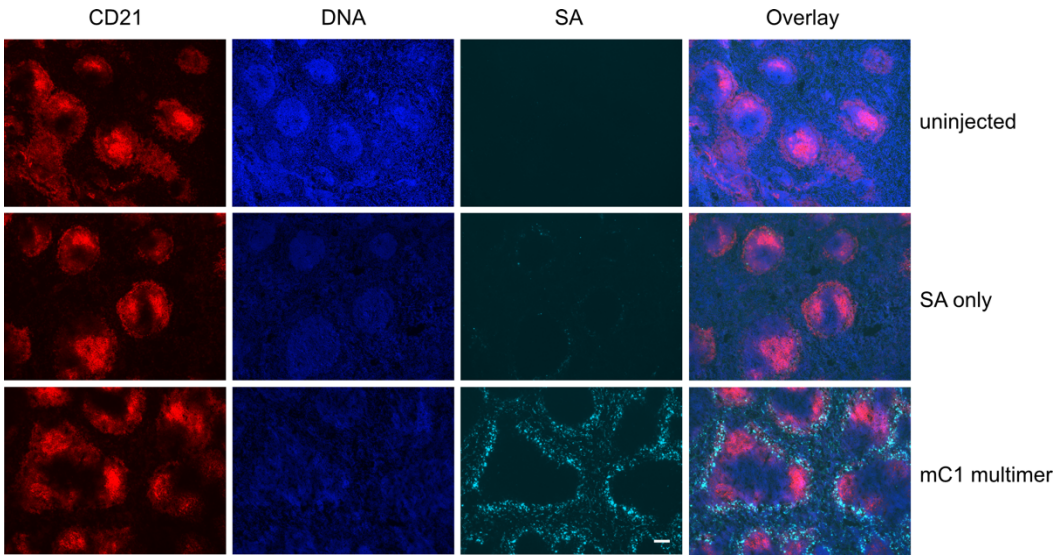

Fig. 5.20: mC1 multimer specifically binds structures in splenic tissue. Mice were either injected with SA(AF647) only or mC1 multimer (cyan). Tissue sections from spleen were prepared and analyzed by fluorescence microscopy. CD21 (red) was used to visualize B cells and follicular dendritic cells. DAPI (blue) was used as DNA dye, scale bar: 100 µm. Histology performed and images taken by Christine Ried.

The applicability of mC1 multimers *in vivo* was tested furthermore in direct comparison with full length mMFG-E8-EGFP by injection in mice and imaging flow cytometry analysis. Whereas injection of mMFG-E8 and counterstain *in vitro* with mC1 multimer (AF647) resulted in an almost exclusive occurrence of double- or multimer positive cells, the reciprocal approach showed a dominant multimer staining *in vivo*. Analysis of the MFG-E8- and multimer-positive population revealed a strong staining of $CD19^-$ $TCR\beta^-$ cells with multimer. Of all analyzed cells, this population was represented by 46% (Fig. 5.21 A).

However, irradiation of the mice caused increased rates of cell death and resulted in a strong increase of multimer staining *in vivo* with multimer-positive cells doubling from 17.5% to 36.6% (Fig. 5.21 B). This further underlines the successful recognition of PS positive cells *in vivo*. Double staining of PS positive cells with both reagents was also proven in single cell analysis. Apoptotic cells showed large areas of signal overlap between mMFG-E8 and multimer (Fig. 5.21 C).

5.4 Multimerized mMFG-E8 C domains can be used as PS detection tools

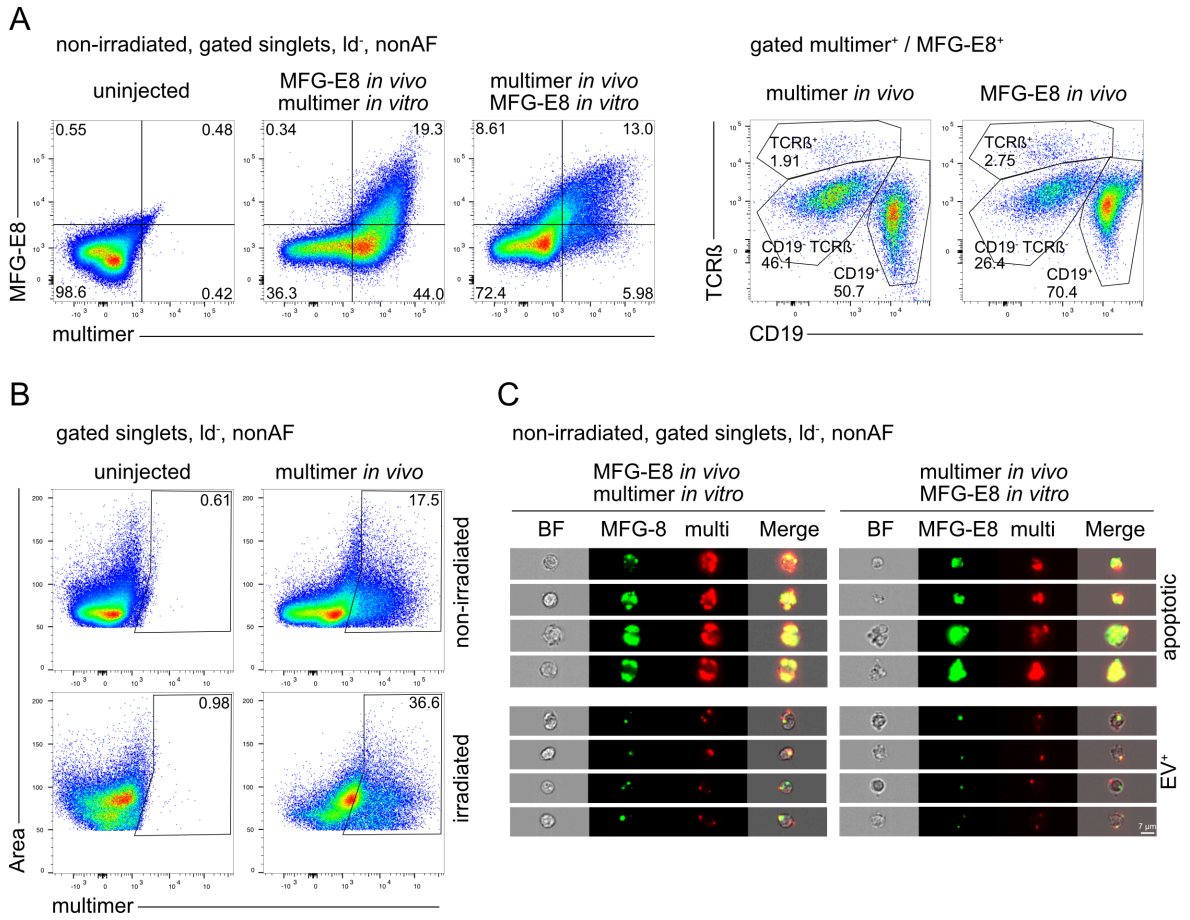

Fig. 5.21: Imaging flow cytometry shows comparable staining of mC1 multimer and mMFG-E8-EGFP *in vivo*.

(A) Mice were injected with either 100 µg mMFG-E8-EGFP or 20 µg mC1 multimer, splenocytes prepared and counterstained *in vitro* (left panel). Live/dead violet was used as viability dye. Cells gated positive for mMFG-E8 and multimer *in vivo* staining were separately analyzed using the CD19 and TCRß markers (right panel).

(B) Analysis of splenocytes from untreated mice or after irradiation with comparable amounts of multimer (20 µg each) injected.

(C) Single cell analysis of splenocytes by imaging flow cytometry. Cells were either classified as associated with EVs (EV^+) or apoptotic with large areas of the surface being marked as PS positive. BF, brightfield.

In addition, PS-positive extracellular vesicles (EVs) associated with cells were also successfully detected with multimer and MFG-E8 (Fig. 5.21 C). The opportunities for applications of the multimer were thereby extended by *in vivo* stainings making the mC1 multimer technology a valuable asset for several *in vitro* and *in vivo* analyses of PS-positive particles.

6 Discussion

Cell death, especially in a controlled way by apoptosis is necessary in developmental processes of multicellular organisms, cellular homeostasis and immune cell development. A central obstacle is the detection of dying cells *in vivo* since during preparation of cell suspensions from tissue cell death can occur, mask the actual fraction of dying cells and make it impossible to differentiate between cell death *in vivo* and *in vitro*. In this study a tool was created to address this issue and provide a versatile platform with various modes of readout to study cell death *in vivo* and assist in experiments *in vitro*. Furthermore, steps were undertaken to create a tool for *in vivo* diagnostic approaches in humans with successful production in bacteria laying the foundation for further research.

6.1 Lessons from hMFG-E8 single PS binding domains and full-length variants obtained from a mammalian expression system

Setting up an *in vitro* assay for comparison of hMFG-E8 single domains and full-length variants it was astonishing to see the high differences in secretion competency of the same construct using either the human or murine ER SS of MFG-E8. It is possible that the human SS is not annotated correctly in the Uniprot database (Identifier: Q08431) and binding by the signal recognition particle (SRP) (Akopian et al., 2013) is weakened or mostly abolished leading to increased fluorescence of the producing cells due to protein retained in the cytoplasm. For production of hMFG-E8 full-length variants the natural SS was sufficient for secretion. Direct comparison with the murine SS using the same protein for ER translocation was not undertaken but would shed more light on potential differences in the homologues' ER SS concerning secretion from HEK 293T cells.

Direct comparison of the single domains with full-length hMFG-E8 revealed a strong binding activity towards dead cells of hC1. This has not been published so far for MFG-E8, only C1 of blood coagulation factor V, also of F5/8 type, was shown to have PS binding activity (Saleh et al., 2004). It is safe to assume that the main ligand for C1 is PS as well since for the full-length molecule exclusive stereoselective binding to this phospholipid was shown (Peterson et al., 1998, Shi et al., 2004) with PE possibly serving a supportive role as ancillary lipid (Otzen et al., 2012).

Usage of high amounts of concentrated HEK SN for staining of mouse thymocytes led to a strong permeabilization of cells in the process as revealed by sequential staining with live/dead

eFluor780, SN and PI. A possible explanation for this phenomenon is enrichment of Pluronic F-68 in the concentration process. This detergent is supplied to serum-free ExCell 293 medium as an anti-foam agent and serves to protect cells from shear forces. However, at high concentrations cytotoxicity was shown (Samith et al., 2013).

In the literature, higher binding of the long isoform of mMFG-E8, containing the P/T-rich domain compared to hMFG-E8 to a PS-coated microtiter plate was shown (Yamaguchi et al., 2008). This circumstance could also be demonstrated in this work in a binding assay with apoptotic cells reflecting the natural state more properly. It is likely that the P/T-rich domain of mMFG-E8 is responsible for this effect since the long isoform showed superior binding over the short isoform lacking this domain (Hanayama et al., 2002).
It would be definitely interesting to see in future studies whether grafting of the mMFG-E8 N-terminus containing the EGF1-EGF2-P/T domains to hC1C2 were able to improve PS binding for the human homologue. In general, a cell- or liposome-based binding assay would always have a more reliable readout than flat, PS-coated plates as mentioned above (Hanayama et al., 2002, Yamaguchi et al., 2008) since MFG-E8 was demonstrated to show a preference for curved membranes (Shi et al., 2004, Otzen et al., 2012).

Concerning hMFG-E8 WT and the IgG3-linker modified variant it could not be determined which factors led to the observed differences in binding between the approach with SN from HEK cells and the respective proteins purified via their Flag tag. One of the speculations, an elevated Albumin concentration could have stabilized hMFG-E8 WT and enhanced its binding properties relative to its IgG3-linker variant was not proven.
In the hMFG-E8 variant array with GS linkers of varying length, 29 aa showed highest binding activity. Comparing purified proteins with linker lengths of e.g. 4, 15 and 29 aa could give valuable information of a trend upon increasing the distance between C1 and C2 domain.
Standardized buffer conditions in this approach would also allow for possible explanation of the observed discrepancies between results obtained from HEK SN and purified proteins.

6.2 Bacterial production and purification of full-length hMFG-E8

Setting up a system for bacterial expression and purification of either single C domains or a full-length hMFG-E8 variant, unspecific binding to the agarose beads used in affinity chromatography was observed. Association was largely independent of the immobilized Ni^{2+} ions as EDTA treatment revealed and could only be resolved by imidazole. Ionic interactions are unlikely to be the reason since the presence of high salt in the lysis buffer did not prevent the unspecific association. Since this occurred with both, glutathione beads for GST affinity chromatography and Ni^{2+}-NTA beads for immobilized metal affinity chromatography (IMAC) the cross-linked agarose bead matrix as lowest common denominator is likely to form the basis for these undesired protein-matrix interactions.
A characteristic of the MFG-E8 C2 domain is the occurrence of solvent-exposed hydrophobic aa, mostly with aromatic side chains such as Phe and Trp which play an important role in the binding event by insertion into the membrane (Ye et al., 2013, Shao et al., 2008, Lin et al., 2007). Imidazole shares the feature of an aromatic structure and assuming the aromatic aa mentioned beforehand play a role in the unspecific binding to the beads, imidazole could shield the solvent-exposed aa residues by engaging in π interactions as it was determined for the imidazole moiety of His (Liao et al., 2013, Wang et al., 2006).

In the three domains of hMFG-E8, a total of six disulfide bonds is present, which are successfully formed only in the eukaryotic ER since all cells feature a reducing cytoplasm. This was mimicked in the *E. coli* expression system by usage of the Origami B (DE3) expression strain featuring mutations in the *trxB* and *gor* genes allowing for disulfide bond formation in the bacterial cytoplasm (Prinz et al., 1997). Since correct folding and establishment of the disulfide bonds could only be controlled by cytoplasmic chaperones, a fusion tag combining both chaperone activity and redox potential like the bacterial DsbA (Bardwell et al., 1991) and DsbC (Missiakas et al., 1994) enabled high expression levels of soluble protein for a MFG-E8 C domain. Especially DsbC has been successfully used for expression of proteins with multiple disulfide bonds (Bessette et al., 1999, Nozach et al., 2013, Zhang et al., 2006). An advantage of DsbC over DsbA is its proofreading activity provided by the disulfide isomerase character (Vertommen et al., 2008, Messens and Collet, 2006) enabling it to correct faulty disulfide bonds. This feature made DsbC a promising fusion tag for expression of a functional fluorescent hMFG-E8 variant. It would be interesting to see whether the observed positional effect of GFP fluorescence also applies for expression in mammalian cells. But assuming the hypothesis of MFG-E8 aggregation interfering with proper establishment of the fluorophore in C-terminal GFP it is also possible for mammalian expression systems to provide elaborate mechanisms preventing MFG-E8 aggregation in the ER.

6.2 Bacterial production and purification of full-length hMFG-E8

Although the procedure previously published to overcome MFG-E8 aggregation using CHAPS in the purification and a SEC buffer with 200 mM L-arginine and 137 mM succinate (Castellanos et al., 2016) was adapted, only an aggregated hMFG-E8 variant could be obtained from bacteria. It is possible that the 15 aa IgG3 linker hMFG-E8 variant behaves differently than wild type hMFG-E8 from the original study. However, it is also likely that MFG-E8 produced in mammalian cells is rather responding to the procedure due to the four N-linked glycosylations in the C2 domain and one between C1 and C2 (Picariello et al., 2008) which are not provided in the bacterial expression system. An Arg/Glu buffer, successfully suppressing aggregation for mC1 multimers at 100 mM did not solve hMFG-E8 aggregates even at 500 mM, though purification previously was performed without CHAPS.

Bacterial expression of full-length hMFG-E8 was undertaken previously (Qiang et al., 2011). The authors employed the BL21 standard expression strain with its reducing cytoplasm for production and did not use any protein tag to assist proper folding or maintenance of disulfide bridges. In addition, expression times were short and protein identity only analyzed via Coomassie staining, Western Blot and mass spectrometry. No analysis of the protein being present as monomer or in aggregates was performed. Although the authors linked effects like e.g. enhancement of phagocytosis of peritoneal macrophages to the recombinant MFG-E8, this purification approach seems to be not applicable to obtain large amounts of the protein.

For further studies and large-scale application of pure bacterially produced hMFG-E8 overcoming protein aggregation will be a necessary, but challenging task. Since imidazole was seen to counteract unspecific association of a hMFG-E8 variant with agarose beads this effect could also be applied in the case of intermolecular association and tested in SEC using an imidazole-containing buffer. In fact, the structurally related aa histidine was demonstrated to protect the recombinant PS binding protein factor VIII SQ against aggregate formation upon freeze-drying alongside with sucrose and polysorbate 80 (Osterberg et al., 1997). His also stabilized an antibody in solution and solid state (Chen et al., 2003) and is readily used in the formulation of pharmaceutically relevant proteins (Arakawa et al., 2007). The soluble nature of MFG-E8 aggregates makes a readout to determine the aggregation state more complicated than just assaying solubility but could be achieved by SEC or an elaborate technique like SEC-MALS (Multiangle light scattering) (Sahin and Roberts, 2012) or dynamic light scattering (DLS) (Stetefeld et al., 2016).

Approaches to label MFG-E8 with chelators for radionuclides or other tracers in a Sortase reaction and usage for diagnostic purposes *in vivo* critically depend on MFG-E8 to be present in a non-aggregated state. Compatibility of the reaction with aggregation-suppressing additives like the aa Arg, Glu and His needs to be determined as well. Coordination of the LPXTG motif

within the active site of *S. aureus* Sortase A is assisted by Arg^{197}, His^{120} is important for transpeptidation whereas Glu^{105}, Glu^{108} and Glu^{171} participate in coordination of the Ca^{2+} ion (Suree et al., 2009, Bentley et al., 2008, Naik et al., 2006). The dependence on Glu residues in the reaction could basically be overcome by usage of a Ca^{2+} independent variant of Sortase A (Hirakawa et al., 2012, Hirakawa et al., 2015).

Introduction of another C-terminal tag to bacterially produced hMFG-E8 could also broaden the application range of additives and successfully select for full-length molecules during the purification process. In case an additive is incompatible with Ni^{2+}-NTA affinity chromatography, the *Strep*-tag II system immobilizing recombinant proteins to a *Strep*-Tactin column with competitive elution using Desthiobiotin could be a promising alternative (Schmidt and Skerra, 2007). Taken together, the DsbC tag and future means to prevent aggregation could help in the production of large amounts of hMFG-E8 for diagnostic purposes and respective single domains for structural, biochemical and biophysical studies of MFG-E8 for basic research.

6.3 MFG-E8 single PS-binding domains provide insight into the molecule and a powerful staining tool

In the literature, single domain studies on MFG-E8 focused on the C2 domain of the murine or bovine homologue, expressed in *E. coli* or *P. pastoris* (Lin et al., 2007, Shao et al., 2008, Ye et al., 2013, Reddy Nanga et al., 2007). mC2 could also be readily produced in the standard bacterial expression strain BL21 (DE3) and kept in a soluble state in a simple buffer system. In early stages of the project a buffer providing stability to the purified bacterially produced MFG-E8 single domains was not available and only surfaced by adaptation of OSB (Kooijmans et al., 2018). Soluble production of mC1 and mC2 was shown to be enhanced with the GST-SUMO3 tag system in combination with the Origami B (DE3) expression strain.

The tag also yielded soluble mC1 in BL21 (DE3), it is therefore possible that the right choice of tag might also circumvent the need for an expression strain with predominantly oxidizing cytoplasm thereby boosting yields as it was already proposed for DsbC fusion proteins (Nozach et al., 2013). Concerning the choice of buffer in the purification procedure, proteolytic activity of Senp2 was greatly diminished in OSB, making a switch to this buffer only possible with the GST-SUMO3 construct after completion of the cleavage steps.

Whereas the purification of mC1 and mC2 was established with the GST-SUMO3 system and yielded pure protein in reasonable amounts, shifting the system to a DsbC fusion protein with a TEV cleavage site separating tag and POI will definitely increase the yield. The advantage of Senp2 being 25fold more catalytically active than TEV (Marblestone et al., 2006) can be

compensated for by the broad tolerance of buffers and additives of the easy-to-produce TEV protease (Sun et al., 2012). In OSB, TEV cleavage was observed to be slightly decreased most likely due to high salt (500 mM) in line with published data (Nallamsetty et al., 2004) but in contrast to Senp2 still possible.

Sortase reaction was demonstrated not to be affected by components of OSB like high salt, glycerol or free aa. Nevertheless, the occurrence of side products in the reaction might be circumvented in the future by shifting the system from batch mode to flow-based approaches using immobilized Sortase A, thereby also decreasing amounts of enzyme and nucleophile (Policarpo et al., 2014). Unspecific association of mMFG-E8 single domains with agarose beads will still be an obstacle to overcome choosing the right, reaction-compatible buffer system. However, SEC revealed no intermolecular association for mC1 and mC2, respectively. Titration of the biotinylated monomers to SA showed complete multimerization at a molar excess of 4-5 of monomer to SA further underlining the presence of mC1 and mC2 in their monomeric form and quantitative biotinylation.
The hypothesis that the observed band pattern for multimers on an SDS gel is a result of the sample preparation, not boiling the samples prior to SDS PAGE analysis, resulted from the occurrence of multiple bands for complete multimerization of mC1-biotin and mC2-biotin, respectively. This mismatch could be approached by comparative analytical ultracentrifugation (AUC) of monomer, incompletely and completely multimerized mixes to probe for actual differences in mass. The AUC approach would be independent from differences in charge (SDS PAGE) or probably poor resolution and interaction of the proteins with column material (SEC) (Howlett et al., 2006, Unzai, 2018).

In multimeric form, mC1 showed stronger binding to apoptotic mouse thymocytes than mC2. Equal amounts of mC1 and mC2 multimers were guaranteed by the same SA input and surveillance of complete assembly via SDS PAGE. To complement this experiment and verify the data it could be repeated using purified multimers with the input normalized according to the SA fluorescence. Comparative studies with bacterially produced and purified sfGFP-mC1 and sfGFP-mC2 will shed further light on the actual binding activity of the single domains. They don’t have any aggregation tendency as shown in this study and definitely reflect the monomeric situation. In addition, a weak signal could be amplified by additional α-GFP(FITC) staining.
Evaluation of C1 and C2 affinities would definitely be interesting taking the biochemical properties into consideration. No free thiol groups were found for both purified domains, but C1 was significantly less stable than C2 in a thermal shift assay.

6.3 MFG-E8 single PS binding domains provide insight into the molecule and a powerful staining tool

Given the status of C1 with two disulfide bonds and C2 with only one, this was counterintuitive and it is tempting to speculate about an evolutionary role. After partial gene duplication giving rise to the homologous C1 and C2 domain in MFG-E8, sacrificing stability in C1 for increased affinity could be an explanation for this conundrum. On the other hand, a conformational switch of C2 in the binding event as already proposed (Shao et al., 2008) could provide this domain with more flexibility and thermal stability. Furthermore, the close proximity of C1 and C2 in the wild type protein, only separated by a 4 aa linker sequence alongside with the biochemical differences observed in this study makes two ways of interaction in the binding event possible assuming C1 has a higher affinity than C2 and makes the primary engagement with the membrane

(1) C1 first associates with the membrane and C2 is only being recruited

(2) C1 induces a conformational switch in C2 making association with the membrane possible

These models would contradict a previously proposed primary engagement of C2 followed by C1 in membrane binding (Otzen et al., 2012). The authors performed stopped-flow kinetics comparing the association of bovine MFG-E8 purified from milk and recombinant bC2 from *E. coli* to PS-containing vesicles.

An experiment to test hypothesis (1) via flow cytometry would be the staining of cells with an sfGFP-Annexin V-mC2 fusion protein, sfGFP-Annexin V and sfGFP-mC2. Importantly, by staining in Annexin V binding buffer and usage of Ca^{2+} free buffer for washing. If staining of cells with Annexin V-mC2-sfGFP is increased relative to mC2-sfGFP, the MFG-E8 domain is actively recruited to the membrane.

A way to address (2) would be to uncouple the binding of both domains by using a fix amount of sfGFP-mC2 for staining with an increasing amount of mC1. If the signal increases for C2, membrane association of C2 is influenced by C1.

To test a potential mutual influence of the C domains, a construct with the positions of C1 and C2 switched could also be tested. Reliable results can be obtained from purified protein either expressed in a mammalian or bacterial system.

6.4 mC1 multimer is a reliable replacement for Annexin V with an even higher potential for usage in various assays

In an *in vitro* staining, the mC1 multimer could be shown to bind to the same cell populations as Annexin V and mMFG-E8-EGFP. Whereas MFG-E8 has a preference for membranes with high curvature (Shi et al., 2004, Otzen et al., 2012), Annexin V was reported to prefer rather flat surfaces and proposed to even lower membrane curvature in the binding event (Swairjo et al., 1994, Andree et al., 1992). Staining of comparable cell populations with all reagents might therefore be surprising at first but could be explained by the *in vitro* approach taken here with excess protein available for binding and optimal conditions for Annexin V due to the used binding buffer.

However, both PS binding proteins also show different modes of association with the membrane. Annexin V was extensively studied in this respect revealing the formation of membrane-bound trimers which are organized in higher 2D arrays (Concha et al., 1992, Voges et al., 1994, Oling et al., 2000). Oligomerization is promoted by intermolecular salt bridge formation (Mo et al., 2003) and Annexin V crystals were proposed to assemble on the membrane laterally (Brisson et al., 1991, Voges et al., 1994) with the Ca^{2+}-mediated PS head group interaction being stabilized by exposure of Trp^{187} and interaction with a PS acyl chain (Meers and Mealy, 1993, Meers and Mealy, 1994).

The MFG-E8 C2 domain on the other hand is hallmarked by three spikes on the PS binding site featuring solvent-exposed hydrophobic aa residues (Shao et al., 2008, Lin et al., 2007) which were demonstrated to insert into the membrane (Ye et al., 2013).

In direct comparison, bMFG-E8 showed superior binding properties to Annexin V concerning sensitivity and staining intensity (Dasgupta et al., 2006). Since the double staining of cells with multimer and Annexin V only gave a qualitative output, evaluation of the cooperative Annexin V binding against the mC1 avidity in multimer context would provide additional data for this new reagent. Due to the common binding mode direct comparison of wild type mMFG-E8 with mC1 multimer is feasible in a fluorescence decay using unlabeled Annexin V as a competitor as performed before for MHC tetramers (Savage et al., 1999).

The applicability of mC1 multimer as a Ca^{2+}- independent alternative to Annexin V was not only demonstrated in terms of a staining reagent but also for removal of dead cells and debris from cell suspensions. The Id^{-} MFG-$E8^{lo}$ population remained largely unaffected by incubation with magnetic α-SA beads and its character as either early apoptotic cells or vesicle-decorated cells could be determined by imaging flow cytometry in a follow-up experiment. It is important to point out that usage of Annexin V binding buffer in flow cytometry staining was always accompanied by a dramatic loss of cells (own observations, Jan Kranich). Cell recovery would

therefore be influenced drastically using commercial Annexin V dead cell depletion kits. In addition, exposure of cells destined for subsequent analysis to high extracellular Ca^{2+} concentrations could induce unwanted side effects. Ca^{2+} ions from an extracellular pool take part in BCR (B-cell receptor) (Numaga et al., 2010) and TCR (T-cell receptor) signaling for activation (Joseph et al., 2014).

In histology as well as imaging flow cytometry binding activity of the mC1 moieties *in vivo* was proven. A preference of mC1 multimer *in vivo* for the $CD19^-$ $TCR\beta^-$ population was detected by imaging flow cytometry. This could result from the RYD motif of Streptavidin, mimicking the RGD motif as a central recognition motif in cell adhesion molecules (Alon et al., 1990) and possibly point towards integrin-expressing monocytes associating with multimer via its RYD motif. In the case of full length MFG-E8, specific staining of PS-positive macrophages and monocytes independent of the RGD motif has been proven by Annexin V counterstain (Kranich et al., 2020). Comparing multimer and MFG-E8, cellular uptake of both molecules but subsequent quenching of the EGFP fluorescence is also possible while multimer fluorescence prevails (Jan Kranich, personal communication).
Altogether, a large overlap of multimer staining *in vivo* / MFG-E8 *in vitro* and vice versa showed PS-specificity of the multimer. This could furthermore be demonstrated by an increase of apoptotic cells upon irradiation of the mice.

Not only apoptotic cells were recognized by the mC1 multimer but also PS-positive EVs. Full-length mMFG-E8-EGFP was previously utilized for this purpose (Kranich et al., 2020) and could now be replaced by the more cost-effective multimer. This will support the investigation of cell fate decisions leading to apoptosis induction and impact of vesicle association by analysis of the marked cells' transcriptome and proteome. The field of EV research gained more attention in the last years, sharply increasing in 2011-2016 (Roy et al., 2018) due to their role in intercellular communication transporting protein, lipid and nucleic acid cargo (Meldolesi, 2018), modulation of immune responses (Robbins and Morelli, 2014) and use as biomarkers for diseases like cancer (Lane et al., 2018). MFG-E8 was already used as a C1C2-Luciferase fusion protein for exosome tracking in mice after injection (Takahashi et al., 2013). In contrast to fluorescently labeled proteins, Luciferase fusion proteins have the advantage of being applicable *in vivo* for even more sensitive and non-invasive monitoring of biological processes (Xu et al., 2016, Mezzanotte et al., 2017).

Multimer application in the isolation of EVs from the bloodstream and their analysis could be driven forward as well. Vesicles targeted by the PS binding probe Tim4 immobilized on magnetic beads are specifically enriched in the surface markers CD9, CD63 and CD81 in

comparison to the vesicle pool obtained by ultracentrifugation and precipitation-based total exosome isolation (TEI) (Nakai et al., 2016). The authors reported low binding of EVs in an ELISA to mMFG-E8- or hMFG-E8-coated 96 well plates. However, they proved PS specificity of Tim4 by MFG-E8-mediated blocking of vesicle binding to Tim4-expressing K562 leukemia cells. Alongside with the successful application of mC1 multimers for dead cell depletion in this study, targeted immobilization of this reagent to anti-Streptavidin beads could be a promising approach for isolation of PS-positive EVs. Direct immobilization of mC1-biotin on magnetic Streptavidin beads or mC1-His_6 on magnetic Ni^{2+}-NTA beads could serve as additional approaches. Recombinant MFG-E8 C2 domain was already used as an alternative for Annexin V in capturing of tumor-derived vesicles from the bloodstream (Shih et al., 2016). The authors faced some problems with coagulation upon addition of Ca^{2+}-containing Annexin V-binding buffer which could not be solved by the anti-coagulant Heparin due to its interference with downstream processing methods such as nucleic acid extraction and PCR. In terms of affinity, mC1-based EV capturing will be a promising further development of this method.

Besides imaging and diagnostic approaches MFG-E8 C1-C2 domains were evaluated as means to target antigen to exosomes. Elevated immune responses against tumor associated antigens were demonstrated by exosome targeting (Hartman et al., 2011) and a higher antitumor response in mice proven for exosome-bound than soluble antigen (Zeelenberg et al., 2008). Targeting of the exosomes themselves to epidermal growth factor receptor (EGFR)-expressing cells was accomplished by fusion of C1C2 to an anti-EGFR nanobody (Kooijmans et al., 2018), opening possibilities for targeted cargo delivery to cells, blocking of receptors and inhibition of tumor growth.

6.5 Conclusion and Outlook

In this work, valuable insight in the MFG-E8 molecule was gathered and the foundation laid for future diagnostic approaches as well as applications in research *in vitro* and *in vivo*.
Binding activity for the C1 domain was proven, which has not been in the focus of study previously. This is likely owed to the fact that soluble C2 is comparatively easy to obtain from a bacterial expression system which most investigators used. In case of C1, the choice of tag and expression host resulted in successful production and purification. DsbC with its chaperone and disulfide bond isomerase activity is a promising tag for future large-scale production of both MFG-E8 single domains and full-length molecules. Purification and structural investigation of C1 or a C1C2 combination alongside with modeling of PS in the binding pocket would provide additional data and hints on the observed differences in binding. As suspected, C1 with its two disulfide bonds could come with a rather fixed structure in comparison to C2 contributing to the observed decrease in stability concomitant with higher PS binding.
Furthermore, the orientation of both domains relative to each other alongside with experiments as described above to determine a possible interplay between C1 and C2 would give valuable insight in the binding mode towards cells with low curvature and vesicles with high curvature. It is definitely noteworthy that for purified hMFG-E8 variants integration of the 15aa linker between C1 and C2 appeared to have no or only a slightly negative impact on binding. In addition, not only intramolecular but also intermolecular interaction should be taken into consideration for the MFG-E8 molecule in the binding event.

In order to improve binding for hMFG-E8, a variant with two C1 domains could be tested against the wild type molecule for higher affinity. The EGF1-EGF2-P/T N-terminal structure of mMFG-E8 contributing to higher binding as compared to the human homologue could represent another future approach. It is possible that the P/T rich sequence does not result in higher binding per se but merely works as a linker separating the EGF-like from the C-domains. Replacement with a random sequence would shed light on this. Independent of the approach undertaken to improve hMFG-E8 binding, large-scale production in bacteria would be at the end of the pipeline and successful application of the molecule critically depends on ways to resolve the observed aggregates as already discussed above.
The work presented in this thesis could support these approaches by large-scale production of MFG-E8 C1C2 and fusion to antigens of choice either genetically or in a Sortase reaction.

For research and diagnostic purposes the mC1 multimer represents a promising platform for various applications. Fluorophores for imaging *in vitro* and *in vivo* can be easily exchanged

with the SA variant used and possibly live cell imaging undertaken investigating processes of cell death and vesicle generation or association with cells.
Readout of a signal can further be accomplished in a setting with Luciferase-fused SA. Applications for this molecule would be e.g. drug screens inducing cell death in a microplate. Taken together, MFG-E8 is a molecule with tremendous potential in diagnosis, imaging, assays and therapeutics. Unraveling the secrets of this molecule further will provide valuable means of tailoring this PS-binding protein to meet the needs of the respective applications.

Bibliography

AKOPIAN, D., SHEN, K., ZHANG, X. & SHAN, S. O. 2013. Signal recognition particle: an essential protein-targeting machine. *Annu Rev Biochem,* 82**,** 693-721.

ALBANYAN, A. M., MURPHY, M. F., RASMUSSEN, J. T., HEEGAARD, C. W. & HARRISON, P. 2009. Measurement of phosphatidylserine exposure during storage of platelet concentrates using the novel probe lactadherin: a comparison study with annexin V. *Transfusion,* 49**,** 99-107.

ALON, R., BAYER, E. A. & WILCHEK, M. 1990. Streptavidin contains an RYD sequence which mimics the RGD receptor domain of fibronectin. *Biochem Biophys Res Commun,* 170**,** 1236-41.

ALTMAN, J. D., MOSS, P. A., GOULDER, P. J., BAROUCH, D. H., MCHEYZER-WILLIAMS, M. G., BELL, J. I., MCMICHAEL, A. J. & DAVIS, M. M. 1996. Phenotypic analysis of antigen-specific T lymphocytes. *Science,* 274**,** 94-6.

ANDERSEN, M. H., BERGLUND, L., RASMUSSEN, J. T. & PETERSEN, T. E. 1997. Bovine PAS-6/7 binds alpha v beta 5 integrins and anionic phospholipids through two domains. *Biochemistry,* 36**,** 5441-6.

ANDERSEN, M. H., GRAVERSEN, H., FEDOSOV, S. N., PETERSEN, T. E. & RASMUSSEN, J. T. 2000. Functional analyses of two cellular binding domains of bovine lactadherin. *Biochemistry,* 39**,** 6200-6.

ANDREE, H. A., STUART, M. C., HERMENS, W. T., REUTELINGSPERGER, C. P., HEMKER, H. C., FREDERIK, P. M. & WILLEMS, G. M. 1992. Clustering of lipid-bound annexin V may explain its anticoagulant effect. *J Biol Chem,* 267**,** 17907-12.

AOKI, N., KISHI, M., TANIGUCHI, Y., ADACHI, T., NAKAMURA, R. & MATSUDA, T. 1995. Molecular cloning of glycoprotein antigens MGP57/53 recognized by monoclonal antibodies raised against bovine milk fat globule membrane. *Biochim Biophys Acta,* 1245**,** 385-91.

ARAKAWA, T., TSUMOTO, K., KITA, Y., CHANG, B. & EJIMA, D. 2007. Biotechnology applications of amino acids in protein purification and formulations. *Amino Acids,* 33**,** 587-605.

ARONSON, D. E., COSTANTINI, L. M. & SNAPP, E. L. 2011. Superfolder GFP is fluorescent in oxidizing environments when targeted via the Sec translocon. *Traffic,* 12**,** 543-8.

ASANO, K., MIWA, M., MIWA, K., HANAYAMA, R., NAGASE, H., NAGATA, S. & TANAKA, M. 2004. Masking of phosphatidylserine inhibits apoptotic cell engulfment and induces autoantibody production in mice. *J Exp Med,* 200**,** 459-67.

ASHKENAZI, A. & DIXIT, V. M. 1998. Death receptors: signaling and modulation. *Science,* 281**,** 1305-8.

BAR, P. R. 1996. Apoptosis--the cell's silent exit. *Life Sci,* 59**,** 369-78.

BARDWELL, J. C., MCGOVERN, K. & BECKWITH, J. 1991. Identification of a protein required for disulfide bond formation in vivo. *Cell,* 67**,** 581-9.

BENTLEY, M. L., LAMB, E. C. & MCCAFFERTY, D. G. 2008. Mutagenesis studies of substrate recognition and catalysis in the sortase A transpeptidase from Staphylococcus aureus. *J Biol Chem,* 283**,** 14762-71.

BESSETTE, P. H., ASLUND, F., BECKWITH, J. & GEORGIOU, G. 1999. Efficient folding of proteins with multiple disulfide bonds in the Escherichia coli cytoplasm. *Proc Natl Acad Sci U S A,* 96**,** 13703-8.

BLANKENBERG, F. G., KATSIKIS, P. D., TAIT, J. F., DAVIS, R. E., NAUMOVSKI, L., OHTSUKI, K., KOPIWODA, S., ABRAMS, M. J., DARKES, M., ROBBINS, R. C., MAECKER, H. T. & STRAUSS, H. W. 1998. In vivo detection and imaging of phosphatidylserine expression during programmed cell death. *Proc Natl Acad Sci U S A,* 95**,** 6349-54.

BRISSON, A., MOSSER, G. & HUBER, R. 1991. Structure of soluble and membrane-bound human annexin V. *J Mol Biol,* 220**,** 199-203.

BRUMATTI, G., SHERIDAN, C. & MARTIN, S. J. 2008. Expression and purification of recombinant annexin V for the detection of membrane alterations on apoptotic cells. *Methods,* 44**,** 235-40.

CANDIANO, G., BRUSCHI, M., MUSANTE, L., SANTUCCI, L., GHIGGERI, G. M., CARNEMOLLA, B., ORECCHIA, P., ZARDI, L. & RIGHETTI, P. G. 2004. Blue silver: a very sensitive colloidal Coomassie G-250 staining for proteome analysis. *Electrophoresis,* 25**,** 1327-33.

CARTER, R. A., BIHANNIC, L., ROSENCRANCE, C., HADLEY, J. L., TONG, Y., PHOENIX, T. N., NATARAJAN, S., EASTON, J., NORTHCOTT, P. A. & GAWAD, C. 2018. A Single-Cell Transcriptional Atlas of the Developing Murine Cerebellum. *Curr Biol,* 28**,** 2910-2920 e2.

CASTELLANOS, E. R., CIFERRI, C., PHUNG, W., SANDOVAL, W. & MATSUMOTO, M. L. 2016. Expression, purification, and characterization of recombinant human and murine milk fat globule-epidermal growth factor-factor 8. *Protein Expr Purif,* 124**,** 10-22.

CHEN, B., BAUTISTA, R., YU, K., ZAPATA, G. A., MULKERRIN, M. G. & CHAMOW, S. M. 2003. Influence of histidine on the stability and physical properties of a fully human antibody in aqueous and solid forms. *Pharm Res,* 20**,** 1952-60.

CHEN, G., NING, B. & SHI, T. 2019. Single-Cell RNA-Seq Technologies and Related Computational Data Analysis. *Front Genet,* 10**,** 317.

CHEN, I., DORR, B. M. & LIU, D. R. 2011. A general strategy for the evolution of bond-forming enzymes using yeast display. *Proc Natl Acad Sci U S A,* 108**,** 11399-404.

CONCHA, N. O., HEAD, J. F., KAETZEL, M. A., DEDMAN, J. R. & SEATON, B. A. 1992. Annexin V forms calcium-dependent trimeric units on phospholipid vesicles. *FEBS Lett,* 314**,** 159-62.

COUTO, J. R., TAYLOR, M. R., GODWIN, S. G., CERIANI, R. L. & PETERSON, J. A. 1996. Cloning and sequence analysis of human breast epithelial antigen BA46 reveals an RGD cell adhesion sequence presented on an epidermal growth factor-like domain. *DNA Cell Biol,* 15**,** 281-6.

CROWLEY, L. C. & WATERHOUSE, N. J. 2016. Detecting Cleaved Caspase-3 in Apoptotic Cells by Flow Cytometry. *Cold Spring Harb Protoc,* 2016.

D'SOUZA-SCHOREY, C. & SCHOREY, J. S. 2018. Regulation and mechanisms of extracellular vesicle biogenesis and secretion. *Essays Biochem,* 62**,** 125-133.

DARZYNKIEWICZ, Z., GALKOWSKI, D. & ZHAO, H. 2008. Analysis of apoptosis by cytometry using TUNEL assay. *Methods,* 44**,** 250-4.

DASGUPTA, S. K., GUCHHAIT, P. & THIAGARAJAN, P. 2006. Lactadherin binding and phosphatidylserine expression on cell surface-comparison with annexin A5. *Transl Res,* 148**,** 19-25.

DUKE, R. C. & COHEN, J. J. 1986. IL-2 addiction: withdrawal of growth factor activates a suicide program in dependent T cells. *Lymphokine Res,* 5**,** 289-99.

ELLIOTT, M. R. & RAVICHANDRAN, K. S. 2010. Clearance of apoptotic cells: implications in health and disease. *J Cell Biol,* 189**,** 1059-70.

ELMORE, S. 2007. Apoptosis: a review of programmed cell death. *Toxicol Pathol,* 35**,** 495-516.

FAIRN, G. D., SCHIEBER, N. L., ARIOTTI, N., MURPHY, S., KUERSCHNER, L., WEBB, R. I., GRINSTEIN, S. & PARTON, R. G. 2011. High-resolution mapping reveals topologically distinct cellular pools of phosphatidylserine. *J Cell Biol,* 194**,** 257-75.

FALBORG, L., WAEHRENS, L. N., ALSNER, J., BLUHME, H., FROKIAER, J., HEEGAARD, C. W., HORSMAN, M. R., RASMUSSEN, J. T. & REHLING, M. 2010. Biodistribution of 99mTc-HYNIC-lactadherin in mice--a potential tracer for visualizing apoptosis in vivo. *Scand J Clin Lab Invest,* 70**,** 209-16.

GALLUZZI, L., VITALE, I., AARONSON, S. A., ABRAMS, J. M., ADAM, D., AGOSTINIS, P., ALNEMRI, E. S., ALTUCCI, L., AMELIO, I., ANDREWS, D. W., ANNICCHIARICO-PETRUZZELLI, M., ANTONOV, A. V., ARAMA, E., BAEHRECKE, E. H., BARLEV, N. A., BAZAN, N. G., BERNASSOLA, F., BERTRAND, M. J. M., BIANCHI, K., BLAGOSKLONNY, M. V., BLOMGREN, K., BORNER, C., BOYA, P., BRENNER, C., CAMPANELLA, M., CANDI, E., CARMONA-GUTIERREZ, D., CECCONI, F., CHAN, F. K., CHANDEL, N. S., CHENG, E. H., CHIPUK, J. E., CIDLOWSKI, J. A., CIECHANOVER, A., COHEN, G. M., CONRAD, M., CUBILLOS-RUIZ, J. R., CZABOTAR, P. E., D'ANGIOLELLA, V., DAWSON, T. M., DAWSON, V. L., DE LAURENZI, V., DE MARIA, R., DEBATIN, K. M., DEBERARDINIS, R. J., DESHMUKH, M., DI DANIELE, N., DI VIRGILIO, F., DIXIT, V. M., DIXON, S. J., DUCKETT, C. S., DYNLACHT, B. D., EL-DEIRY, W. S., ELROD, J. W., FIMIA, G. M., FULDA, S., GARCIA-SAEZ, A. J., GARG, A. D., GARRIDO, C., GAVATHIOTIS, E., GOLSTEIN, P., GOTTLIEB, E., GREEN, D. R., GREENE, L. A., GRONEMEYER, H., GROSS, A., HAJNOCZKY, G., HARDWICK, J. M., HARRIS, I. S., HENGARTNER, M. O., HETZ, C., ICHIJO, H., JAATTELA, M., JOSEPH, B., JOST, P. J., JUIN, P. P., KAISER, W. J., KARIN, M., KAUFMANN, T., KEPP, O., KIMCHI, A., KITSIS, R. N., KLIONSKY, D. J., KNIGHT, R. A., KUMAR, S., LEE, S. W., LEMASTERS, J. J., LEVINE, B., LINKERMANN, A., LIPTON, S. A., LOCKSHIN, R. A., LOPEZ-OTIN, C., LOWE, S. W., LUEDDE, T., LUGLI, E., MACFARLANE, M., MADEO, F., MALEWICZ, M., MALORNI, W., MANIC, G., et al. 2018. Molecular mechanisms of cell death: recommendations of the Nomenclature Committee on Cell Death 2018. *Cell Death Differ,* 25**,** 486-541.

GAVRIELI, Y., SHERMAN, Y. & BEN-SASSON, S. A. 1992. Identification of programmed cell death in situ via specific labeling of nuclear DNA fragmentation. *J Cell Biol,* 119**,** 493-501.

GIBSON, D. G. 2011. Enzymatic assembly of overlapping DNA fragments. *Methods Enzymol,* 498**,** 349-61.

GLAMOCLIJA, V., VILOVIC, K., SARAGA-BABIC, M., BARANOVIC, A. & SAPUNAR, D. 2005. Apoptosis and active caspase-3 expression in human granulosa cells. *Fertil Steril,* 83**,** 426-31.

GOLOVANOV, A. P., HAUTBERGUE, G. M., WILSON, S. A. & LIAN, L. Y. 2004. A simple method for improving protein solubility and long-term stability. *J Am Chem Soc,* 126**,** 8933-9.

GORCZYCA, W., BRUNO, S., DARZYNKIEWICZ, R., GONG, J. & DARZYNKIEWICZ, Z. 1992. DNA strand breaks occurring during apoptosis - their early insitu detection by the terminal deoxynucleotidyl transferase and nick translation assays and prevention by serine protease inhibitors. *Int J Oncol,* 1**,** 639-48.

GUIMARAES, C. P., WITTE, M. D., THEILE, C. S., BOZKURT, G., KUNDRAT, L., BLOM, A. E. & PLOEGH, H. L. 2013. Site-specific C-terminal and internal loop labeling of proteins using sortase-mediated reactions. *Nat Protoc,* 8**,** 1787-99.

GUO, M. F., ZHAO, Y., TIAN, R., LI, L., GUO, L., XU, F., LIU, Y. M., HE, Y. B., BAI, S. & WANG, J. 2009. In vivo99mTc-HYNIC-annexin V imaging of early tumor apoptosis in mice after single dose irradiation. *J Exp Clin Cancer Res,* 28**,** 136.

HANAYAMA, R., MIYASAKA, K., NAKAYA, M. & NAGATA, S. 2006. MFG-E8-dependent clearance of apoptotic cells, and autoimmunity caused by its failure. *Curr Dir Autoimmun,* 9**,** 162-72.

HANAYAMA, R. & NAGATA, S. 2005. Impaired involution of mammary glands in the absence of milk fat globule EGF factor 8. *Proc Natl Acad Sci U S A,* 102**,** 16886-91.

HANAYAMA, R., TANAKA, M., MIWA, K., SHINOHARA, A., IWAMATSU, A. & NAGATA, S. 2002. Identification of a factor that links apoptotic cells to phagocytes. *Nature,* 417**,** 182-7.

HANAYAMA, R., TANAKA, M., MIYASAKA, K., AOZASA, K., KOIKE, M., UCHIYAMA, Y. & NAGATA, S. 2004. Autoimmune disease and impaired uptake of apoptotic cells in MFG-E8-deficient mice. *Science,* 304**,** 1147-50.

HARPER, S. & SPEICHER, D. W. 2011. Purification of proteins fused to glutathione S-transferase. *Methods Mol Biol,* 681**,** 259-80.

HARTMAN, Z. C., WEI, J., GLASS, O. K., GUO, H., LEI, G., YANG, X. Y., OSADA, T., HOBEIKA, A., DELCAYRE, A., LE PECQ, J. B., MORSE, M. A., CLAY, T. M. & LYERLY, H. K. 2011. Increasing vaccine potency through exosome antigen targeting. *Vaccine,* 29**,** 9361-7.

HIRAKAWA, H., ISHIKAWA, S. & NAGAMUNE, T. 2012. Design of Ca2+-independent Staphylococcus aureus sortase A mutants. *Biotechnol Bioeng,* 109**,** 2955-61.

HIRAKAWA, H., ISHIKAWA, S. & NAGAMUNE, T. 2015. Ca2+ -independent sortase-A exhibits high selective protein ligation activity in the cytoplasm of Escherichia coli. *Biotechnol J,* 10**,** 1487-92.

HOWLETT, G. J., MINTON, A. P. & RIVAS, G. 2006. Analytical ultracentrifugation for the study of protein association and assembly. *Curr Opin Chem Biol,* 10**,** 430-6.

HU, C. Y., WU, C. S., TSAI, H. F., CHANG, S. K., TSAI, W. I. & HSU, P. N. 2009. Genetic polymorphism in milk fat globule-EGF factor 8 (MFG-E8) is associated with systemic lupus erythematosus in human. *Lupus,* 18**,** 676-81.

HVARREGAARD, J., ANDERSEN, M. H., BERGLUND, L., RASMUSSEN, J. T. & PETERSEN, T. E. 1996. Characterization of glycoprotein PAS-6/7 from membranes of bovine milk fat globules. *Eur J Biochem,* 240**,** 628-36.

ILICIC, T., KIM, J. K., KOLODZIEJCZYK, A. A., BAGGER, F. O., MCCARTHY, D. J., MARIONI, J. C. & TEICHMANN, S. A. 2016. Classification of low quality cells from single-cell RNA-seq data. *Genome Biol,* 17**,** 29.

JOSEPH, N., REICHER, B. & BARDA-SAAD, M. 2014. The calcium feedback loop and T cell activation: how cytoskeleton networks control intracellular calcium flux. *Biochim Biophys Acta,* 1838**,** 557-68.

KENIS, H., VAN GENDEREN, H., BENNAGHMOUCH, A., RINIA, H. A., FREDERIK, P., NARULA, J., HOFSTRA, L. & REUTELINGSPERGER, C. P. 2004. Cell surface-expressed phosphatidylserine and annexin A5 open a novel portal of cell entry. *J Biol Chem,* 279**,** 52623-9.

KERR, J. F., WYLLIE, A. H. & CURRIE, A. R. 1972. Apoptosis: a basic biological phenomenon with wide-ranging implications in tissue kinetics. *Br J Cancer,* 26**,** 239-57.

KHEDDO, P., TRACKA, M., ARMER, J., DEARMAN, R. J., UDDIN, S., VAN DER WALLE, C. F. & GOLOVANOV, A. P. 2014. The effect of arginine glutamate on the stability of monoclonal antibodies in solution. *Int J Pharm,* 473**,** 126-33.

KIETSELAER, B. L., HOFSTRA, L., DUMONT, E. A., REUTELINGSPERGER, C. P. & HEIDENDAL, G. A. 2003. The role of labeled Annexin A5 in imaging of programmed cell death. From animal to clinical imaging. *Q J Nucl Med,* 47**,** 349-61.

KIMPLE, M. E., BRILL, A. L. & PASKER, R. L. 2013. Overview of affinity tags for protein purification. *Curr Protoc Protein Sci,* 73**,** 9 9 1-9 9 23.

KOOIJMANS, S. A. A., GITZ-FRANCOIS, J., SCHIFFELERS, R. M. & VADER, P. 2018. Recombinant phosphatidylserine-binding nanobodies for targeting of extracellular vesicles to tumor cells: a plug-and-play approach. *Nanoscale,* 10**,** 2413-2426.

KRANICH, J., CHLIS, N.-K., RAUSCH, L., LATHA, A., SCHIFFERER, M., KURZ, T., KIA, A. F.-A., SIMONS, M., THEIS, F. J. & BROCKER, T. 2020. In vivo identification of apoptotic and extracellular vesicle-bound live cells using image-based deep learning. *bioRxiv***,** 2020.04.14.040691.

KRANICH, J., KRAUTLER, N. J., HEINEN, E., POLYMENIDOU, M., BRIDEL, C., SCHILDKNECHT, A., HUBER, C., KOSCO-VILBOIS, M. H., ZINKERNAGEL, R., MIELE, G. & AGUZZI, A. 2008. Follicular dendritic cells control engulfment of apoptotic bodies by secreting Mfge8. *J Exp Med,* 205**,** 1293-302.

KUGE, Y., ZHAO, S., TAKEI, T. & TAMAKI, N. 2009. Molecular imaging of apoptosis with radio-labeled Annexin A5 focused on the evaluation of tumor response to chemotherapy. *Anticancer Agents Med Chem,* 9**,** 1003-11.

LANE, R. E., KORBIE, D., HILL, M. M. & TRAU, M. 2018. Extracellular vesicles as circulating cancer biomarkers: opportunities and challenges. *Clin Transl Med,* 7**,** 14.

LAROCCA, D., PETERSON, J. A., URREA, R., KUNIYOSHI, J., BISTRAIN, A. M. & CERIANI, R. L. 1991. A Mr 46,000 human milk fat globule protein that is highly expressed in human breast tumors contains factor VIII-like domains. *Cancer Res,* 51**,** 4994-8.

LEVENTIS, P. A. & GRINSTEIN, S. 2010. The distribution and function of phosphatidylserine in cellular membranes. *Annu Rev Biophys,* 39**,** 407-27.

LIAO, S. M., DU, Q. S., MENG, J. Z., PANG, Z. W. & HUANG, R. B. 2013. The multiple roles of histidine in protein interactions. *Chem Cent J,* 7**,** 44.

LIN, L., HUAI, Q., HUANG, M., FURIE, B. & FURIE, B. C. 2007. Crystal structure of the bovine lactadherin C2 domain, a membrane binding motif, shows similarity to the C2 domains of factor V and factor VIII. *J Mol Biol,* 371**,** 717-24.

LOGUE, S. E., ELGENDY, M. & MARTIN, S. J. 2009. Expression, purification and use of recombinant annexin V for the detection of apoptotic cells. *Nat Protoc,* 4**,** 1383-95.

MARBLESTONE, J. G., EDAVETTAL, S. C., LIM, Y., LIM, P., ZUO, X. & BUTT, T. R. 2006. Comparison of SUMO fusion technology with traditional gene fusion systems: enhanced expression and solubility with SUMO. *Protein Sci,* 15**,** 182-9.

MARTIN, S. J., REUTELINGSPERGER, C. P., MCGAHON, A. J., RADER, J. A., VAN SCHIE, R. C., LAFACE, D. M. & GREEN, D. R. 1995. Early redistribution of plasma membrane phosphatidylserine is a general feature of apoptosis regardless of the initiating stimulus: inhibition by overexpression of Bcl-2 and Abl. *J Exp Med,* 182**,** 1545-56.

MEERS, P. & MEALY, T. 1993. Relationship between annexin V tryptophan exposure, calcium, and phospholipid binding. *Biochemistry,* 32**,** 5411-8.

MEERS, P. & MEALY, T. 1994. Phospholipid determinants for annexin V binding sites and the role of tryptophan 187. *Biochemistry,* 33**,** 5829-37.

MELDOLESI, J. 2018. Exosomes and Ectosomes in Intercellular Communication. *Curr Biol,* 28**,** R435-R444.

MESSENS, J. & COLLET, J. F. 2006. Pathways of disulfide bond formation in Escherichia coli. *Int J Biochem Cell Biol,* 38**,** 1050-62.

MEZZANOTTE, L., VAN 'T ROOT, M., KARATAS, H., GOUN, E. A. & LOWIK, C. 2017. In Vivo Molecular Bioluminescence Imaging: New Tools and Applications. *Trends Biotechnol,* 35**,** 640-652.

MISSIAKAS, D., GEORGOPOULOS, C. & RAINA, S. 1994. The Escherichia coli dsbC (xprA) gene encodes a periplasmic protein involved in disulfide bond formation. *EMBO J,* 13**,** 2013-20.

MIYASAKA, K., HANAYAMA, R., TANAKA, M. & NAGATA, S. 2004. Expression of milk fat globule epidermal growth factor 8 in immature dendritic cells for engulfment of apoptotic cells. *Eur J Immunol,* 34**,** 1414-22.

MO, Y., CAMPOS, B., MEALY, T. R., COMMODORE, L., HEAD, J. F., DEDMAN, J. R. & SEATON, B. A. 2003. Interfacial basic cluster in annexin V couples phospholipid binding and trimer formation on membrane surfaces. *J Biol Chem,* 278**,** 2437-43.

MOORE, E. W. 1970. Ionized calcium in normal serum, ultrafiltrates, and whole blood determined by ion-exchange electrodes. *J Clin Invest,* 49**,** 318-34.

NAGATA, S. 2018. Apoptosis and Clearance of Apoptotic Cells. *Annu Rev Immunol,* 36**,** 489-517.

NAIK, M. T., SUREE, N., ILANGOVAN, U., LIEW, C. K., THIEU, W., CAMPBELL, D. O., CLEMENS, J. J., JUNG, M. E. & CLUBB, R. T. 2006. Staphylococcus aureus Sortase A transpeptidase. Calcium promotes sorting signal binding by altering the mobility and structure of an active site loop. *J Biol Chem,* 281**,** 1817-26.

NAKAI, W., YOSHIDA, T., DIEZ, D., MIYATAKE, Y., NISHIBU, T., IMAWAKA, N., NARUSE, K., SADAMURA, Y. & HANAYAMA, R. 2016. A novel affinity-based method for the isolation of highly purified extracellular vesicles. *Sci Rep,* 6**,** 33935.

NALLAMSETTY, S., KAPUST, R. B., TOZSER, J., CHERRY, S., TROPEA, J. E., COPELAND, T. D. & WAUGH, D. S. 2004. Efficient site-specific processing of fusion proteins by tobacco vein mottling virus protease in vivo and in vitro. *Protein Expr Purif,* 38**,** 108-15.

NAMURA, S., ZHU, J., FINK, K., ENDRES, M., SRINIVASAN, A., TOMASELLI, K. J., YUAN, J. & MOSKOWITZ, M. A. 1998. Activation and cleavage of caspase-3 in apoptosis induced by experimental cerebral ischemia. *J Neurosci,* 18**,** 3659-68.

NOZACH, H., FRUCHART-GAILLARD, C., FENAILLE, F., BEAU, F., RAMOS, O. H., DOUZI, B., SAEZ, N. J., MOUTIEZ, M., SERVENT, D., GONDRY, M., THAI, R., CUNIASSE, P., VINCENTELLI, R. & DIVE, V. 2013. High throughput screening identifies disulfide isomerase DsbC as a very efficient partner for recombinant expression of small disulfide-rich proteins in E. coli. *Microb Cell Fact,* 12**,** 37.

NUMAGA, T., NISHIDA, M., KIYONAKA, S., KATO, K., KATANO, M., MORI, E., KUROSAKI, T., INOUE, R., HIKIDA, M., PUTNEY, J. W., JR. & MORI, Y. 2010. Ca2+ influx and protein scaffolding via TRPC3 sustain PKCbeta and ERK activation in B cells. *J Cell Sci,* 123**,** 927-38.

OGURA, K., NARA, K., WATANABE, Y., KOHNO, K., TAI, T. & SANAI, Y. 1996. Cloning and expression of cDNA for O-acetylation of GD3 ganglioside. *Biochem Biophys Res Commun,* 225**,** 932-8.

OLING, F., SANTOS, J. S., GOVORUKHINA, N., MAZERES-DUBUT, C., BERGSMA-SCHUTTER, W., OOSTERGETEL, G., KEEGSTRA, W., LAMBERT, O., LEWIT-BENTLEY, A. & BRISSON, A. 2000. Structure of membrane-bound annexin A5 trimers: a hybrid cryo-EM - X-ray crystallography study. *J Mol Biol,* 304**,** 561-73.

OSHIMA, K., AOKI, N., KATO, T., KITAJIMA, K. & MATSUDA, T. 2002. Secretion of a peripheral membrane protein, MFG-E8, as a complex with membrane vesicles. *Eur J Biochem,* 269**,** 1209-18.

OSHIMA, K., AOKI, N., NEGI, M., KISHI, M., KITAJIMA, K. & MATSUDA, T. 1999. Lactation-dependent expression of an mRNA splice variant with an exon for a multiply O-glycosylated domain of mouse milk fat globule glycoprotein MFG-E8. *Biochem Biophys Res Commun,* 254**,** 522-8.

OSHIMA, K., YASUEDA, T., NISHIO, S. & MATSUDA, T. 2014. MFG-E8: Origin, Structure, Expression, Functions and Regulation. *In:* WANG, P. (ed.) *MFG-E8 and Inflammation.* Dordrecht: Springer Netherlands.

OSTERBERG, T., FATOUROS, A. & MIKAELSSON, M. 1997. Development of freeze-dried albumin-free formulation of recombinant factor VIII SQ. *Pharm Res,* 14**,** 892-8.

OTZEN, D. E., BLANS, K., WANG, H., GILBERT, G. E. & RASMUSSEN, J. T. 2012. Lactadherin binds to phosphatidylserine-containing vesicles in a two-step mechanism sensitive to vesicle size and composition. *Biochim Biophys Acta,* 1818**,** 1019-27.

PETERSON, J. A., PATTON, S. & HAMOSH, M. 1998. Glycoproteins of the human milk fat globule in the protection of the breast-fed infant against infections. *Biol Neonate,* 74**,** 143-62.

PICARIELLO, G., FERRANTI, P., MAMONE, G., ROEPSTORFF, P. & ADDEO, F. 2008. Identification of N-linked glycoproteins in human milk by hydrophilic interaction liquid chromatography and mass spectrometry. *Proteomics,* 8**,** 3833-47.

POLICARPO, R. L., KANG, H., LIAO, X., RABIDEAU, A. E., SIMON, M. D. & PENTELUTE, B. L. 2014. Flow-based enzymatic ligation by sortase A. *Angew Chem Int Ed Engl,* 53**,** 9203-8.

POULSEN, R. H., RASMUSSEN, J. T., EJLERSEN, J. A., FLO, C., FALBORG, L., HEEGAARD, C. W. & REHLING, M. 2013. Pharmacokinetics of the phosphatidylserine tracers 99mTc-lactadherin and 99mTc-annexin V in pigs. *EJNMMI Res,* 3**,** 15.

PRINZ, W. A., ASLUND, F., HOLMGREN, A. & BECKWITH, J. 1997. The role of the thioredoxin and glutaredoxin pathways in reducing protein disulfide bonds in the Escherichia coli cytoplasm. *J Biol Chem,* 272**,** 15661-7.

QIANG, X., LI, J., WU, R., JI, Y., CHAUNG, W., DONG, W. & WANG, P. 2011. Expression and characterization of recombinant human milk fat globule-EGF factor VIII. *Int J Mol Med,* 28**,** 1071-6.

RAYNAL, P. & POLLARD, H. B. 1994. Annexins: the problem of assessing the biological role for a gene family of multifunctional calcium- and phospholipid-binding proteins. *Biochim Biophys Acta,* 1197**,** 63-93.

RECORD, M., SILVENTE-POIROT, S., POIROT, M. & WAKELAM, M. J. O. 2018. Extracellular vesicles: lipids as key components of their biogenesis and functions. *J Lipid Res,* 59**,** 1316-1324.

REDDY NANGA, R. P., VIVEKANANDAN, S. & YOON, H. S. 2007. Expression, purification and characterization of C2 domain of milk fat globule-EGF-factor 8-L. *Protein Expr Purif,* 52**,** 329-33.

RICHARDSON, J. S. & RICHARDSON, D. C. 1989. Principles and patterns of protein conformation. *Prediction of protein structure and the principles of protein conformation.* Springer.

RIEDL, S. J. & SHI, Y. 2004. Molecular mechanisms of caspase regulation during apoptosis. *Nat Rev Mol Cell Biol,* 5**,** 897-907.

ROBBINS, P. D. & MORELLI, A. E. 2014. Regulation of immune responses by extracellular vesicles. *Nat Rev Immunol,* 14**,** 195-208.

ROY, S., HOCHBERG, F. H. & JONES, P. S. 2018. Extracellular vesicles: the growth as diagnostics and therapeutics; a survey. *J Extracell Vesicles,* 7**,** 1438720.

SAHIN, E. & ROBERTS, C. J. 2012. Size-exclusion chromatography with multi-angle light scattering for elucidating protein aggregation mechanisms. *Methods Mol Biol,* 899**,** 403-23.

SALEH, M., PENG, W., QUINN-ALLEN, M. A., MACEDO-RIBEIRO, S., FUENTES-PRIOR, P., BODE, W. & KANE, W. H. 2004. The factor V C1 domain is involved in membrane binding: identification of functionally important amino acid residues within the C1 domain of factor V using alanine scanning mutagenesis. *Thromb Haemost,* 91**,** 16-27.

SAMITH, V. D., MIÑO, G., RAMOS-MOORE, E. & ARANCIBIA-MIRANDA, N. 2013. Effects of pluronic F68 micellization on the viability of neuronal cells in culture. *Journal of Applied Polymer Science,* 130**,** 2159-2164.

SAVAGE, P. A., BONIFACE, J. J. & DAVIS, M. M. 1999. A kinetic basis for T cell receptor repertoire selection during an immune response. *Immunity,* 10**,** 485-92.

SCHMIDT, T. G. & SKERRA, A. 2007. The Strep-tag system for one-step purification and high-affinity detection or capturing of proteins. *Nat Protoc,* 2**,** 1528-35.

SEGAWA, K., KURATA, S., YANAGIHASHI, Y., BRUMMELKAMP, T. R., MATSUDA, F. & NAGATA, S. 2014. Caspase-mediated cleavage of phospholipid flippase for apoptotic phosphatidylserine exposure. *Science,* 344**,** 1164-8.

SEGAWA, K. & NAGATA, S. 2015. An Apoptotic 'Eat Me' Signal: Phosphatidylserine Exposure. *Trends Cell Biol,* 25**,** 639-650.

SHAKERI, R., KHEIROLLAHI, A. & DAVOODI, J. 2017. Apaf-1: Regulation and function in cell death. *Biochimie,* 135**,** 111-125.

SHAO, C., NOVAKOVIC, V. A., HEAD, J. F., SEATON, B. A. & GILBERT, G. E. 2008. Crystal structure of lactadherin C2 domain at 1.7A resolution with mutational and computational analyses of its membrane-binding motif. *J Biol Chem,* 283**,** 7230-41.

SHI, J. & GILBERT, G. E. 2003. Lactadherin inhibits enzyme complexes of blood coagulation by competing for phospholipid-binding sites. *Blood,* 101**,** 2628-36.

SHI, J., HEEGAARD, C. W., RASMUSSEN, J. T. & GILBERT, G. E. 2004. Lactadherin binds selectively to membranes containing phosphatidyl-L-serine and increased curvature. *Biochim Biophys Acta,* 1667**,** 82-90.

SHI, J., SHI, Y., WAEHRENS, L. N., RASMUSSEN, J. T., HEEGAARD, C. W. & GILBERT, G. E. 2006. Lactadherin detects early phosphatidylserine exposure on immortalized leukemia cells undergoing programmed cell death. *Cytometry A,* 69**,** 1193-201.

SHIH, C. L., CHONG, K. Y., HSU, S. C., CHIEN, H. J., MA, C. T., CHANG, J. W., YU, C. J. & CHIOU, C. C. 2016. Development of a magnetic bead-based method for the collection of circulating extracellular vesicles. *N Biotechnol,* 33**,** 116-22.

STETEFELD, J., MCKENNA, S. A. & PATEL, T. R. 2016. Dynamic light scattering: a practical guide and applications in biomedical sciences. *Biophys Rev,* 8**,** 409-427.

STUART, M. C., REUTELINGSPERGER, C. P. & FREDERIK, P. M. 1998. Binding of annexin V to bilayers with various phospholipid compositions using glass beads in a flow cytometer. *Cytometry,* 33**,** 414-9.

STUBBS, J. D., LEKUTIS, C., SINGER, K. L., BUI, A., YUZUKI, D., SRINIVASAN, U. & PARRY, G. 1990. cDNA cloning of a mouse mammary epithelial cell surface protein reveals the existence of epidermal growth factor-like domains linked to factor VIII-like sequences. *Proc Natl Acad Sci U S A,* 87**,** 8417-21.

SUN, C., LIANG, J., SHI, R., GAO, X., ZHANG, R., HONG, F., YUAN, Q. & WANG, S. 2012. Tobacco etch virus protease retains its activity in various buffers and in the presence of diverse additives. *Protein Expr Purif,* 82**,** 226-31.

SUREE, N., LIEW, C. K., VILLAREAL, V. A., THIEU, W., FADEEV, E. A., CLEMENS, J. J., JUNG, M. E. & CLUBB, R. T. 2009. The structure of the Staphylococcus aureus sortase-substrate complex reveals how the universally conserved LPXTG sorting signal is recognized. *J Biol Chem,* 284**,** 24465-77.

SUZUKI, J., DENNING, D. P., IMANISHI, E., HORVITZ, H. R. & NAGATA, S. 2013. Xk-related protein 8 and CED-8 promote phosphatidylserine exposure in apoptotic cells. *Science,* 341**,** 403-6.

SWAIRJO, M. A., ROBERTS, M. F., CAMPOS, M. B., DEDMAN, J. R. & SEATON, B. A. 1994. Annexin V binding to the outer leaflet of small unilamellar vesicles leads to altered inner-leaflet properties: 31P- and 1H-NMR studies. *Biochemistry,* 33**,** 10944-50.

SZABO, P. A., LEVITIN, H. M., MIRON, M., SNYDER, M. E., SENDA, T., YUAN, J., CHENG, Y. L., BUSH, E. C., DOGRA, P., THAPA, P., FARBER, D. L. & SIMS, P. A. 2019. Single-cell transcriptomics of human T cells reveals tissue and activation signatures in health and disease. *Nat Commun,* 10**,** 4706.

TAKADA, Y., YE, X. & SIMON, S. 2007. The integrins. *Genome Biol,* 8**,** 215.

TAKAGI, J. 2004. Structural basis for ligand recognition by RGD (Arg-Gly-Asp)-dependent integrins. *Biochem Soc Trans,* 32**,** 403-6.

TAKAHASHI, Y., NISHIKAWA, M., SHINOTSUKA, H., MATSUI, Y., OHARA, S., IMAI, T. & TAKAKURA, Y. 2013. Visualization and in vivo tracking of the exosomes of murine melanoma B16-BL6 cells in mice after intravenous injection. *J Biotechnol,* 165**,** 77-84.

TAYLOR, M. R., COUTO, J. R., SCALLAN, C. D., CERIANI, R. L. & PETERSON, J. A. 1997. Lactadherin (formerly BA46), a membrane-associated glycoprotein expressed in human milk and breast carcinomas, promotes Arg-Gly-Asp (RGD)-dependent cell adhesion. *DNA Cell Biol,* 16**,** 861-9.

THERY, C., REGNAULT, A., GARIN, J., WOLFERS, J., ZITVOGEL, L., RICCIARDI-CASTAGNOLI, P., RAPOSO, G. & AMIGORENA, S. 1999. Molecular characterization of dendritic cell-derived exosomes. Selective accumulation of the heat shock protein hsc73. *J Cell Biol,* 147**,** 599-610.

TRAUTZ, B., WIEDEMANN, H., LUCHTENBORG, C., PIERINI, V., KRANICH, J., GLASS, B., KRAUSSLICH, H. G., BROCKER, T., PIZZATO, M., RUGGIERI, A., BRUGGER, B. & FACKLER, O. T. 2017. The host-cell restriction factor SERINC5 restricts HIV-1 infectivity without altering the lipid composition and organization of viral particles. *J Biol Chem,* 292**,** 13702-13713.

UNZAI, S. 2018. Analytical ultracentrifugation in structural biology. *Biophys Rev,* 10**,** 229-233.

VAN NIEL, G., D'ANGELO, G. & RAPOSO, G. 2018. Shedding light on the cell biology of extracellular vesicles. *Nat Rev Mol Cell Biol,* 19**,** 213-228.

VERMES, I., HAANEN, C., STEFFENS-NAKKEN, H. & REUTELINGSPERGER, C. 1995. A novel assay for apoptosis. Flow cytometric detection of phosphatidylserine expression on early apoptotic cells using fluorescein labelled Annexin V. *J Immunol Methods,* 184**,** 39-51.

VERTOMMEN, D., DEPUYDT, M., PAN, J., LEVERRIER, P., KNOOPS, L., SZIKORA, J. P., MESSENS, J., BARDWELL, J. C. & COLLET, J. F. 2008. The disulphide isomerase DsbC cooperates with the oxidase DsbA in a DsbD-independent manner. *Mol Microbiol,* 67**,** 336-49.

VOGES, D., BERENDES, R., BURGER, A., DEMANGE, P., BAUMEISTER, W. & HUBER, R. 1994. Three-dimensional structure of membrane-bound annexin V. A correlative electron microscopy-X-ray crystallography study. *J Mol Biol,* 238**,** 199-213.

WANG, L., SUN, N., TERZYAN, S., ZHANG, X. & BENSON, D. R. 2006. A histidine/tryptophan pi-stacking interaction stabilizes the heme-independent folding core of microsomal apocytochrome b5 relative to that of mitochondrial apocytochrome b5. *Biochemistry,* 45**,** 13750-9.

WEBER, P. C., OHLENDORF, D. H., WENDOLOSKI, J. J. & SALEMME, F. R. 1989. Structural origins of high-affinity biotin binding to streptavidin. *Science,* 243**,** 85-8.

WUEST, M., PERREAULT, A., RICHTER, S., KNIGHT, J. C. & WUEST, F. 2019. Targeting phosphatidylserine for radionuclide-based molecular imaging of apoptosis. *Apoptosis,* 24**,** 221-244.

XU, T., CLOSE, D., HANDAGAMA, W., MARR, E., SAYLER, G. & RIPP, S. 2016. The Expanding Toolbox of In Vivo Bioluminescent Imaging. *Front Oncol,* 6**,** 150.

YAMAGUCHI, H., FUJIMOTO, T., NAKAMURA, S., OHMURA, K., MIMORI, T., MATSUDA, F. & NAGATA, S. 2010. Aberrant splicing of the milk fat globule-EGF factor 8 (MFG-E8) gene in human systemic lupus erythematosus. *Eur J Immunol,* 40**,** 1778-85.

YAMAGUCHI, H., TAKAGI, J., MIYAMAE, T., YOKOTA, S., FUJIMOTO, T., NAKAMURA, S., OHSHIMA, S., NAKA, T. & NAGATA, S. 2008. Milk fat globule EGF factor 8 in the serum of human patients of systemic lupus erythematosus. *J Leukoc Biol,* 83**,** 1300-7.

YANG, S. K., ATTIPOE, S., KLAUSNER, A. P., TIAN, R., PAN, D., RICH, T. A., TURNER, T. T., STEERS, W. D. & LYSIAK, J. J. 2006. In vivo detection of apoptotic cells in the testis using fluorescence labeled annexin V in a mouse model of testicular torsion. *J Urol,* 176**,** 830-5.

YE, H., LI, B., SUBRAMANIAN, V., CHOI, B. H., LIANG, Y., HARIKISHORE, A., CHAKRABORTY, G., BAEK, K. & YOON, H. S. 2013. NMR solution structure of C2 domain of MFG-E8 and insights into its molecular recognition with phosphatidylserine. *Biochim Biophys Acta,* 1828**,** 1083-93.

YEUNG, T., GILBERT, G. E., SHI, J., SILVIUS, J., KAPUS, A. & GRINSTEIN, S. 2008. Membrane phosphatidylserine regulates surface charge and protein localization. *Science,* 319**,** 210-3.

ZEELENBERG, I. S., OSTROWSKI, M., KRUMEICH, S., BOBRIE, A., JANCIC, C., BOISSONNAS, A., DELCAYRE, A., LE PECQ, J. B., COMBADIERE, B., AMIGORENA, S. & THERY, C. 2008. Targeting tumor antigens to secreted membrane vesicles in vivo induces efficient antitumor immune responses. *Cancer Res,* 68**,** 1228-35.

ZHANG, S. T., SHI, J., ZHAO, J., QI, Y. F. & GUO, A. G. 2006. Expression of soluble and functional snake venom fibrinolytic enzyme fibrolase via the co-expression of DsbC in Escherichia coli. *Protein Pept Lett,* 13**,** 559-63.

Acknowledgements

Ich möchte mich ganz herzlich bei Prof. Dr. Thomas Brocker bedanken, dass ich meine Arbeit in seiner Arbeitsgruppe anfertigen konnte. Ich wusste die Möglichkeit, mich frei zu entfalten sehr zu schätzen, wobei ich bei Fragen immer auf eine offene Tür und wichtige Ratschläge zählen konnte.

Dr. Jan Kranich danke ich für die unermüdliche Einsatzbereitschaft, Hilfe und Rat bei verschiedenen Experimenten, die Gewährleistung einer lockeren Arbeitsatmosphäre und das Korrekturlesen dieser Arbeit.

Meinen beiden Masteranden Larissa Köppel und Filip Zubic gilt ein herzliches Dankeschön für die produktive, motivierte und entspannte Zusammenarbeit. Ihr wart eine wichtige Unterstützung für mich.

Meiner Graduiertenschule QBM möchte ich für die umfassende Finanzierung danken und der Möglichkeit, auch einmal weiter über den Tellerrand hinauszuschauen und auf unzähligen Gebieten dazuzulernen.

Bei Christine Ried möchte ich mich besonders für das Labormanagement, die unzähligen Bestellungen mit Sonderwünschen meinerseits und die Anfertigung/Bearbeitung der Histologieschnitte bedanken, außerdem bei Agnieszka Foltyn-Arfa Kia und Amelie Frohmann für technische Unterstützung.

Meine beiden direkten Kolleginnen Lisa Rausch und Ashreta Latha möchte ich besonders erwähnen für die unkomplizierte Zusammenarbeit, Hilfsbereitschaft und einem kollegialen, humorvollen Umgang.

Hervorheben möchte ich zudem Dr. Gunnar Knobloch für die Starthilfe in Sachen SEC, die beständige kritische Diskussionsbereitschaft und eine zweite Meinung in biochemischen Angelegenheiten.

Für das Bereitstellen von verschiedenen Plasmiden gilt ein besonderes Dankeschön dem EMBL in Heidelberg und den AGs von Dr. Felix Müller-Planitz, Prof. Dr. Karl-Peter Hopfner und Prof. Dr. Andreas Ladurner.

Supplementary figures

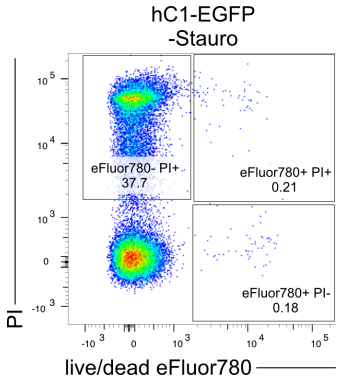

Supp. Fig. 1: High levels of SN from transfected HEK cells used for staining permeabilize cells in the staining procedure.
Untreated thymocytes were first stained with amino-reactive live/dead dye eFluor780, then with SN containing hC1-EGFP as done in Fig. 5.2 C and finally with PI to monitor SN-induced permeabilization of cells in the staining procedure.

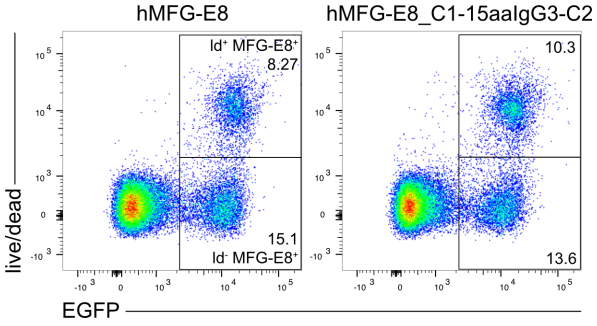

Supp. Fig. 2: No difference in binding is detected between hMFG-E8 and the linker variant
Staurosporine-treated mouse thymocytes were stained with equimolar amounts of wild type hMFG-E8 and hMFG-E8_C1-15aaIgG3-C2. Live/dead dye eFluor780 was used.

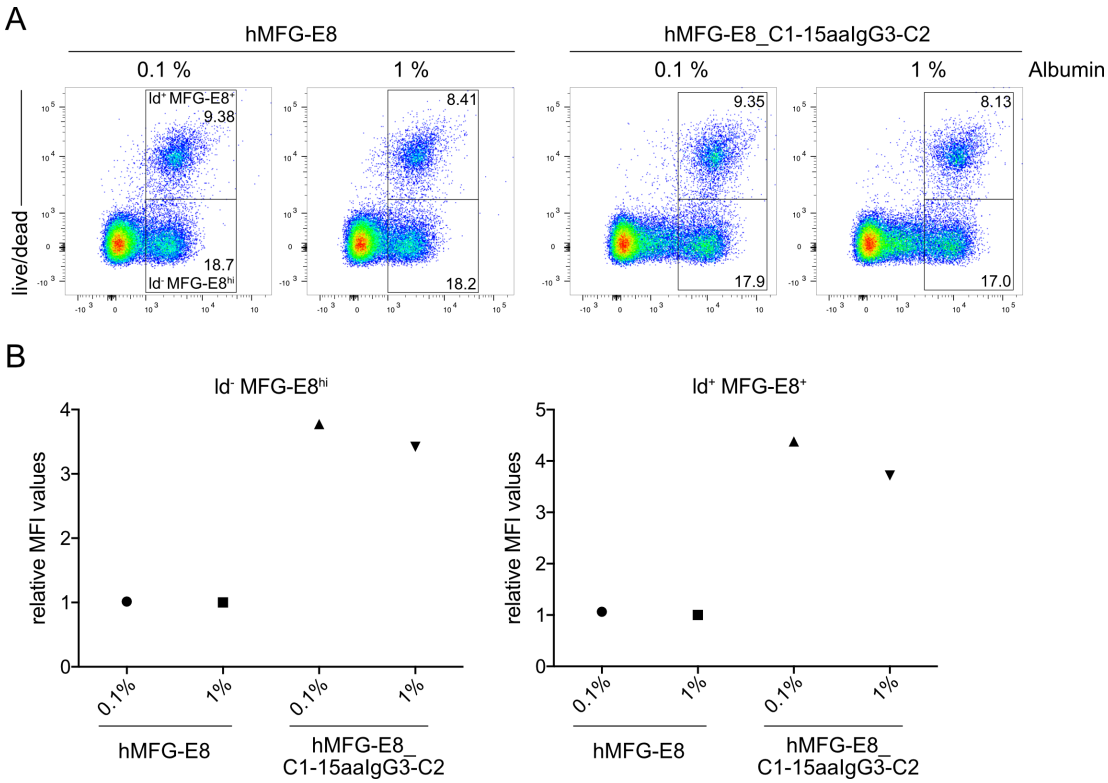

Supp. Fig. 3: Albumin content in the SN has no impact on hMFG-E8 variant binding properties.
(A) Staurosporine-treated thymocytes were stained with equimolar amounts of wild type hMFG-E8 and the 15aa IgG3-linker modified variant. SN for staining contained either 0.1% or 1% Albumin final concentration.
(B) MFI analysis for the EGFP signal in the Id^{-} MFG-E8^{hi} and Id^{+} MFG-E8^{+} gate. For comparison, the lowest value (hMFG-E8, 1% Albumin) was set to 1.